



## MASTER'S THESIS 2011

SUBJECT AREA: Concrete Structures	DATE: 17 December 2011	NO. OF PAGES: 84 +33
--------------------------------------	---------------------------	-------------------------

TITLE:

**Calculation and evaluation of crack risk in hardening concrete structures:  
Effects of thermal dilation, autogenous shrinkage and structural restraint on culverts**

Beregning og evaluering av rissrisiko i herdefasen:  
Anvendelse av det nye beregningsprogrammet CRACKTEST COIN på Møllenberg  
løsmassetunnel

BY:

Christian Kareliussen Sandvik



SUMMARY:

This thesis deals with prediction of early age cracking during the hardening phase. Concrete curing will generate stresses if the motions caused by hydration are restrained. The two major reasons for these motions are thermal dilation and autogenous shrinkage. The criterion for prediction of cracking risk in young concrete has usually been based on temperature. This has been found to be quite inaccurate, while stress-strain analysis contains all crucial factors and is therefore considered more reliable.

There are tailor made FE software products for temperature based stress analysis for predicting risk of cracking caused by restraint. In this thesis a Swedish two-dimensional FE software called "CrackTeSt COIN" has been used. It has been compared with similar software with focus on assessing the differences. The study also included taking a closer look at three different concrete mixtures and what impact various parameters have on the probability of cracks.

The Møllenberg culvert has been used as a basis for comparing the software as this is a massive structure with significant structural restraint. The objective of the computer simulations has been to outline measures that could be executed to prevent cracking. The computations were adapted to fit the concrete and conditions actually used in construction. Results from "CrackTeSt COIN" did, as expected, turn out to be conservative compared to simulations done in 3D. When compared with "4C Temp&Stress" the terms of concrete creep seem to be somewhat better represented in "CrackTeSt COIN". This statement is based on the shape of the time dependent stress development in the TSTM test results.

The parameter study displays how different different concrete materials behave under similar boundary conditions and what significance tensile strength has in prediction of cracking risk. The study also shows how the use of insulation will postpone the time of maximum crack index, but has not any positive effect.

Finally some improvement to help "CrackTeSt COIN" become as user-friendly as possible are proposed.

RESPONSIBLE TEACHER: Prof. Terje Kanstad

SUPERVISORS: Dr. Øyvind Bjøntegaard (Statens vegvesen) and Adj. Prof. Sverre Smepllass (Skanska)

CARRIED OUT AT: Department of Structural Engineering, NTNU.





## **MASTER'S THESIS FALL 2011**

*for stud. techn.  
Christian K. Sandvik*

***Calculation and evaluation of crack risk in hardening concrete structures:***

***Effects of thermal dilation, autogenous shrinkage and structural restraint on culvert structures***

*Beregning og evaluering av rissrisiko i herdefasen:  
Anvendelse av det nye beregningsprogrammet CRACKTEST COIN på  
Møllenberg løsmassetunnel*

### **Introduction**

In construction of large scale concrete structures effects of restrained thermal dilation and autogenous shrinkage may give large probability of cracking in the hardening phase. The consequence might be reduced functionality and durability, and visible cracks. The risk of this type of cracking can be assessed by application of special purpose FEM programs, presumed that the material property development and the structural system can be reasonably accurately described. Experimental determination of the material properties is time- and resource demanding, and it has therefore been common practice to estimate some properties based on previous results from previous testing of similar concretes.

In the comprehensive road project E6 East in Trondheim low-heat concrete is used to a large extent because it is favourable regarding the risk of cracking in the hardening phase. This master thesis is related to the culvert structures at Møllenberg, and measured material properties will be available for the most relevant concrete mixes.

In this thesis the new calculation program Cracktest COIN (2011) shall be used and the results shall be compared with previously reported results from the alternative programs 4CTemp&Stress and Diana.

### **Problem**

The course is to carry out calculations of stresses and cracking risk for the new culvert structures at Møllenberg, and relate the results to previous results obtained by the special purpose program 4CTemp&Stress and the general FEM program system Diana.

The master thesis shall in addition to the calculation part contain a theoretical part which gives background for result evaluation and discussion of the deviations between the results obtained by the different programs.

### **General**

The master project was initiated 4<sup>th</sup> August 2011, and shall be finalized within 22<sup>nd</sup> December 2011.

2011-12-10

Terje Kanstad

Professor





*There is also a kind of powder which, by nature, produces wonderful results. It is found in the neighbourhood of Baiae and in the lands of the municipalities round Mount Vesuvius. This being mixed with lime and rubble, not only furnishes strength to other buildings, but also, when piers are built in the sea, they set under water. And there would not be unless deep down they had huge blazing fires of sulphur, alum or pitch. Therefore the fire and vapors of flame within, flowing through the cracks, make that earthlight. And the tufa, which is found to come up there, is free from moisture. Therefore, when three substances formed in like manner by the violence of fire come into one mixture, they suddenly take up water and cohere together. They are quickly hardened by the moisture and made solid, and can be dissolved neither by the waves nor the power of the water.*

- Marcus Vitruvius Pollio, 25 B.C.[1]



# Preface

The Master's thesis is written in the course TKT4920 "Prosjektering av konstruksjoner, masteroppgave" and is the final paper of my MSc at NTNU. The thesis is prepared individually with supervision from Professor Terje Kanstad, Dr. Øyvind Bjøndegaard from the Norwegian Public Roads Administration and Adjunct Professor Sverre Smeplass from Skanska Norge.

The subject for the thesis is chosen by me in collaboration with my professor and supervisor Dr. Terje Kanstad. The purpose of this thesis is to compare the FEM-program CrackTeSt COIN to results from a FEM-program called 4C Temp & Stress and results from other Master thesis on the topic. The goal is to look closer on stress development and cracking tendencies in concretes hardening phase.

The thesis is related with COIN, Concrete Innovation Centre, which is a part of NTNU and SINTEF's Centre for Research-based Innovation. COIN started up in 2007 with the goal of creating more attractive concrete buildings and constructions. This implies development of new and sustainable design concepts together with more environmentally friendly material production.

I would like to thank everyone who have helped me with the Master thesis. Specially I want to express my gratitude to my supervisor Terje Kanstad for his help and support. I am also grateful to the contribution I have got from Jan-Erik Jonasson from Luleå Technical University, Øyvind Bjøntegaard and Sverre Smeplass.

I will finally thank Oliver B. Skjølsvik, Skanska Norge, for all help he has given me and for always being available on e-mail and telephone when I had questions.

Trondheim, 20<sup>th</sup> December 2011

Christian K Sandvik



# Abstract

This thesis deals with prediction of early age cracking during the hardening phase. Concrete curing will generate stresses if the motions caused by hydration are restrained. The two major reasons for these motions are thermal dilation and autogenous shrinkage. The criterion for prediction of cracking risk in young concrete has usually been based on temperature. This has been found to be quite inaccurate, while stress-strain analysis contains all crucial factors and is therefore considered more reliable.

There are tailor made FE software products for temperature based stress analysis for predicting risk of cracking caused by restraint. In this thesis a Swedish two-dimensional FE software called "CrackTeSt COIN" has been used. It has been compared with similar software with focus on assessing the differences. The study also included taking a closer look at three different concrete mixtures and what impact various parameters have on the probability of cracks.

The Møllenberg culvert has been used as a basis for comparing the software as this is a massive structure with significant structural restraint. The objective of the computer simulations has been to outline measures that could be executed to prevent cracking. The computations were adapted to fit the concrete and conditions actually used in construction. Results from "CrackTeSt COIN" did, as expected, turn out to be conservative compared to simulations done in 3D. When compared with "4C Temp&Stress" the terms of concrete creep seem to be somewhat better represented in "CrackTeSt COIN". This statement is based on the shape of the time dependent stress development in the TSTM test results.

The parameter study displays how different different concrete materials behave under similar boundary conditions and what significance tensile strength has in prediction of cracking risk. The study also shows how the use of insulation will postpone the time of maximum crack index, but has not any positive effect.

Finally some improvement to help "CrackTeSt COIN" become as user-friendly as possible are proposed.



# Contents

<b>1</b>	<b>Introduction</b>	<b>1</b>
1.1	Background . . . . .	1
1.2	Møllenberg tunnel through a clay deposit . . . . .	2
1.3	Computer-based curing technology . . . . .	4
<b>2</b>	<b>Theory</b>	<b>5</b>
2.1	Object and purpose . . . . .	5
2.2	Curing technology . . . . .	5
2.2.1	Maturity . . . . .	6
2.2.2	Activation energy . . . . .	6
2.2.3	Heat generation . . . . .	7
2.2.4	Autogenous shrinkage . . . . .	9
2.3	Restraint . . . . .	10
2.3.1	Internal restraint . . . . .	10
2.3.2	External restraint . . . . .	10
2.4	Stress development . . . . .	12
2.4.1	General . . . . .	12
2.4.2	Material models . . . . .	12
2.4.3	Crack index . . . . .	14
2.5	Input to simulation programs . . . . .	14
<b>3</b>	<b>Difference in Mathematical Models of Young Concrete Behaviour</b>	<b>17</b>
3.1	Basis . . . . .	17
3.2	Heat . . . . .	19
3.2.1	General . . . . .	19
3.2.2	Results . . . . .	19
3.3	Strength development . . . . .	21
3.3.1	General . . . . .	21
3.3.2	Results . . . . .	21
3.4	Creep . . . . .	24
3.4.1	Linear viscoelasticity for ageing materials . . . . .	25
3.4.2	Maxwell model . . . . .	25
3.4.3	Kelvin-Voigt model . . . . .	26
3.4.4	Burger model - 4C Temp&Stress . . . . .	27
3.4.5	Double power law - RELAX . . . . .	28
3.4.6	Maxwell chain model - CrackTeSt COIN . . . . .	29

3.5	Tensile stress and crack index . . . . .	30
3.5.1	Stress development . . . . .	30
3.5.2	Results . . . . .	30
<b>4</b>	<b>Material Properties</b>	<b>35</b>
4.1	Boundary conditions and geometry . . . . .	35
4.2	Compression strength development and activation energy . . . . .	36
4.3	Young's modulus . . . . .	38
4.4	Tensile strength . . . . .	39
4.5	Heat development . . . . .	39
4.6	Stiffness development summary . . . . .	40
<b>5</b>	<b>Analysis and Results</b>	<b>41</b>
5.1	Temperature . . . . .	41
5.2	Stress . . . . .	43
5.3	Crack index . . . . .	45
<b>6</b>	<b>Parameter Study</b>	<b>47</b>
6.1	General . . . . .	47
6.2	Temperature . . . . .	48
6.3	Stress . . . . .	49
6.4	Crack index . . . . .	51
6.5	Insulation . . . . .	52
<b>7</b>	<b>Software Useability</b>	<b>55</b>
7.1	General . . . . .	55
7.2	Graphical user interface . . . . .	55
7.3	Simulations . . . . .	56
7.4	Proposed changes . . . . .	57
<b>8</b>	<b>Conclusion</b>	<b>59</b>
<b>9</b>	<b>Further Work</b>	<b>61</b>
	<b>References</b>	<b>62</b>
<b>A</b>	<b>Material Parameters from Oliver</b>	<b>65</b>
<b>B</b>	<b>Material Parameters for NCC 50% FA per binder</b>	<b>69</b>
<b>C</b>	<b>Material Parameters for Anlegg 33.3% FA per binder</b>	<b>77</b>
<b>D</b>	<b>Material Parameters for Anlegg 30% FA per binder from the Bjørvika tunnel</b>	<b>85</b>
<b>E</b>	<b>Geometry of the Møllenberg tunnel</b>	<b>95</b>

# List of Figures

- 1.1 Different phases of concrete - schematic diagram [3] . . . . . 2
- 1.2 Illustration of Day zone west [5] . . . . . 3
- 1.3 Sketch map of the Strindheim tunnel [5] . . . . . 3
  
- 2.1 Cross section of heat in a concrete wall on cold continuous footing on the ground 5
- 2.2 Activation Energy  $E(\theta)$  with  $A = 20 \text{ kJ} \cdot \text{mol}^{-1}$  and  $B = 1.25 \text{ kJ} \cdot \text{mol}^{-1} \cdot ^\circ\text{C}^{-1}$  [8] 7
- 2.3 Total chemical shrinkage and external volumetric autogenous deformation in cement paste. 20 °C isothermal conditions. Schematic diagram [3] . . . . . 10
- 2.4 Temperature gradients and stress due to internal restraint[3] . . . . . 11
- 2.5 Degree of external restraint decreases with the distance from joint[2] . . . . . 11
- 2.6 Wall on slab from a FEM-analysis[3] . . . . . 11
- 2.7 Stress development during the hardening phase – schematic diagram[3] . . . . . 12
- 2.8 Relative development of Young’s modulus ( $E$ ), tensile strength ( $f_t$ ), and compressive strength ( $f_c$ ). All properties are 1.0 at 28 days (672 h). The curves are based on experimental data[3]. . . . . 13
- 2.9 Stress and strength development during the hardening phase because of external restraint . . . . . 14
- 2.10 Factors influencing the formation of cracks in hardening concrete[13] . . . . . 16
  
- 3.1 Measurements for wall on slab. The left drawing shows how the structure looks in ”CrackTeSt COIN” and the star shows where the results are gathered. . . . . 18
- 3.2 Temperature development versus maturity for traditional structural concrete (TSC) 20
- 3.3 Temperature development versus Maturity for FA20 concrete . . . . . 20
- 3.4 Temperature development versus Maturity for FA40 concrete . . . . . 20
- 3.5 Tensile strength development, TSC . . . . . 22
- 3.6 Tensile strength development, FA20 . . . . . 23
- 3.7 Tensile strength development, FA40 . . . . . 23
- 3.8 Compressive strength development, TSC . . . . . 23
- 3.9 Compressive strength development, FA20 . . . . . 24
- 3.10 Compressive strength development, FA40 . . . . . 24
- 3.11 Mechanical models for viscoelasticity . . . . . 27
- 3.12 Maxwell chain model . . . . . 30
- 3.13 Tensile stress development, TSC . . . . . 31
- 3.14 Tensile stress development, FA20 . . . . . 31
- 3.15 Tensile stress development, FA40 . . . . . 32
- 3.16 Crack Index as a function of maturity, TSC . . . . . 32
- 3.17 Crack Index as a function of maturity, FA20 . . . . . 32

3.18 Crack Index as a function of maturity, FA40 . . . . . 33

4.1 Cross section of the tunnel’s geometry in ”CrackTeSt COIN”. With a lateral X-axis and vertical Y-axis. . . . . 36

4.2 Compressive strength development before adjusting for activations energy . . . . 37

4.3 Compressive strength development after adjusting for activations energy . . . . . 38

4.4 Development of Young’s modulus and compressive strength with the matching adapted functions. . . . . 38

4.5 Tensile strength development plotted against maturity . . . . . 39

4.6 Relative development of Young’s modulus ( $E$ ), tensile strength ( $f_t$ ) and compressive strength ( $f_c$ ). The properties are all normalized with regard to their 28-day value. . . . . 40

5.1 Illustration of where the computed results were obtained . . . . . 42

5.2 Temperature development at an air temperature of -7 °C, ground and slab temperature of 2 °C and a concrete cast temperature of 13 °C . . . . . 42

5.3 Temperature development where all thermal boundary conditions are 20 °C . . . . 43

5.4 Color maps from the two software products at the time, 502 h, with maximum stress . . . . . 44

5.5 Stress development at an air temperature of -7 °C, ground and slab temperature of 2 °C and a concrete cast temperature of 13 °C . . . . . 45

5.6 Stress development where all thermal boundary conditions are 20 °C . . . . . 45

5.7 Crack index at an air temperature of -7 °C, ground and slab temperature of 2 °C and a concrete cast temperature of 13 °C . . . . . 46

5.8 Crack index where all thermal boundary conditions are 20 °C . . . . . 46

6.1 Charts from isothermal laboratory tests of autogenous shrinkage . . . . . 48

6.2 Temperature development at an air temperature of -7 °C, ground and slab temperature of 2 °C and a concrete cast temperature of 13 °C . . . . . 48

6.3 Temperature development where all thermal boundary conditions are 20 °C . . . . 49

6.4 Stress development at an air temperature of -7 °C, ground and slab temperature of 2 °C and a concrete cast temperature of 13 °C . . . . . 50

6.5 Stress development where all thermal boundary conditions are 20 °C . . . . . 50

6.6 Crack index at an air temperature of -7 °C, ground and slab temperature of 2 °C and a concrete cast temperature of 13 °C . . . . . 51

6.7 Crack index where all thermal boundary conditions are 20 °C . . . . . 52

6.8 Temperature development at an air temperature of -7 °C, ground and slab temperature of 2 °C and a concrete cast temperature of 13 °C . . . . . 53

6.9 Temperature development where all thermal boundary conditions are 20 °C . . . . 53

6.10 Crack index at an air temperature of -7 °C, ground and slab temperature of 2 °C and a concrete cast temperature of 13 °C . . . . . 54

6.11 Crack index where all thermal boundary conditions are 20 °C . . . . . 54

---

7.1	Graphical user interface . . . . .	55
7.2	Difference between the piecemeal linear and the piecemeal constant functions [17]	57
7.3	Example of color-map results for crack index . . . . .	57



# List of Tables

- 3.1 Structure used in analyses . . . . . 18
- 3.2 Transmission coefficients . . . . . 18
  
- 4.1 Heat transfer coefficients . . . . . 35
- 4.2 Stress case: Degree of restraint . . . . . 36
- 4.3 Parameters for compression strength . . . . . 37
- 4.4 Parameters for Activation Energy . . . . . 37
- 4.5 Parameters for Young’s modulus . . . . . 38
- 4.6 Parameters for tensile strength . . . . . 39
- 4.7 Parameters for heat development according to Swedish model . . . . . 40



# Chapter 1

## Introduction

### 1.1 Background

The first few days and weeks after mixing and casting are crucial for concrete structures. Concrete is a strong material, but volume instability, however, is a negative property which may cause cracking problems on-site. These volume instabilities and cracking tendencies are magnified in massive structures built with high quality concrete. By high quality it is referred to concretes with low w/b-ratio and high compressive strength. The concept of Curing Technology was introduced in the late 70's by the two Danes, Freisleben Hansen and Pedersen. These two are known for proposing a new function to compute maturity index from the recorded temperature history of the concrete. The maturity is set to correspond to the concrete's age when cured at 20 °C. Today National standards, like Eurocode, refer to maturity hours and not actual hours when it is written hours.

This thesis will concentrate on the hardening phase, and on crack assessment due to heat generation and restraint. This is the basis for stress-based computations. Differences in temperature between already hardened concrete and the adjoining new concrete in the hardening phase are the major cause of this kind of cracks. It has become more and more common to require documentation of the concrete's probability to crack, in terms of a crack index, during. To prepare this documentation, customized FEM computer software has been developed. One of these has been applied in this thesis.

Concrete as a material is constantly developing and goes through three main phases: fresh phase, hardening phase and service phase. The fresh phase, or plastic phase, includes mixing, transport, casting and early setting, see Figure 1.1. During this phase there is not much hydration to talk about before the next part, the semi-plastic phase. Here the concrete gradually loses all consistency due to weak physical bonds between particles and initial hydration products [2].

When the concrete reaches  $t_0$ , the final setting, it has already gained some measurable mechanical properties.  $t_0$  is usually from 6 to 12 hours after mixing, but varies with the concrete

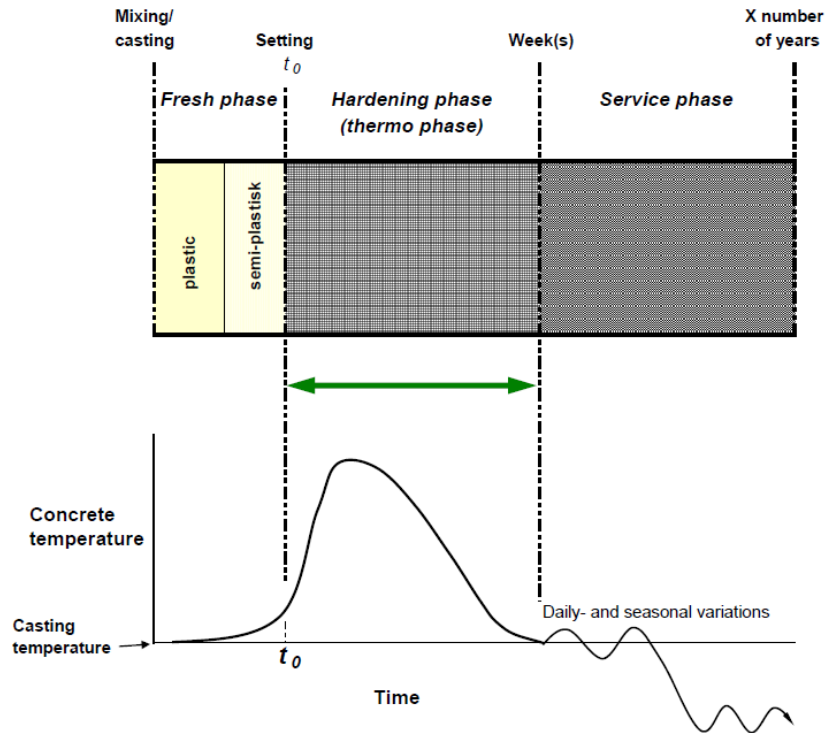


Figure 1.1: Different phases of concrete - schematic diagram [3]

temperature, type of cement and additives. It is in the hardening phase (thermo phase) the concrete develops most of its properties. The result of the exothermal hydration reaction is a significant heat generation. For a massive construction the temperature can reach as much as 50 °C or more. As one can see in Figure 1.1 the concrete temperature will after an amount of time rise to a maximum usually in between 18-48 hours after  $t_0$ , dependent of the structure. Then the concrete will cool down.

In the service phase the concrete will be exposed to service loads etc.

The three most important factors in prediction of early age cracking are[4]:

- the temperature and shrinkage development
- the development of material properties
- restraint conditions

## 1.2 Møllenberg tunnel through a clay deposit

The "Strindheim tunnel" is a part of the "E6 Trondheim–Stjørdal" project. The 2.5 km long [5] tunnel is built by The Norwegian Public Roads Administration, to handle the through traffic from the east of Trondheim city centre to Strindheim, near Nidar chocolate factory.

Most of the tunnel is surrounded by solid rock, but at the Møllenberg side, the west side of the tunnel, a section of approximately 0.5 km is much more challenging to construct. This end of the tunnel is known as "Day zone west", see Figure 1.2 and 1.3, and around here the surrounding soil consists of either quick clay or very hard rock. Several buildings have been temporarily moved to a storage area further east and some even got demolished and will be replaced when the tunnel is finished. The "Strindheim tunnel" project is scheduled to be finished end of 2012 and the road is scheduled to be opened for traffic in 2014.



Figure 1.2: Illustration of Day zone west [5]

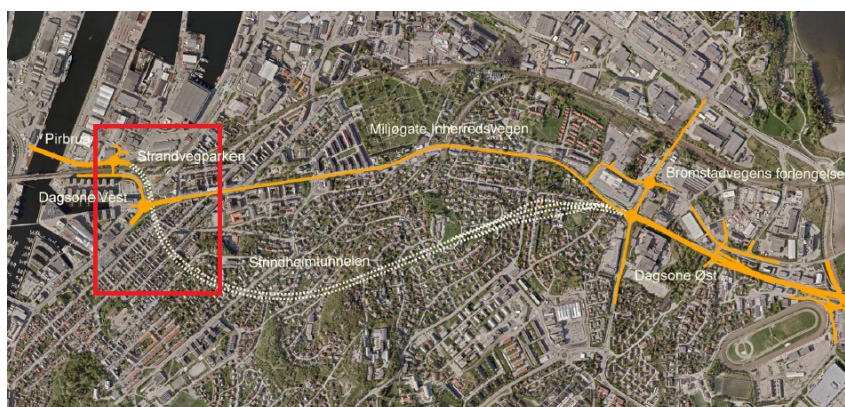


Figure 1.3: Sketch map of the Strindheim tunnel [5]

The Norwegian Public Roads Administration usually requires SV40 concrete for their tunnel projects, but in this case a special low heat concrete with high content of fly ash is selected. The analysis done in this thesis apply data from two different concretes, one "Anlegg-FA" concrete with 40 % fly ash and one special developed concrete with 100 % fly ash. These percentage shares are according to the Norwegian Public Roads Administration notations, Equation 1.1, and refer to the amount of fly ash compared to the amount of cement clinker. The risk of cracks is greatest in the wall that will be cast on a cold concrete foundation.

$$\text{Fly ash content} = \frac{\text{Fly ash mass}}{\text{Cement mass}} \quad (1.1)$$

$$\text{Fly ash content} = \frac{\text{Fly ash mass}}{\text{Fly ash mass} + \text{Cement mass}} \quad (1.2)$$

A notation for concrete's amount of fly ash, Equation 1.2, will consequently be used as the standard notation in the rest of this thesis. 40 % fly ash, according to Equation 1.1, will then have a fly ash content of 28,6 %, according to Equation 1.2.

### 1.3 Computer-based curing technology

There are several computer programs made to estimate temperature, maturity and mechanical property development. The most common ones use FEA and a variation of 2D, 2<sup>1/2</sup>D or 3D; theory, while models and functions differ from program to program. The computer calculations reported in this thesis are made in "CrackTeSt COIN", a Norwegian version of the original Swedish program ConTest Pro, made by Jan-Erik Jonasson from Luleå Technical University. "CrackTeSt-COIN" used finite-element stress analysis. I have also used a program called "RELAX". This program converts creep data into relaxation data which is used as input data for "CrackTeSt COIN".

The data program "ConTest Pro" is based on adiabatic and semi-adiabatic hydration tests on commonly used Self-Compacting Concrete (SCC) and Traditional Concrete (TC) for civil engineering, obtained by the Luleå Technical University. Apart from the calorimetric tests, results from compressive-, pull-, creep- and shrinkage tests were obtained[6]. This thesis also compares theory used in "CrackTeSt COIN" with a similar Danish program called "4C Temp & Stress".

# Chapter 2

## Theory

### 2.1 Object and purpose

The purpose of this chapter is to present the theory which will form the basis for this thesis. There will also be clarification in the use of symbols and technical terms, because these may vary in different literature.

### 2.2 Curing technology

Concrete is created mainly by a reaction between cement and water. In the reaction it will form a solid material consisting of partially water-filled pores. The reaction is called hydration and is exothermic, it generates heat. This heat causes thermal dilatation  $\varepsilon_{TD}$  (thermal expansion) of the concrete. At the same time the partially water-filled pores will cause autogenous shrinkage  $\varepsilon_{AS}$  (chemical contraction) due to self-desiccation. It is mainly these two factors, thermal dilatation and autogenous shrinkage, that are responsible for volume changes in hardening concrete. The

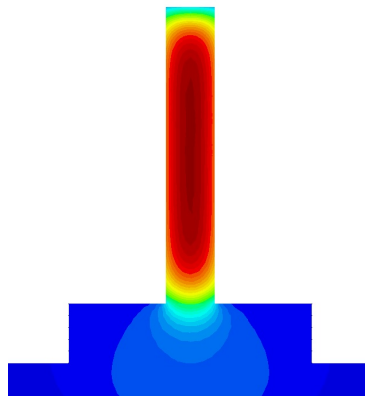


Figure 2.1: Cross section of heat in a concrete wall on cold continuous footing on the ground

commonly used equation to describe concrete deformation is the sum of these independent terms, expressed as:

$$\varepsilon_{tot} = \varepsilon_{TD} + \varepsilon_{AS} \quad (2.1)$$

### 2.2.1 Maturity

The principle of maturity, developed by Freisleben Hansen and Pedersen, makes it possible to compare concretes cured at different temperatures[7]. That applies, as long as the strength development is known. It uses a concept called equivalent time. Equivalent time, or maturity time ( $t_e$ ), is the amount of time which has been needed to achieve the same maturity as if the concrete had cured at 20 °C. Maturity is found by integrating the rate of hydration ( $H$ ) from  $t_0$  to  $t$ , see Equation 2.2:

$$t_e = \int_{t_0}^t H(\theta) dt, \quad \theta = \theta(t) \quad (2.2)$$

where

$$\begin{aligned} H(\theta) &= \exp \left[ \frac{E(\theta)}{R} \cdot \left( \frac{1}{293} - \frac{1}{273 + \theta} \right) \right] \\ E(\theta) &= \text{activation energy [J mol}^{-1}\text{]} \\ R &= \text{ideal gas constant} = 8.3144621 \text{ J mol}^{-1} \text{ K}^{-1} \\ \theta &= \text{temperature [}^\circ\text{C]} \end{aligned} \quad (2.3)$$

To help to do this numerically and with measured data, one can write equation 2.2 into a formula with a summation operator for easier computations:

$$t_e = \sum_{i=1}^{i=n} H(\theta_i) \Delta t_i \quad (2.4)$$

### 2.2.2 Activation energy

A maturity model makes it possible to compare curing process that take place during different time/temperature histories and compare this with equivalent curing at 20 °C. To achieve this, one must know the cement reaction rate with water at different temperatures. This is expressed by a Arrhenius function, the rate of hydration ( $H$ ), shown in Equation 2.3 and Equation 2.5 shows the activation energy,  $E(\theta)$ , expressed by the empirical constants  $A$  and  $B$ . The parameters  $A$  and  $B$  are determined by curve fitting of strength development at different points of time

and temperatures up to 28 days strength. The constant  $A$  will increase while  $B$  will decrease with higher levels of fly ash. In Figure 2.2 one can see the activations energy for a typical cement.

$$E(\theta) = \begin{cases} A + B(20 - \theta) & \theta \leq 20 \text{ }^\circ\text{C} \\ A & \theta > 20 \text{ }^\circ\text{C} \end{cases} \quad (2.5)$$

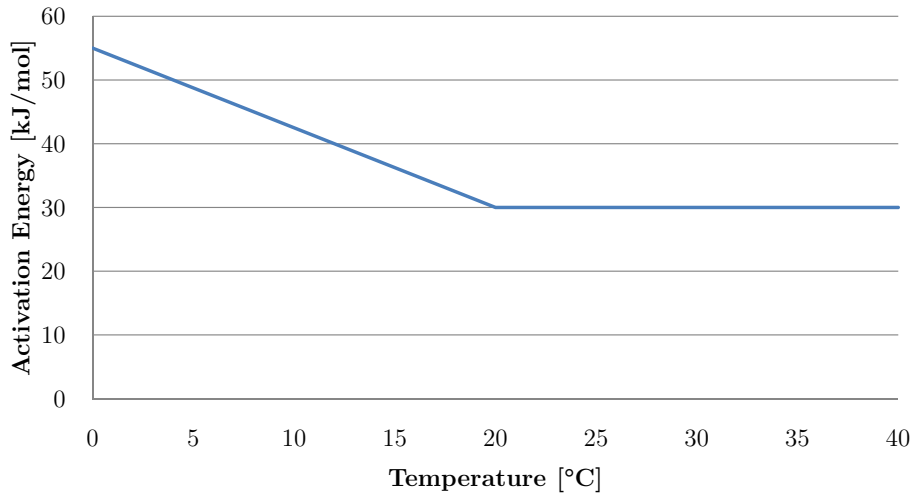


Figure 2.2: Activation Energy  $E(\theta)$  with  $A = 20 \text{ kJ} \cdot \text{mol}^{-1}$  and  $B = 1.25 \text{ kJ} \cdot \text{mol}^{-1} \cdot \text{ }^\circ\text{C}^{-1}$  [8]

### 2.2.3 Heat generation

As shown in the introduction of the figure 1.1, concrete will produce a lot of heat at the start of the curing phase. Different compositions of clinker in the cement cause differences in the heat generation. A typical Portland cement develops 400-500 kJ/kg cement at full hydration[9]. The relationship between the developed heat and temperature increase under adiabatic conditions can according to Smeplass [9] be expressed as:

$$\Delta\theta = \frac{Q_\infty \cdot C}{\rho_r \cdot c_b} \quad (2.6)$$

where:

$\Delta\theta$  = temperature increase in the concrete [°C]

$Q_\infty$  = amount of heat developed per kilogram of cement [kJ/kg]

$C$  = amount of cement [kg]

$$\begin{aligned}\rho_c &= \text{concrete density [kg/m}^3\text{]} \\ c_b &= \text{the concrete specific heat capacity [kJ/m}^3\text{ }^\circ\text{C]}\end{aligned}$$

The correlation between temperature change  $\Delta\theta$  and thermal dilation  $\varepsilon_{TD}$  is displayed in equation 2.7, where  $\alpha_\theta$  is the thermal expansion coefficient. The commonly used, and CrackTeSt COIN's default, value for  $\alpha_\theta$  is  $10 \cdot 10^{-6}/\text{K}$ , but varies considerably depending on aggregate type and moisture condition.

$$\varepsilon_{TD} = \alpha_\theta \cdot \Delta\theta \quad (2.7)$$

The heat development has often been described mathematically in Norway with equation 2.8. This is an empirical shape function introduced by Freisleben Hansen. This is the Danish model and for instance the simulation program "4C Temp and Stress" uses this function [3]:

$$Q(t_e) = Q_\infty \cdot \exp \left[ - \left( \frac{\tau}{t_e} \right)^\alpha \right] \quad (2.8)$$

where:

$$\begin{aligned}Q(t_e) &= \text{the heat generation as a function of maturity time [J/kg]} \\ Q_\infty &= \text{the final heat generation after "infinite" time [J/kg]} \\ t_e &= \text{maturity [h]} \\ \tau[\text{h}] \text{ and } \alpha &= \text{curve fitting parameters}\end{aligned}$$

The simulation program used in this thesis, "CrackTeSt COIN", is made in Sweden and therefore uses a Swedish exponential function that differs slightly from the Danish model:

$$Q(t_e) = W_\infty \cdot \exp \left[ -\lambda_1 \cdot \ln \left( 1 + \frac{t_e}{t_1} \right) \right]^{-\kappa_1} \quad (2.9)$$

where:

$$\begin{aligned}Q(t_e) &= \text{the heat generation as a function of maturity time [J/kg]} \\ W_\infty &= \text{the final heat generation after "infinite" time [J/kg]} \\ t_e &= \text{maturity [h]} \\ \lambda_1, t_1[\text{h}] \text{ and } \kappa_1 &= \text{curve fitting parameters}\end{aligned}$$

The parameter  $\lambda_1$  is mathematically coupled with  $\kappa_1$ , therefore  $\lambda_1 \equiv 1.0$  is normally used without changing the degree of freedom of the function.

An Excel-based spreadsheet developed by Smeplass [10] is typically used in Norway to convert measured temperatures from semi-adiabatic calorimeters to isothermal heat data..

#### 2.2.4 Autogenous shrinkage

When cement reacts with water the total concrete volume is reduced because the reaction product has less volume than the reactants, this effect is called chemical shrinkage and constitutes approximately  $0.06 \text{ cm}^3$  per gram of reacted cement, this corresponds to about 8 volume percentage of a fully hydrated concrete with a w/c-ratio of 0.4 [9], assuming complete hydration. Chemical shrinkage starts when water meets cement in the mixing process and continues as long as the hydration process goes on in the concrete.

During hydration, the degree of water saturation in the pore structure is reduced since the water is consumed as cement hydration processes. The decrease in water saturation is called self-desiccation, and will lead to a decline in relative humidity (RH) in the pore system. This drop in RH will increase in high performance concretes, with low w/b-ratio [3]. Self-desiccation is together with negative capillary pressure assumed to be the main mechanism behind autogenous shrinkage in concrete. In figure 2.3 the fundamental relationship between chemical shrinkage (internal contraction) and autogenous deformation (external contraction) is shown. The difference between the curves expresses the empty pore volume in the binder phase that is formed by chemical shrinkage. It also shows that the chemical shrinkage and autogenous deformation are equal in the initial phase.

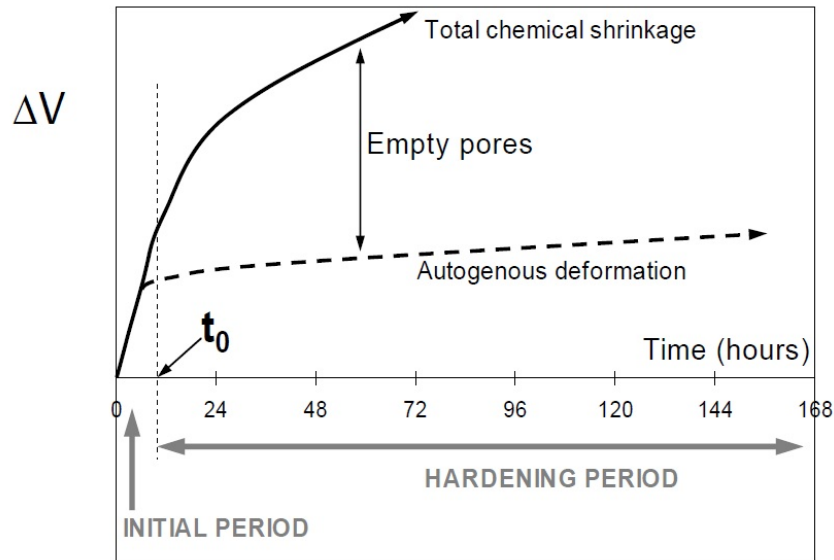


Figure 2.3: Total chemical shrinkage and external volumetric autogenous deformation in cement paste. 20 °C isothermal conditions. Schematic diagram [3]

## 2.3 Restraint

Volume changes in young concrete combined with some kind of restraint will cause stresses to develop. This may again lead to cracking

### 2.3.1 Internal restraint

Internal restraint is a phenomenon that occurs when the surfaces of a young concrete structure are exposed to ambient temperature, and is due to temperature gradients over the concrete cross section and compatibility requirements as the "Navier-Bernoulli hypothesis". The surfaces that are exposed to air will cool down quickly, while the core will keep the heat for a longer amount of time. This temperature difference will lead to various expansions in the structure and will cause tension that may result in cracks. Surface cracks due to internal restraint, however, tend to be on self-closing, as the core with time obtains the same temperature as its surroundings, thereby eliminating the temperature gradient [9]. Though it, nonetheless, can be unfortunate with "initial" damage serving as weak point during later climate exposure.

### 2.3.2 External restraint

An example of external restraint is casting joints to stiff adjacent structural components as older cast elements or solid rock. The concrete will during the hardening phase expand due to heat; this is possible because the concrete has not developed much strength yet. As the structural component hardens, the stiffness and restraint will increase. When it in the cooling phase contracts and it has achieved a higher Young's modulus, the restraint from the stiff adjoining

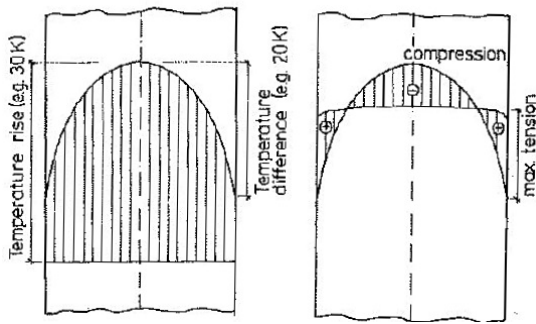


Figure 2.4: Temperature gradients and stress due to internal restraint[3]

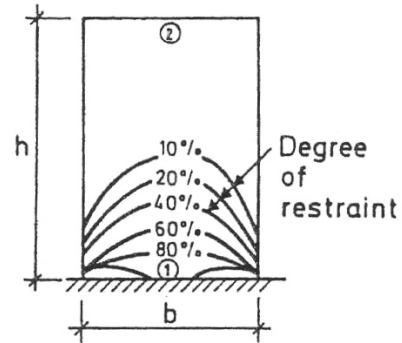
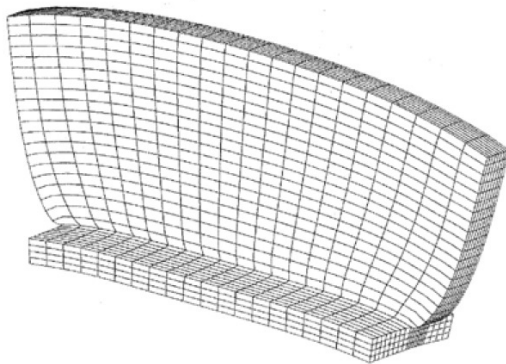
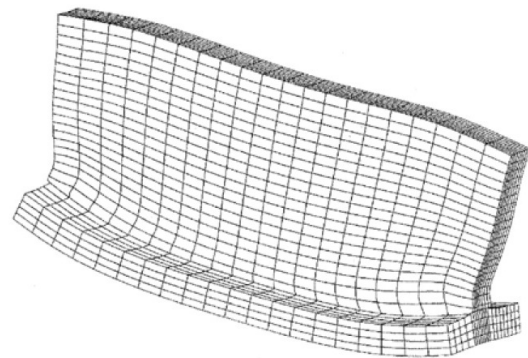


Figure 2.5: Degree of external restraint decreases with the distance from joint[2]

structure will result in mainly longitudinal stress in the concrete. The stress that arises might again lead to cracks in typically 1-2 weeks after casting. Unless the concrete has reached sufficient tensile strength it will get "trough-cracks", i.e. transverse cracks that span through the entire cross section. It is common that cracks are close to the joint, where the combination of restraint and temperature gradients are the most unfavourable, according to Jonasson [11] the critical position is about 0.7 wall width above the construction joint. The crack will then develop vertically in both directions during further cooling.



(a) Deformation at maximum wall temperature



(b) Deformation after the end of the cooling phase

Figure 2.6: Wall on slab from a FEM-analysis[3]

The degree of external restraint in a hardening concrete wall depends on the following issues [3]:

- The geometry of the structure (the L/H-ratio) influences the stress distribution over the height and over the length. High L/H-ratio give larger areas with high degree of restraint and possible cracking may occur over a larger portion of the wall.
- Stiffness (E-modulus and cross-section area) of the restraining structure has significant influence.

- Joint-end slip failure decreases the degree of restraint, but is difficult to model and generally not included in analysis. However, some simulation programs may take this effect into account.
- The flexibility and stiffness of the ground (for wall on slab).

## 2.4 Stress development

### 2.4.1 General

It is thus restrained volume changes combined with the development of Young's modulus which is the reason for the tensile stress that may cause cracking. The easiest way to describe this is by Hook's law:

$$\sigma = E\varepsilon \quad (2.10)$$

$\sigma$  = stress[MPa]

$E$  = Young's modulus[MPa]

$\varepsilon$  = strain [-]

FEM-calculation software computes temperature and stress development over time. These programs identify critical positions in the structure, based on material properties, structural design and ambient service conditions. Thermal dilation and autogenous shrinkage are the driving forces, while the other parameters can in simplification be called "response". Figure 2.7 shows the major factors for early age cracking.

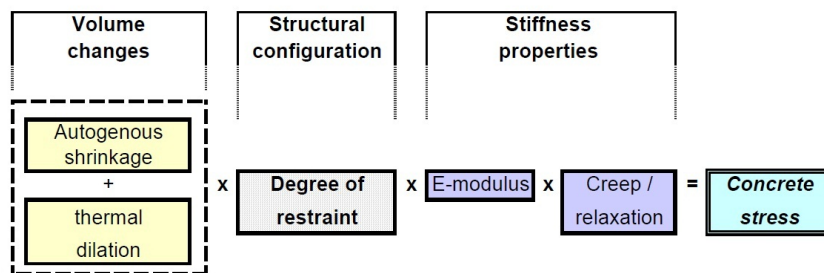


Figure 2.7: Stress development during the hardening phase – schematic diagram[3]

### 2.4.2 Material models

Most of the parameters in Figure 2.7 have been mentioned in the earlier subsections, while the concrete viscoelastic properties (stiffness properties) will be further discussed in the next chapter.

Concrete creep and relaxation properties determine the ability to reduce stress over time. A "soft" concrete, i.e. with low Young's modulus and/or high relaxation capacity, is beneficial in the sense that the tension is relative low for a given retained deformation. Kanstad et al. [12] have based on a general shape function proposed three property development equations, Equation 2.11, 2.12 and 2.13.  $s$  and  $n$  are curve fitting parameters. The parameter  $t_0$  ensures consistent coupling between the different mechanical properties and between the hydration heat and strength development.

$$f_c(t_e) = f_{c28} \cdot \exp \left[ s \left( 1 - \sqrt{\frac{28}{\frac{t_e}{24} - \frac{t_0}{24}}} \right) \right] \quad (2.11)$$

$$f_t(t_e) = f_{t28} \cdot \left\{ \exp \left[ s \left( 1 - \sqrt{\frac{28}{\frac{t_e}{24} - \frac{t_0}{24}}} \right) \right] \right\}^{n_t} \quad (2.12)$$

$$E_c(t_e) = E_{c28} \cdot \left\{ \exp \left[ s \left( 1 - \sqrt{\frac{28}{\frac{t_e}{24} - \frac{t_0}{24}}} \right) \right] \right\}^{n_E} \quad (2.13)$$

The relative development of the E-modulus is faster than the tensile strength, and even slower is the compressive strength development. This is principally unfortunate, and generally means that the concrete can develop tensile stresses before it is able to withstand them. A graphical representation of these mechanical properties is shown in Figure 2.8.

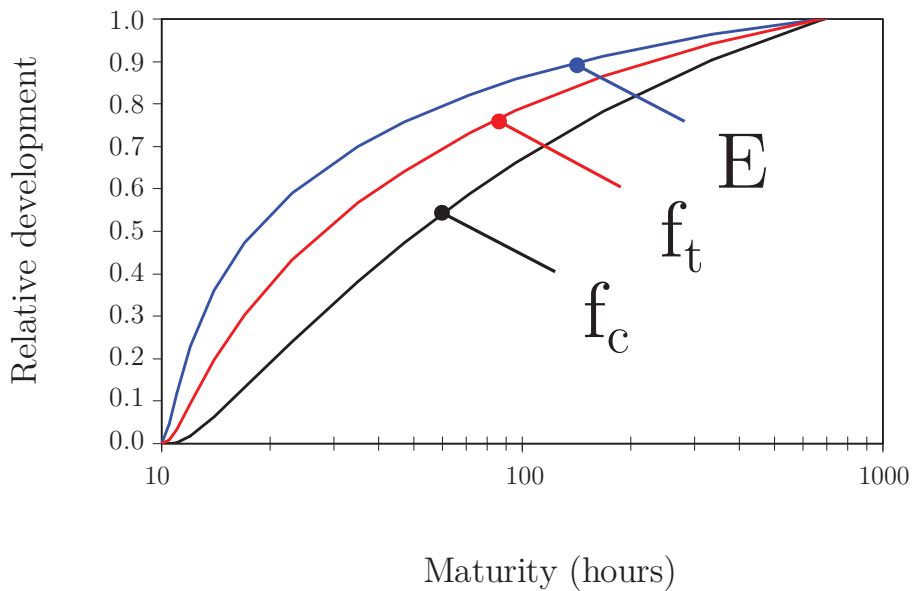


Figure 2.8: Relative development of Young's modulus ( $E$ ), tensile strength ( $f_t$ ), and compressive strength ( $f_c$ ). All properties are 1.0 at 28 days (672 h). The curves are based on experimental data[3].

### 2.4.3 Crack index

The risk of cracks can now be expressed as the time-dependent relationship between the generated stress and developed concrete tensile strength. This ratio is called "the crack index" [3],  $C_i(t)$ , or relative stress, see Equation 2.14:

$$C_i(t) = \frac{\sigma(t)}{f_t(t)} \quad (2.14)$$

The crack index is highest some time into the cooling phase. A calculated crack index of 1.0 or higher indicates that cracking will occur. Figure 2.9 shows a typical diagram of stress development and strength development during the hardening phase. In the thermal phase tensile stresses are avoided partly due to chemical contraction, so it is in the cooling phase the concrete is most likely to fracture. Because of computational uncertainties and the fact that several factors can vary considerably from laboratory to construction site, the crack index is in practice usually limited to be below 0.7 to be sure to avoid cracks. In this case, Figure 2.9, cracks are prevented in theory, but will exceed a crack index of 0.7. The crack index presented as a part of the design documentation should be the average crack index through a cross section [11].

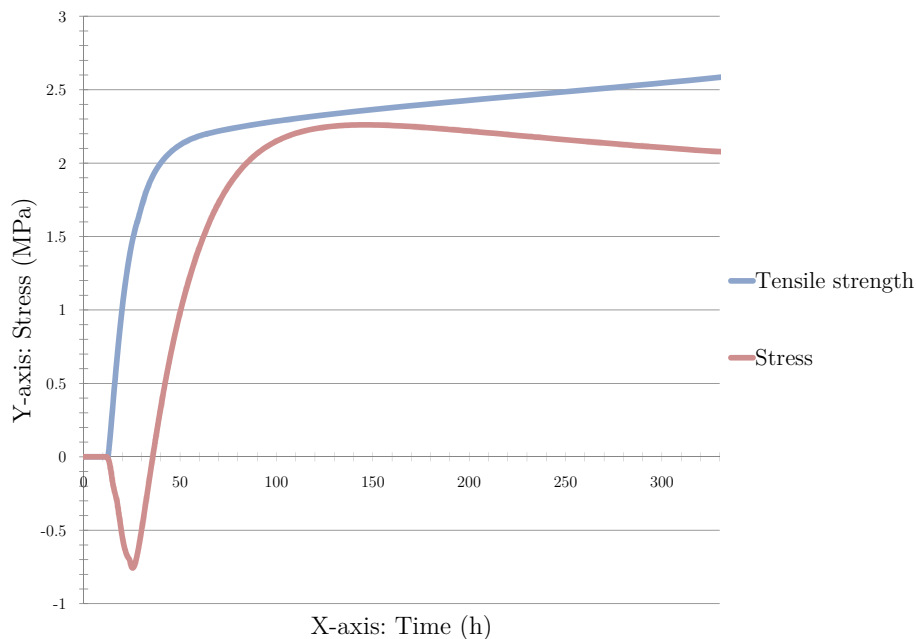


Figure 2.9: Stress and strength development during the hardening phase because of external restraint

## 2.5 Input to simulation programs

Input data for the analysis of stresses are generated by a number of assorted laboratory experiments. Only the measurements of curing heat can in practice be done on site. This is also the

parameter which, together with the concrete tensile strength, has the greatest impact on the analysis results. All experience show that heat generation can vary between different concrete truck deliveries, and should be tested regularly. Calculations are done with the finite element method and made on the basis of input parameters shown in Figure 2.10.

Figure 2.10 shows the "flow" of the computer program CrackTeSt COIN and factors influencing the formation of cracks during hardening. The avoidance of cracks can be divided into the following areas [13]:

- Structural design
  - Reducing restraining
- Material choices
  - Type of cement
  - Concrete recipe
  - Concrete temperature at casting
- Measures on site
  - Cooling of newly cast structure
  - Heating of adjacent structure
  - Thermal insulation

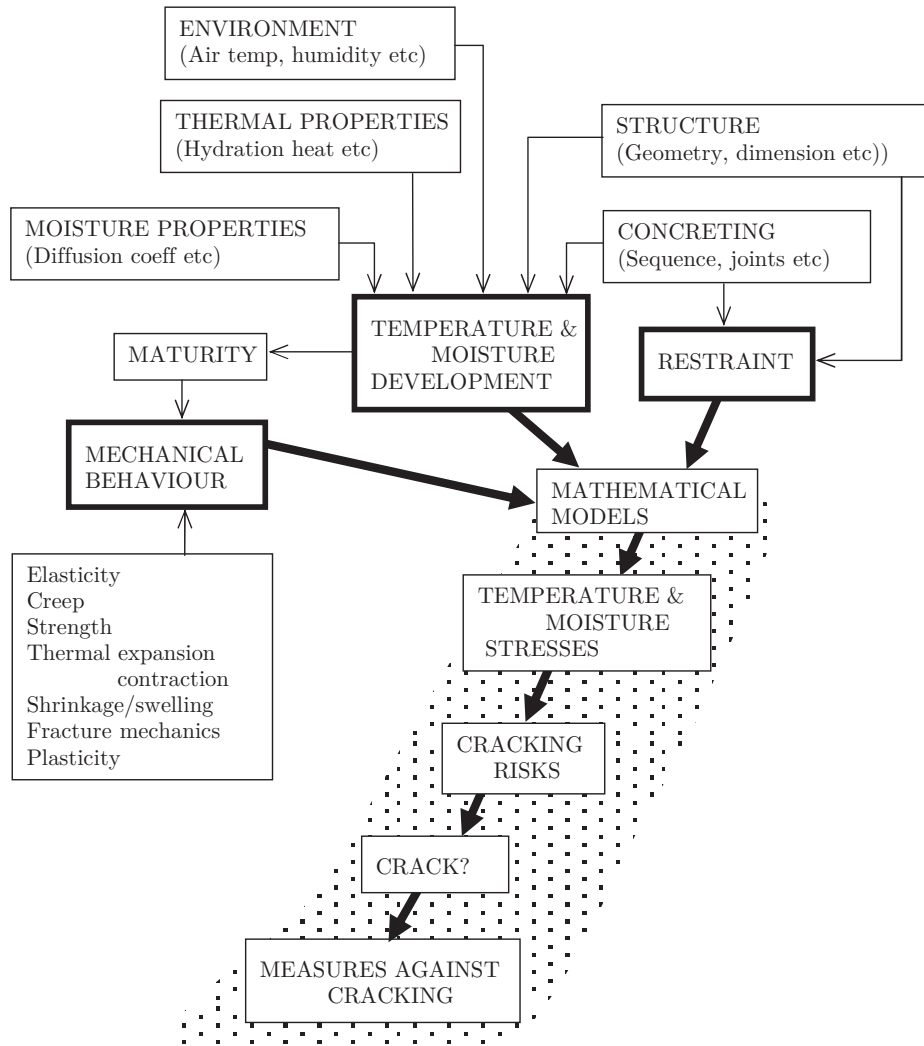


Figure 2.10: Factors influencing the formation of cracks in hardening concrete[13]

## Chapter 3

# Difference in Mathematical Models of Young Concrete Behaviour

### 3.1 Basis

This chapter will present different theories used in the simulation software, with focus on CrackTeSt COIN. A comparison between the two programs "CrackTeSt COIN" and "4C Temp&Stress" based on their use of different theories and equations will be given. The results from "4C Temp&Stress" are taken from an internal report [14] worked out by O. B. Skjølvik for Skanska, while all the results from "CrackTeSt COIN" are first computed by Skjølvik and then recomputed in this study.

Three different concrete mixtures have been applied to compare the two simulation programs. The structure used is shown in Figure 3.1. Because the programs rely on different theories they also need different input data. The parameters are as good as possible adjusted so that they provide virtually the same input data to the two programs. One can therefore assume that boundary conditions are equal, see Table 3.1 and 3.2. The three concretes used were:

- Traditional structural concrete (CEM I), from now on referred to as "TSC".
- Semi low-heat concrete (CEM II/A-V with 20 % fly-ash), from now on referred to as "20 %FA".
- Low-heat concrete (40 % fly-ash), from now on referred to as "40 %FA".

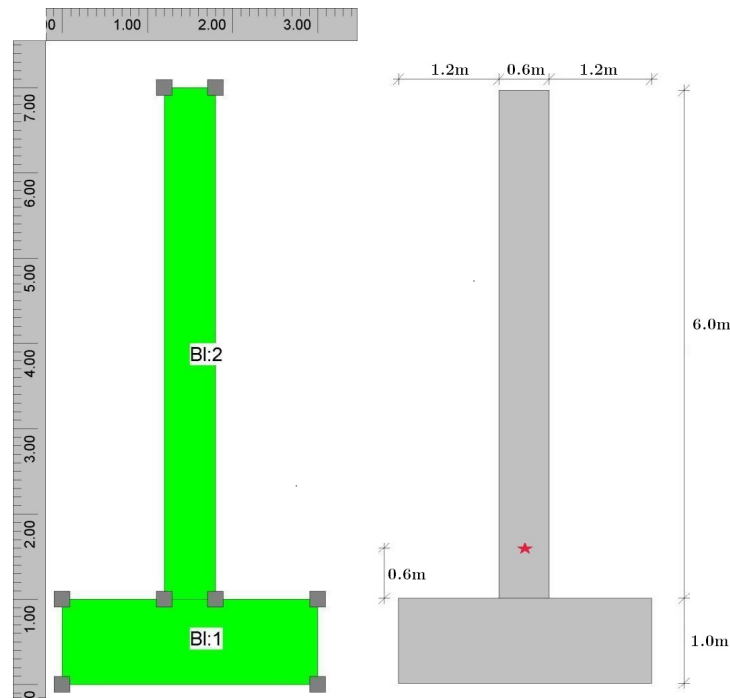


Figure 3.1: Measurements for wall on slab. The left drawing shows how the structure looks in "CrackTeSt COIN" and the star shows where the results are gathered.

Table 3.1: Structure used in analyses

	Wall	Foundation	Air	Ground
Concrete	Fresh	Hardened	-	-
Measurements	$0.6 \times 6$ m	$1 \times 13$ m	-	-
Temperature	$20$ °C	$10$ °C	$5$ °C	$5$ °C
Wind	-	-	$1$ m/s	-

Table 3.2: Transmission coefficients

	CrackTeSt COIN [ $W/K \cdot m^2$ ]	4C Temp&Stress [ $kJ/m^2 \cdot h \cdot ^\circ C$ ]
Free surface	9.46	24.06
Form work 0-24 h	3.82	13.74
Form work 24-672 h	9.46	34.05
Ground	900	3240

## 3.2 Heat

### 3.2.1 General

While "4C temp and Stress" is using the Danish model (2.8) for the heat computation, "CrackTeSt COIN" is using the Swedish model (2.9), with a small simplification setting  $\lambda_1 = 1$ . Equation 3.2 is a maturity time function similar to Equation 2.2, with parameters regarding starting time and size.

$$Q(t_e) = C \cdot W_\infty \cdot \exp \left[ -\ln \left( 1 + \frac{t_e}{t_1} \right) \right]^{-\kappa_1} \quad (3.1)$$

$$t_e = t_{e0} + \beta_D \int \beta_T dt \quad (3.2)$$

where:

$Q(t_e)$  = the heat generation as a function of maturity time [J/kg]

$C$  = cement content [kg/m<sup>3</sup>]

$W_\infty$  = the final heat generation after "infinite" time [J/kg]

$\beta_D$  = curve fitting parameter (should typically be =1) [days]

$\beta_T$  = time [days]

$t_{e0}$  = equivalent time at the start of assessment, for postponed cast (should typically be =0) [days]

$t_1$  = curve fitting parameter to make the formula dimension less [days]

$\kappa_1$  = curve fitting parameters

### 3.2.2 Results

The two different models, the Swedish (3.1) and the Danish (2.8) shall in principle not give any major differences in temperature development which corresponds well with the graphs in Figure 3.2, 3.3 and 3.4. The results, which are calculated temperatures for the wall shown in Figure 3.1, show that the Danish model has a tendency to react a bit slower than the Swedish one, but these differences are not significant. The calculated maximum temperatures are quite close and the differences will not have significant influence on the calculated stresses. The parameters used in the models are found by curve fitting to the same discrete data, thus only minor differences are expected to occur.

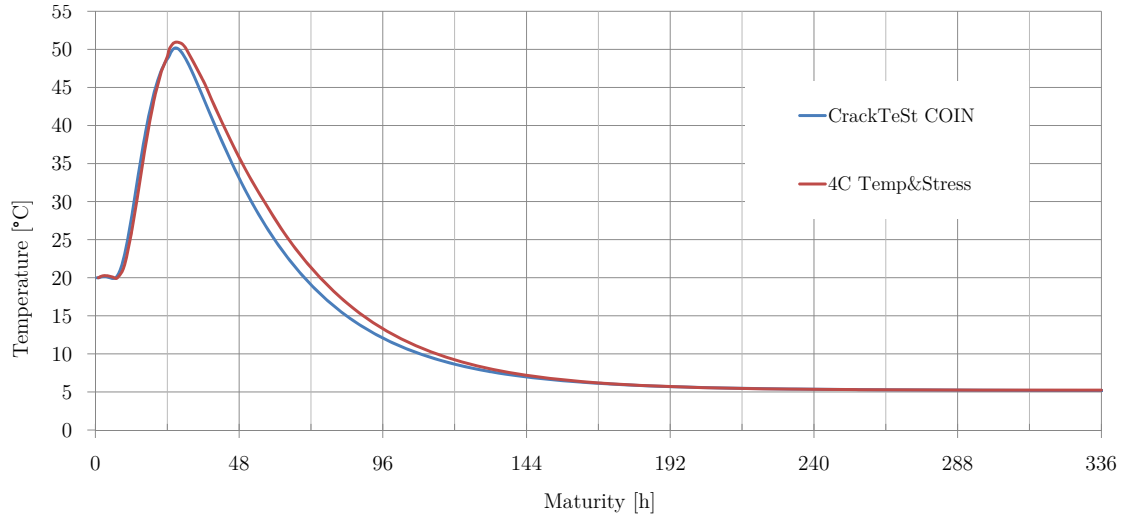


Figure 3.2: Temperature development versus maturity for traditional structural concrete (TSC)

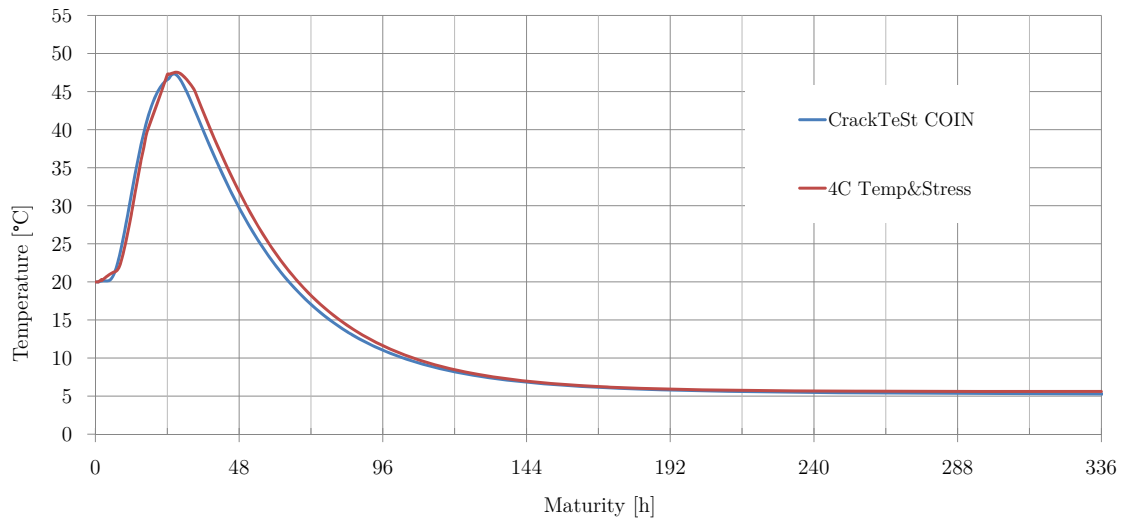


Figure 3.3: Temperature development versus Maturity for FA20 concrete

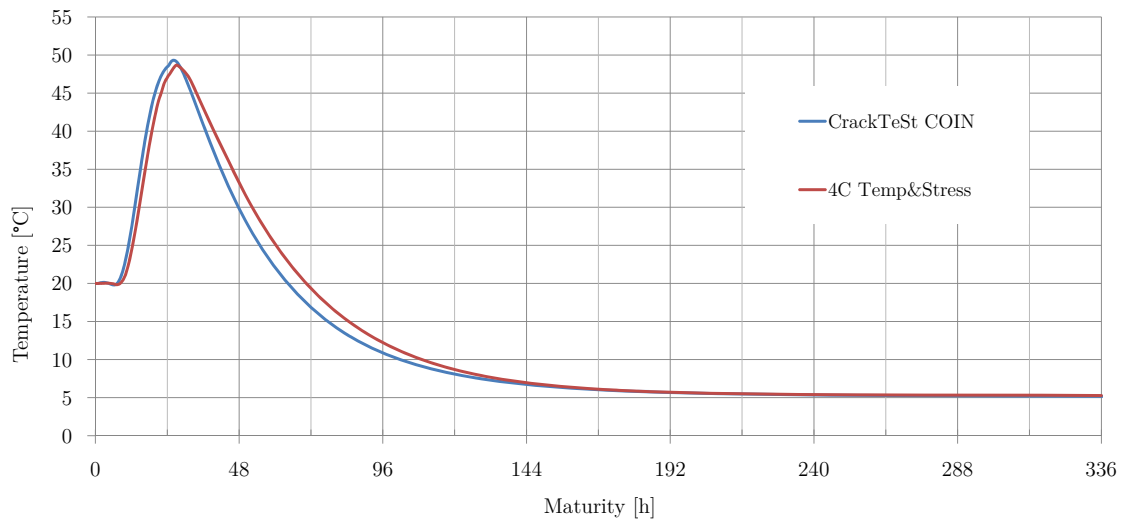


Figure 3.4: Temperature development versus Maturity for FA40 concrete

### 3.3 Strength development

#### 3.3.1 General

The computer program "CrackTeSt COIN" uses the same equation as mentioned in Subsection 2.4.2, apart from that it adjusts the values at the beginning to avoid numerical problems. The program uses 3 equations (3.3)[15]<sup>1</sup>. The first sets the strength equal to zero until a chosen start time  $t_S$ , while the second ensures a smooth transition between the zero function and the main feature, from  $t_S$  to  $t_A$ . The  $n_{cc,28}$  and  $s$  in the third equations are curve fitting parameters and have the same effect, that's why  $n_{cc,28}$  (3.3) should be set equal to one for the compression strength function. In this way one can find the  $s$  that will be used in Equations 2.12 and 2.13 and then later adjust  $n_t$  and  $n_E$  for the particular equation.

$$f_{cc}^{ref} = \begin{cases} 0 & \text{for } 0 \leq t_{eT} < t_S \\ \left(\frac{t_{eT}-t_S}{t_A-t_S}\right)^{n_A} \cdot f_A & \text{for } t_S \leq t_{eT} < t_A \\ \exp\left(s \left[1 - \left(\frac{672h-t^*}{t_{eT}-t^*}\right)^{n_{cc,28}}\right]\right) \cdot f_{cc,28} & \text{for } t_{eT} \geq t_A \end{cases} \quad (3.3)$$

where  $f_{cc,28d}$ [MPa],  $s$  [-],  $n_{cc,28d}$ [-],  $t_s$ [h],  $t_A$ [h],  $f_A$ [MPa] and  $n_A$ [-] are parameters that are determined from experiments. In this case the time is given in maturity days.

$$f_{cc}^{ref}(t_A) = f_A \quad (3.4)$$

$$t^* = \frac{672 - \delta_c \cdot t_A}{1 - \delta_c} \quad (3.5)$$

$$\delta_c = \left[1 - \frac{\ln(f_A/f_{cc,28d})}{s}\right]^{\frac{1}{n_{cc,28d}}} \quad (3.6)$$

#### 3.3.2 Results

In addition to the initial conditions, are "CrackTeSt COIN" and "4C Temp and Stress" using slightly different models for strength development. It is therefore in this case the first adapted a strength development function for "CrackTeSt COIN", according to equation 2. Then there are selected discrete values from this function which then is used in "4C Temp and Stress". It uses linear regression between the discrete points as strength development in its simulations. Figure 3.5, 3.6 and 3.7 shows the development of tensile strength, which as assumed are similar. As mentioned earlier in the chapter, all results displayed here are recomputed and equal to

<sup>1</sup>It is uncertainties regarding Equation 3.3, which was sent over from one of the "CrackTeSt COIN" creators, Jonasson, since it is not identical to Equation 2.11. This has no effect on the calculations as long as  $n_{cc,28} = 1$

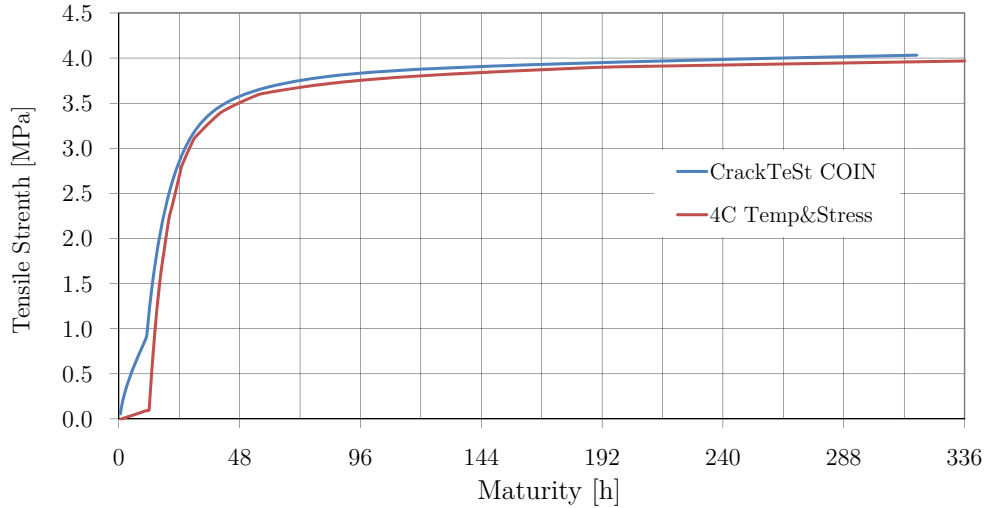


Figure 3.5: Tensile strength development, TSC

Skjølsvik's Skanska rapport [14]. Some improvements of the simulations in "CrackTeSt COIN" will therefore be proposed.

The major difference appears the first 24 hours. An important matter is "CrackTeSt COIN's" relatively steep progression from the starting point. This is due to the transition curve, between  $t_S$  and  $t_A$ , in Equation 3.3. The ideal case is a strength development of zero until  $t_0$ . In order to settle a more correct strength development the first 24 hours, the choice of  $t_S$  and  $t_A$  is essential. By choosing a  $t_S$  and a  $t_A$  that don't differ too much from  $t_0$ , a more correct development the first hours after casting will be obtained.. One could typically choose a  $t_S$  half an hour lower than  $t_0$  and a  $t_A$  half an hour greater than  $t_0$ . "4C temp and Stress" uses a different approach to  $t_0$  where the program assumes a moderate linear increase until the actual strength development function proceeds.

The differences that occur after passing 24 hours are minor and may be due to small differences in input parameters and differences in the simulation programs' choice of elements or similar.

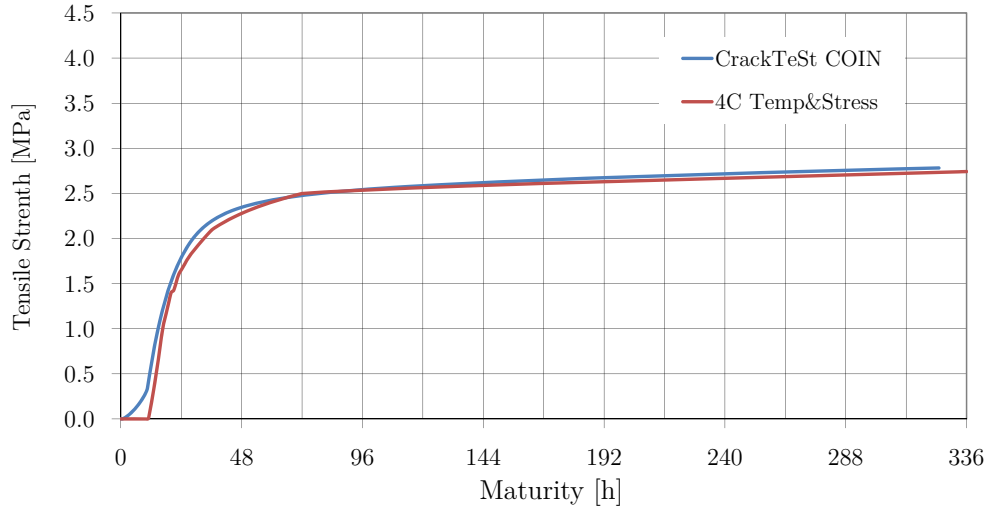


Figure 3.6: Tensile strength development, FA20

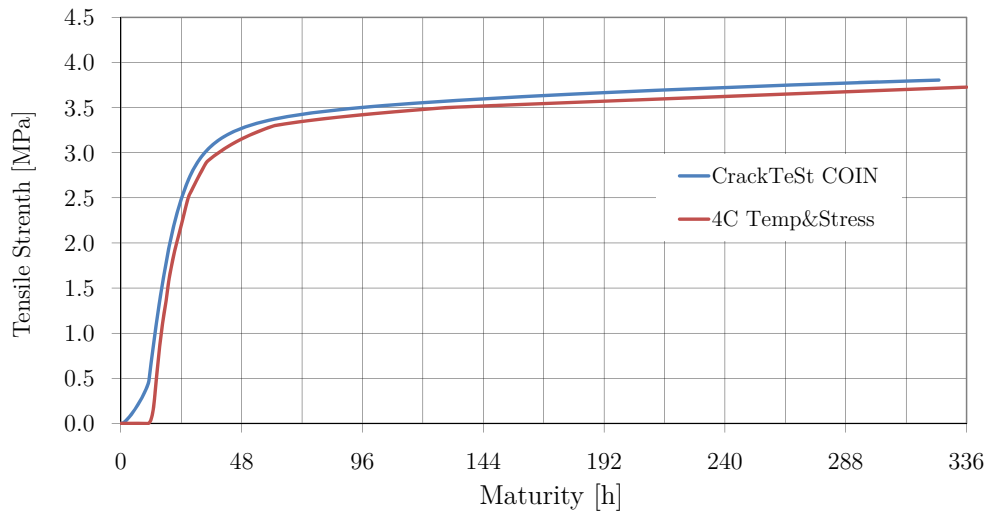


Figure 3.7: Tensile strength development, FA40

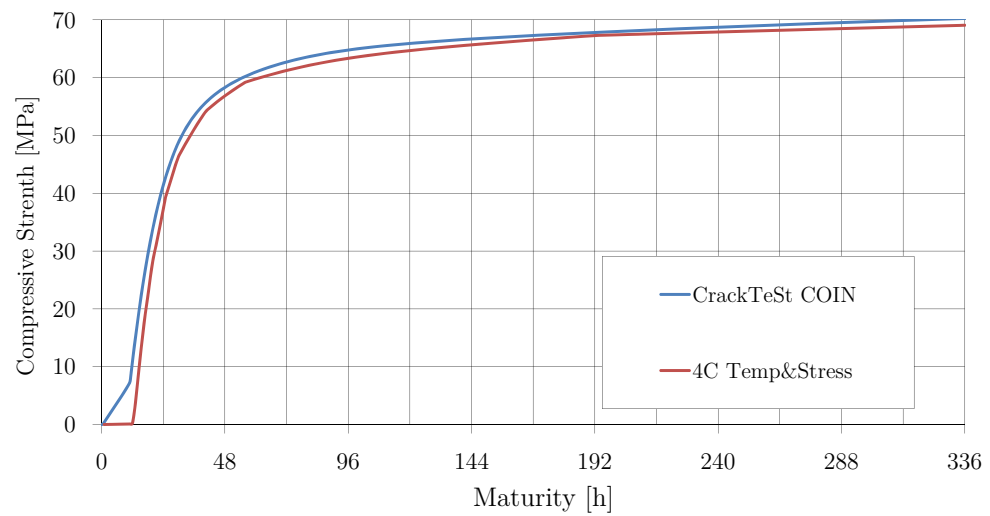


Figure 3.8: Compressive strength development, TSC

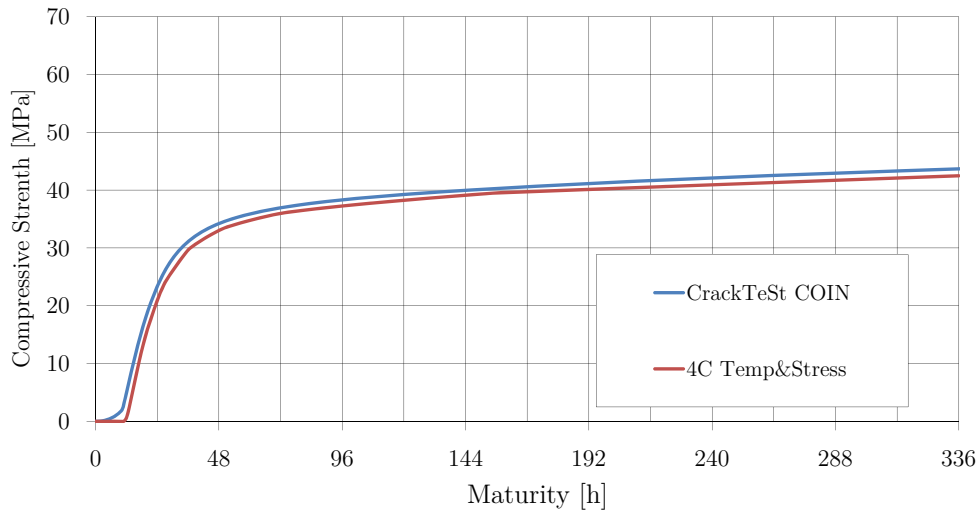


Figure 3.9: Compressive strength development, FA20

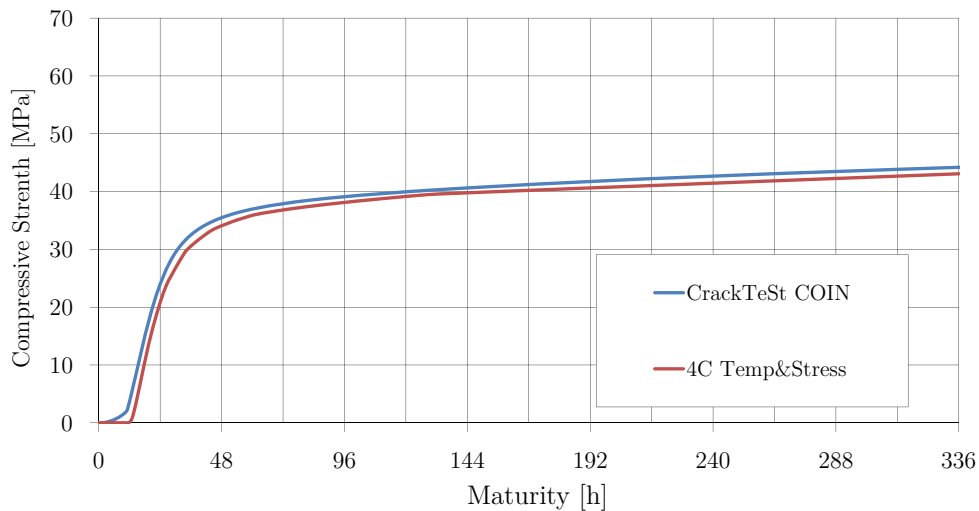


Figure 3.10: Compressive strength development, FA40

Figure 3.8, 3.9 and 3.10 show the same results that have been commented in the previous paragraphs, but here for compressive strength. As for the tensile strength, one can see that the differences for the strength development are most significant the first 24 hours for the strength development, and otherwise also come to the same conclusion.

One can, by the way, also notice that the concrete with fly ash has a much greater tensile strength - compressive strength ratio than the one without, due to the slow hydration process, and the shape of the equations.

### 3.4 Creep

In this section creep due to thermal stresses will be explored, as well as comparing different creep models used in computer software.

### 3.4.1 Linear viscoelasticity for ageing materials

Concrete exhibits time-dependent behaviour like basic creep, drying creep, creep recovery and stress relaxation. These effects have been attempted described for many years, e.g. Boltzmann came up with a theory for isotropic viscoelasticity already in the 1870s. The fact that concrete has a viscoelastic behaviour means that the strain due to creep is assumed proportional to the corresponding stress. When young concrete is subjected to loading, it will deform instantly. Creep is defined as the time-dependent deformation due to applied stress history, whereas relaxation is defined as stress development due to applied strain history. It is difficult to detect the division between creep and relaxation outside diagnostic labs, so in everyday use creep is often used as a generic term about both phenomena.

Several factors contribute to determine the creep deformations, a list of external and internal factors follows:

- Internal
  - cement type
  - w/c-ratio
  - aggregate
  
- External
  - duration and size of the load
  - type of load (tension/compression)
  - age of concrete when loading
  - relative humidity and relative humidity variation
  - temperature and temperature variation

### 3.4.2 Maxwell model

There are many mechanical linear viscoelastic models which can be used for concrete, for instance those shown in Figure 3.11. They are made of linear springs and linear viscous dashpots, inertia effects are neglected. The spring model may be expressed like in Equation 3.7, where  $K$  can be interpreted as a linear spring constant or a Young's modulus.

$$\sigma = K \cdot \varepsilon \quad (3.7)$$

$$\sigma = \eta \frac{d\varepsilon}{dt} \quad (3.8)$$

For the dashpot element the constant  $\eta$  is called the coefficient of viscosity [16], and in this model the strain rate  $\dot{\varepsilon}$  is proportional to the stress, or in other words the dashpot will be deformed at a constant rate when it is subjected to constant stress. At the instant moment a constant strain is imposed to the dashpot elements, the stress will be infinite and will thereafter rapidly decrease to zero. An infinite stress is impossible in reality, thus finite deformation can not be imposed instantaneously to the dashpot.

One of the most known models of this kind is the Maxwell model. It is a two element model that consists of one linear spring and one linear viscous dashpot connected in series as shown in Figure 3.11(a). Adding the time derivative of [3.7] with [3.8] ( $\dot{\varepsilon} = \dot{\varepsilon}_{Spring} + \dot{\varepsilon}_{Dashpot}$ ) one can obtain the stress-strain rate differential equation 3.9 [16]. By solving the differential equation and applying a constant stress  $\sigma = \sigma_0$  at  $t = 0$  (3.9) becomes a first order differential equation of  $\varepsilon(t)$ . Equation 3.10 shows the Maxwell models creep equation for linear material behaviour, where  $J(t) = \varepsilon(t)/\sigma_0$ . The function  $J(t)$  is often called the "creep compliance" and is the creep strain per unit of applied stress. Important to point out is that (3.10) and (3.11) only apply if  $K$  and  $\eta$  are constants.

$$\sigma + \frac{\eta}{K}\dot{\sigma} = \eta\dot{\varepsilon} \quad (3.9)$$

$$J(t) = \frac{1}{K} + \frac{t}{\eta} \quad (3.10)$$

$$E(t) = Ke^{-Kt/\eta} \quad (3.11)$$

Relaxation modulus for linear material behaviour can be represented by  $E(t) = \sigma(t)/\varepsilon_0$ , the stress per unit applied strain, and is material dependent. Subjecting the Maxwell model to constant strain  $\varepsilon_0$  at time  $t = 0$  and integrating (3.9), the stress response  $\sigma(t)$  will be obtained and with that Equation 3.11.

### 3.4.3 Kelvin-Voigt model

The Kelvin-Voigt model is represented by the same two elements, but here in parallel. This results in adding up the stresses ( $\sigma = \sigma_{Spring} + \sigma_{Dashpot}$ ) from the dashpot and spring equations to get the differential equation, see (3.12). Under constant stress  $\sigma_0$  applied at  $t = 0$ , Kelvin-Voigt's creep compliance is as shown in Equation 3.13. A sudden applied stress on this model response is called delayed elasticity[16]. Where, at first, the viscous element  $\eta$  will take all the stress that was applied and then transfer larger and larger portions of the load to the elastic element  $K$ . Thus, finally the elastic element carries the entire stress.

The Kelvin-Voigt model does not exhibit time-independent strain on loading, or unloading, nor does it show a time-dependent relaxation. The relaxation equation 3.14 are obtained from the differential equation 3.12 by using Dirac delta function  $\delta(t)$  and Heaviside step function.

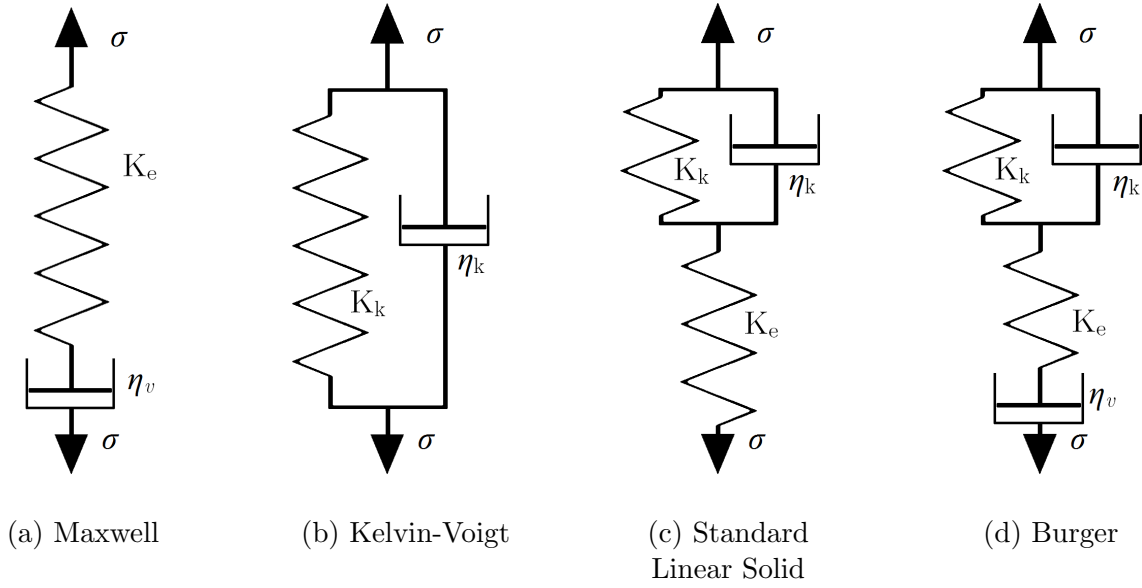


Figure 3.11: Mechanical models for viscoelasticity

$$\dot{\epsilon} + \frac{K}{\eta} \epsilon = \frac{\sigma}{\eta} \quad (3.12)$$

$$J(t) = \frac{1}{K} \cdot \left(1 - e^{-Kt/\eta}\right) \quad (3.13)$$

$$E(t) = K + \eta \delta(t) \quad (3.14)$$

Neither Maxwell nor Kelvin-Voigt models are capable of representing real material behaviour. Kelvin-Voigt does not exhibit instant elastic strain on loading, nor a permanent strain unloading. While Maxwell model is not able to show decreasing strain rate, which is characteristic for primary creep. None are able to show a rapid initial strain rate. This can to some degree be improved by adding more elements, like in the three element Standard linear solid model, Figure 3.11 (c) and the four element Burger model, Figure 3.11 (d).

### 3.4.4 Burger model - 4C Temp&Stress

The Burger model is a Maxwell and a Kelvin-Voigt model connected in series. The total strain will be the sum of a spring (3.7), a dashpot (3.8) and a Kelvin-Voigt (3.12) unit ( $\epsilon = \epsilon_{Spring} + \epsilon_{Dashpot} + \epsilon_{Kelvin-Voigt}$ ). Adding these three together results in the Burger model's differential Equation 3.15 [16]:

$$\sigma + \left(\frac{\eta_e}{E_e} + \frac{\eta_e}{E_k} + \frac{\eta_k}{E_k}\right) \dot{\sigma} + \frac{\eta_e \eta_k}{E_e E_k} \ddot{\sigma} = \eta_e \dot{\epsilon} + \frac{\eta_e \eta_k}{E_k} \ddot{\epsilon} \quad (3.15)$$

$$J(t, t_0) = \frac{1}{E_e} + \frac{1}{E_k} \left(1 - e^{-R_k(t-t_0)/\eta_k}\right) + \frac{t-t_0}{\eta_e} \quad (3.16)$$

$$E(t) = \frac{[(q_e - q_k r_e) e^{r_e t} - (q_e - q_k r_k) e^{-r_k t}]}{A} \quad (3.17)$$

where

$$r_e, r_k = \frac{\left(\frac{\eta_e}{E_e} + \frac{\eta_e}{E_k} + \frac{\eta_k}{E_k}\right) \mp A}{2 \frac{\eta_e \eta_k}{E_e E_k} A}$$

$$q_e = \eta_e$$

$$q_k = \frac{\eta_e \eta_k}{E_k}$$

$$A = \sqrt{\left(\frac{\eta_e}{E_e} + \frac{\eta_e}{E_k} + \frac{\eta_k}{E_k}\right)^2 - 4 \frac{\eta_e \eta_k}{E_e E_k}}$$

One of the disadvantages of the Burger model is the difficulties of adopting discrete data to fit the model. To do this it is necessary to set up a particular program, like they do in Denmark.

### 3.4.5 Double power law - RELAX

Input data on creep and relaxation in CrackTeSt COIN are done through a command prompt program called RELAX. Although command-line interpreters are rarely used and people don't like writing commands anymore, "RELAX" is basic and quite easy to use. Nonetheless, it would have been even easier for the user if the software producers, JEJMS, could have implemented "RELAX", or parts of it, into "CrackTeSt COIN". For the Norwegian version of "ConTeSt Pro", i.e. "CrackTeSt COIN", one only needs to add the part "RELAX" called "KTYPE=7", which is NTNU's request for creep and relaxation computation. "KTYPE=7 NTNU E-formula + Double power law", uses Equation 3.18 and 3.19 [17]:

$$J(t, t_0) = \frac{1}{E(t_0)} \cdot \left\{ 1 + \varphi_1 \left[ \left( \frac{t_0}{t_B} \right)^{-m} + \varsigma \right] \cdot \left[ \frac{t - t_0}{t_A} \right]^n \right\} \quad (3.18)$$

$$E(t_0) = E_{ref} \cdot \left\{ \exp \left[ s \cdot \left( 1 - \frac{1}{\sqrt{\frac{t_0 - t_s}{t_{ref} - t_s}}} \right) \right] \right\}^\kappa \quad (3.19)$$

where:

$E(t_0)$  = elastic modulus at age  $t_0$  [GPa]

$E_{ref}$  = elastic modulus at chosen reference age [GPa]

$t_0$  = load application [h]

$\varphi_1, \varsigma$  = material parameters [-]

$m, n$  = material parameters [-]

$$\begin{aligned}
 s, \kappa &= \text{parameters reflecting the time development of elastic modulus [-]} \\
 t_A, t_B &= \text{chosen reference time [h]}
 \end{aligned}$$

For describing the time shape of creep curves as well as their age dependence the "double power law" is a commonly used equation for basic creep. It is a simple creep function with only three parameters, the calculation is therefore quite easy without any numerical problems[4].

After running RELAX, the program creates six output files. These output files have different purposes, but they mainly contain tables of relaxation data to be used in Maxwell chain calculations. This data will then be input for "CrackTeSt COIN", "Diana" or similar programs with the need of relaxation data.

### 3.4.6 Maxwell chain model - CrackTeSt COIN

"CrackTeSt COIN" uses Maxwell chains in its calculations of relaxation, Equation 3.20. Maxwell chains are a series of parallel Maxwell models, consisting of a spring ( $E_\mu$ ) and a dashpot ( $\eta_\mu$ ) see Figure 3.12, and may be determined from a experimental relaxation curve. Every separate dash-pot is characterized by its retardation time ( $\tau_\mu$ ) according to [17]:

$$\tau_\mu = \frac{\eta_\mu}{E_\mu} \quad (3.20)$$

$$R(t, t_0) = \sum_{\mu=1}^N E_\mu(t_0) \exp \left[ -\frac{(t - t_0)}{\tau_\mu} \right] \quad (3.21)$$

If only creep curves are available, creep should be converted into relaxation. Because of the large number of degrees of freedom in this model small variations in data can cause large variations of the parameters. It is therefore important that  $\tau_\mu$  is chosen in advance and must cover the entire time of interest [4].

When using "RELAX" one can choose the number of decades in the time spans. Since the first relaxation time already is set by the program, the number of spring- and dashpot elements in the output file's Maxwell chain are one plus the number of decades chosen. This means that with use of default settings in "RELAX", the input to "CrackTeSt COIN" will contain eight spring- and dashpot elements. When a load is applied all Maxwell elements are active, but the contribution of each element decreases with time. In the end only the last element is operative [18]. For calculations of arbitrary loading age, interpolation between relaxation data is done for each spring- and dashpot element by assuming linearity in relaxation modulus by a logarithm in loading age.

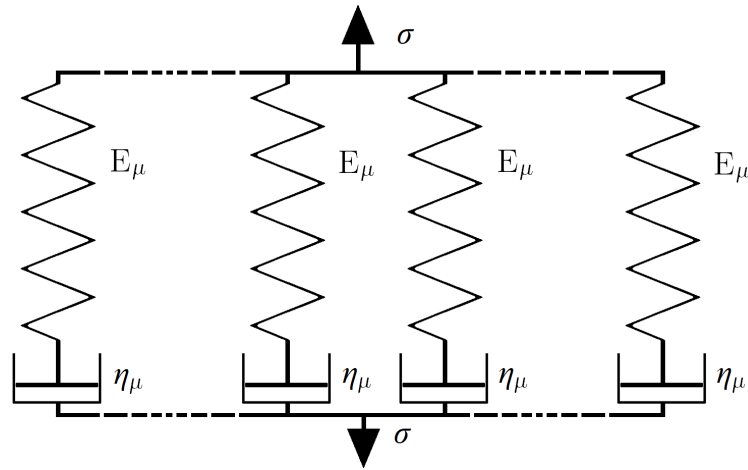


Figure 3.12: Maxwell chain model

## 3.5 Tensile stress and crack index

### 3.5.1 Stress development

Stress generation of hardening concrete is a very complex topic, since so many phenomena are involved. To simplify the calculation of stress, it is assumed that strain rate may be decomposed as follows [4], here also including cracking:

$$\dot{\epsilon} = \dot{\epsilon}_{elastic} + \dot{\epsilon}_{creep} + \dot{\epsilon}_{TD} + \dot{\epsilon}_{AS} + \dot{\epsilon}_{crack} \quad (3.22)$$

### 3.5.2 Results

The following stress development graphs will illustrate the difference between "CrackTeSt COIN" and "4C temp and Stress", and the theories behind them. Figure 3.13, 3.14 and 3.15 display the Tensile stress for the three concretes over the 336 first equivalent hours and all have the same tendency. The "4C Temp&Stress" curves seem to start later, but when first started they are steeper compared to the "CrackTeSt COIN" curves. The curves' maxima are also higher and occur earlier, and when the curves decrease the decline is significant. The "CrackTeSt COIN" tensile stress tends to stay high when the point of maximum is reached.

The difference between the two models is primarily due to the choice of creep models. "Double power law" is using superposition, and the parameters are obtained by fitting calculated strains to the experimental one using least square method. "Burgers model", on the other hand, obtains the strains using Equation 3.23 [4] to obtain the stress parameters. The two models also differ in their temperature dependence, where in "Burgers model's" Young's moduli and viscosities are made equivalent age dependent, this will effect in age dependent retardation time in the Kelvin-Voigt unit, i.e. ageing influences the rate of creep. While "Double power law" influences the creep through the instantaneous Young's modulus, keeping the creep function unchanged.

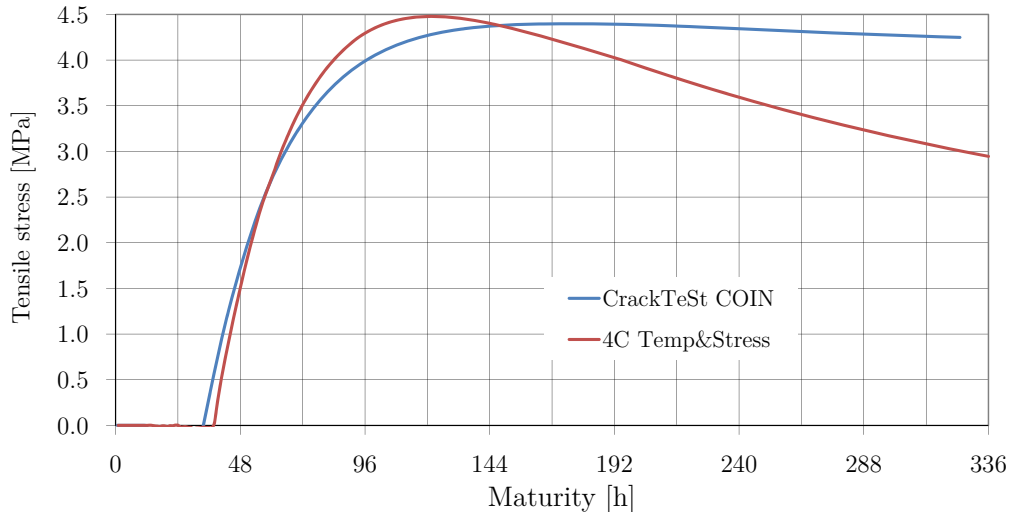


Figure 3.13: Tensile stress development, TSC

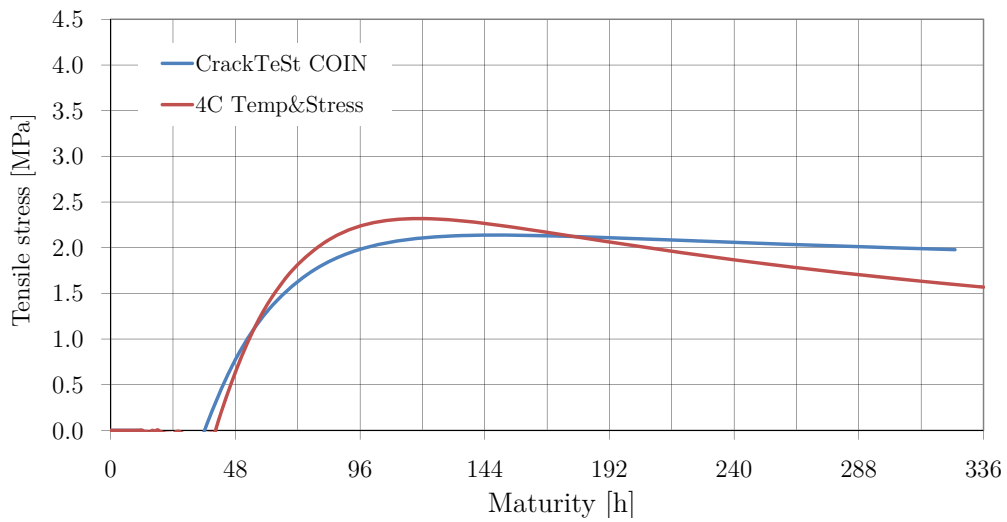


Figure 3.14: Tensile stress development, FA20

$$\dot{\varepsilon}_{creep} = \sum_{\mu=1}^2 \left( \frac{1}{\eta_{\mu}} \cdot \sigma - \frac{E_{\mu}}{\eta_{\mu}} \cdot \varepsilon_{\mu,creep} \right) \quad (3.23)$$

Similar to the compressive strength the tensile stress compared to the tensile strength also tend to be smaller for the concrete with fly ash. This will have quite an influence on the crack index.

The crack indexes in Figure 3.16, 3.17 and 3.18 are basically showing the same results as the stress cases. Also here the "Burger model" is higher in the beginning and lower in the end than stresses/crack indexes computed with "Double Power Law". Explained by "Burgers model" giving less creep in early age and higher after a while.

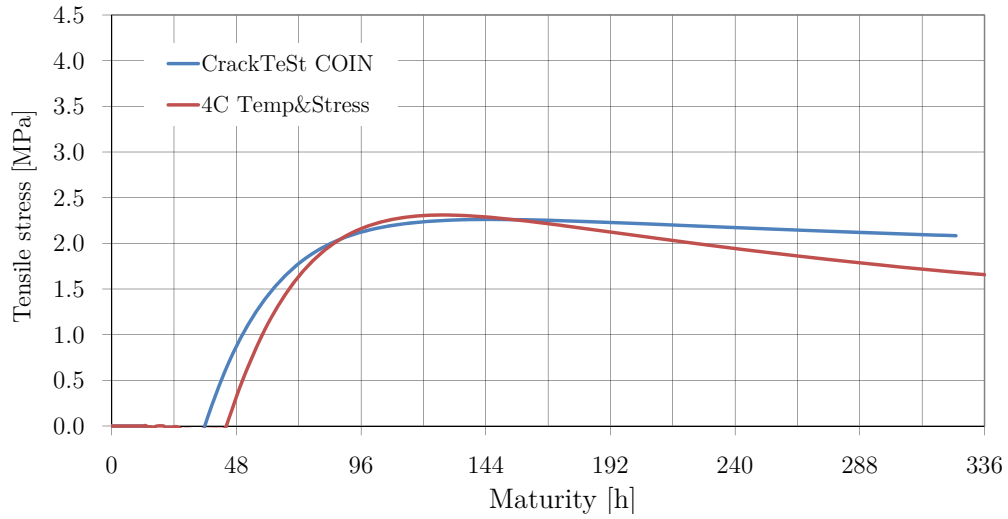


Figure 3.15: Tensile stress development, FA40

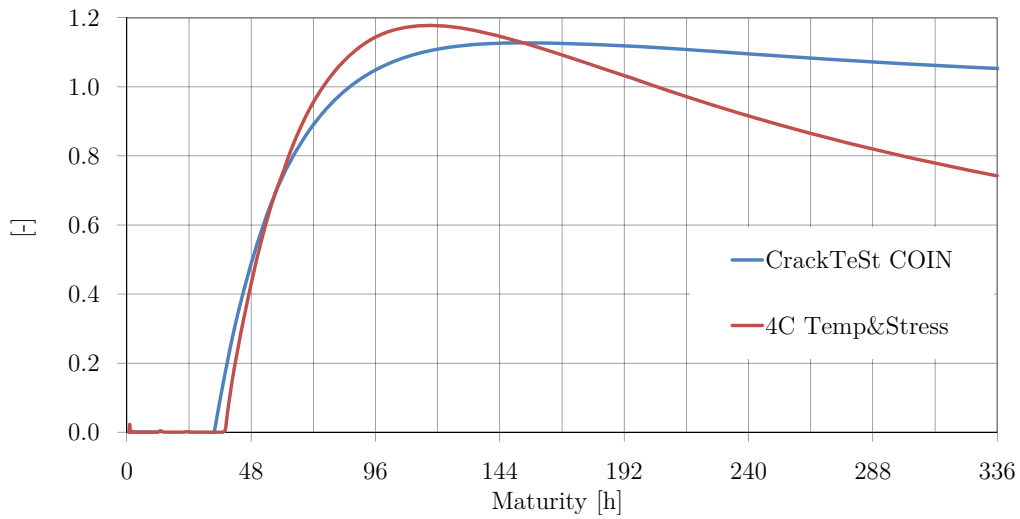


Figure 3.16: Crack Index as a function of maturity, TSC

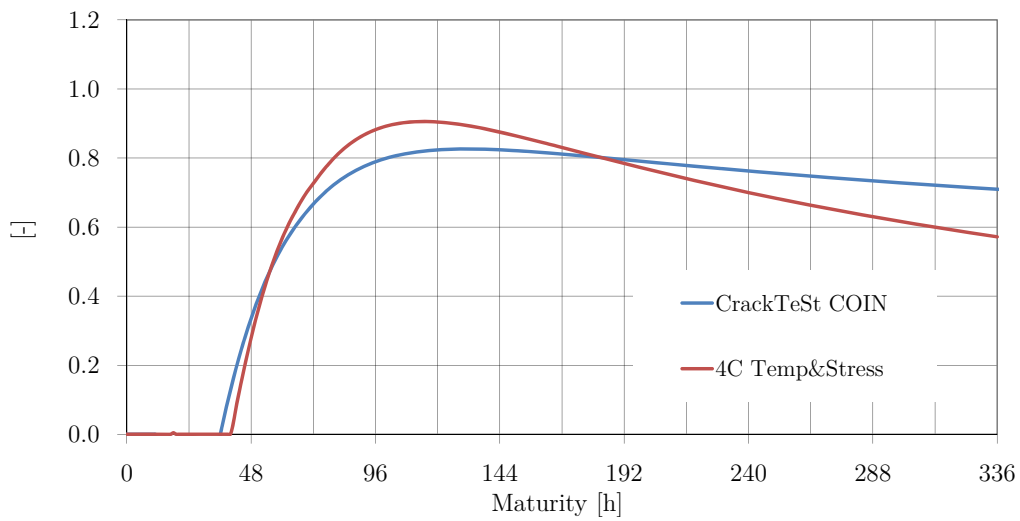


Figure 3.17: Crack Index as a function of maturity, FA20

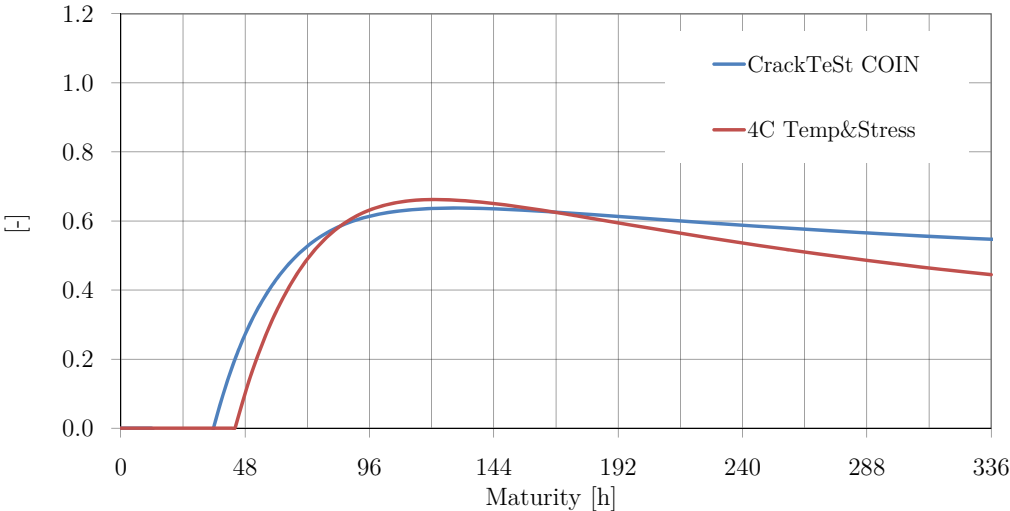


Figure 3.18: Crack Index as a function of maturity, FA40



# Chapter 4

## Material Properties

### 4.1 Boundary conditions and geometry

The object for this chapter is to provide a basis for the boundary conditions and material parameters used in the next chapters.

Material data will be computed for two concretes, a concrete with 50 % fly ash called "NCC" and one with 33 % fly ash called "Anlegg FA". They will both be simulated at two assorted boundary conditions to check the behaviour under various ambient conditions. The concretes will first be computed at an air temperature of  $-7\text{ }^{\circ}\text{C}$ , a ground and slab temperature of  $2\text{ }^{\circ}\text{C}$  and with a concrete temperature of  $13\text{ }^{\circ}\text{C}$  at cast. This is kind of a worst case scenario. Simulation will also be done with all temperatures, ambient and concrete, set to  $20\text{ }^{\circ}\text{C}$ .

The tunnel's exterior formwork is permanent, while the formwork inside is torn down after 72 hours. The roof, or upper surface, of the tunnel is in the simulations cast after 28 days and will not be discussed here. Convection values used in the calculations are found in Table 4.1. As Figure 4.1 shows the bottom plate is 1.2 meters thick, while the wall thickness is 1 meter. Abnormally high thermal conductivity parameters are selected for the ground. This is because the simulation program otherwise affects the ground temperature while the ground temperature should affect the concrete's temperature.

Table 4.1: Heat transfer coefficients

Convection values		The ground's heat properties	
72 h formwork	$4.12\text{ W/K m}^2$	Heat capacity	$449\text{ J/kg K}$
Permanent formwork	$0.412\text{ W/K m}^2$	Heat conductivity	$9000\text{ W/m K}$
Free surface	$12.5\text{ W/K m}^2$		
Moving boundary	$12.5\text{ W/K m}^2$		
Ground	$9 \cdot 10^8\text{ W/K m}^2$		

Before calculating the stress the user of "CrackTeSt COIN" can decide the impact of restraint, see Table 4.2. When setting the stress case one also have the option to include length to height

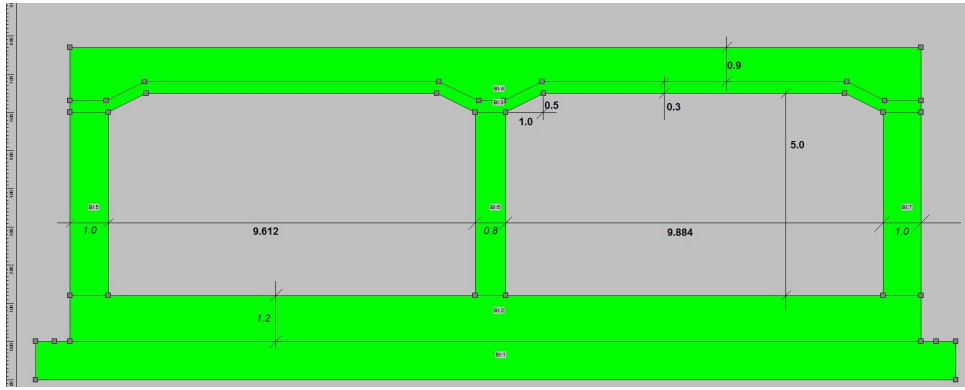


Figure 4.1: Cross section of the tunnel's geometry in "CrackTeSt COIN". With a lateral X-axis and vertical Y-axis.

ratio in the simulation, but since "CrackTeSt COIN" does its simulations in 2D and the tunnel is as long as 2.5 km, the section's length is not taken into account in the calculations in this thesis.

Table 4.2: Stress case: Degree of restraint

Restraint	
Translation	Free
Rotation around X-axis	Free
Rotation around Y-axis	Full

## 4.2 Compression strength development and activation energy

It has not been done a separate laboratory program for this thesis. Used property data were taken from SINTEFs' test reports [19, 20] for the two concretes actually used in the construction of Møllenberg tunnel. The reports include i.a. test of compressive strength at different occasions during the 28 first days where the concrete test blocks are stored at a constant temperature of 5 °C, 20 °C and 38 °C, see Appendix B and C.

The first thing done was to calculate the parameters  $f_{c28}$ ,  $t_0$  and  $s$  using the the reports' results from testing compressive strength of specimens stored at 20 °C. For both concretes the  $t_0$  was found by logarithmic extrapolation from the measured data and back to where the compression strength was zero. This method gave  $t_0$  as shown in Table 4.3. As a cross-check,  $t_0$  was recalculated with respect to heat measurements, based on NOR-CRACK report 3.2 [21]. Equation 4.1 indicates that  $t_0$  is found by locating the time where the heat production is 12 kJ and adding 2.6 hours, with a standard deviation of 0.6 hours. By running through the calculations with measured data from the respective concretes,  $t_0$  values were found to be 12.4 h for "NCC" and 7.9 h for "Anlegg FA". This confirmed that the results found by the extrapolation were sufficiently accurate, so there was no reason to change these. The  $s$  and  $f_{c28}$  parameter were found by model fitting, iterating using least square method, with Equation 2.11. Figure 4.2 displays

measured data for compressive strength and the material model with parameters according to Table 4.3.

$$t_0 = t_{Q=12 \text{ kJ}} + 2.6 \text{ h} \quad (\text{stdev}(t_0) = \pm 0.6 \text{ h}) \quad (4.1)$$

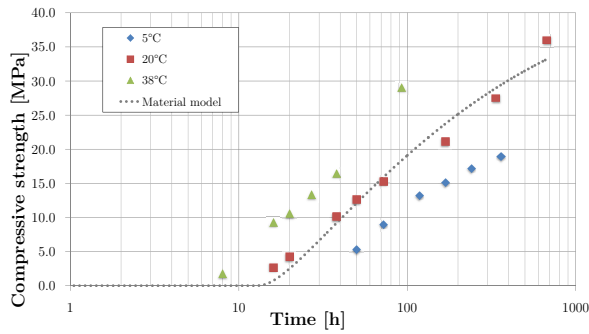
Table 4.3: Parameters for compression strength

NCC 50 % FA		Anlegg 33.3 % FA	
$f_{c28}$	33.27 MPa	$f_{c28}$	47.75 MPa
$t_0$	12.10 h	$t_0$	8.07 h
$s$	0.31	$s$	0.26

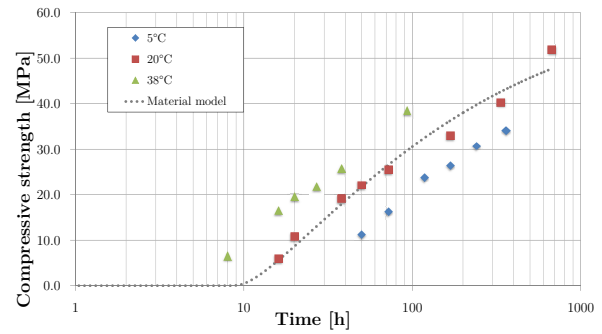
Activation energy is calculated by using the principle of same compressive strength should give the same maturity. This is done by adjusting the parameters  $A$  and  $B$  in  $E(\theta)$ , Equation 2.5, so that the compressive strength for various temperatures follow the same graph in terms of maturity, see subsection 2.2.2. Figure 4.2 shows the chart of measured compressive strengths and the adjusted material model for the two concretes, where Figure 4.3 illustrates the chart after calibration of activation energy. As for  $s$  and  $f_{c28}$ , the parameters  $A$  and  $B$  are found by iteration using the least square method based on measured data at different temperatures, see Table 4.4 for the results.

Table 4.4: Parameters for Activation Energy

NCC 50 % FA		Anlegg 33.3 % FA	
A	40 742 J/mol	A	33792 J/mol
B	273 J/mol °C	B	386 J/mol °C

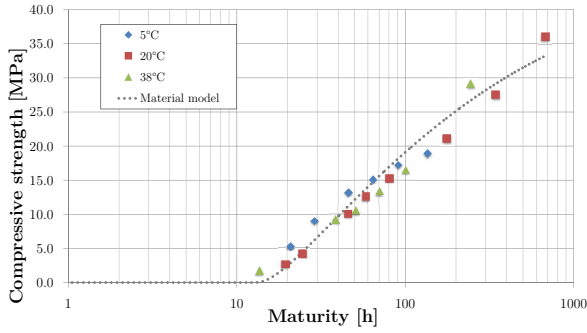


(a) NCC 50% FA

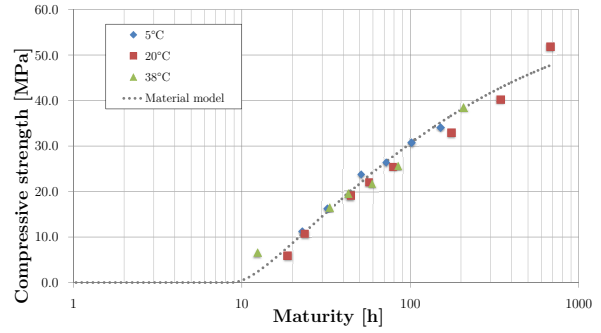


(b) Anlegg 33.3% FA

Figure 4.2: Compressive strength development before adjusting for activations energy



(a) NCC 50% FA



(b) Anlegg 33.3% FA

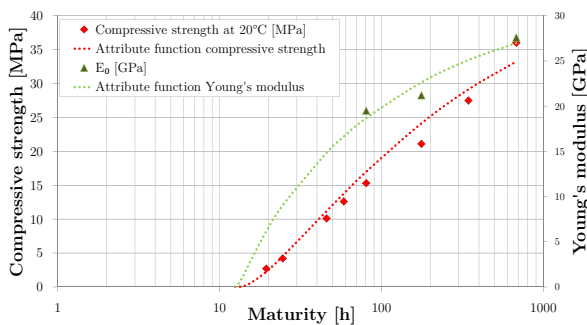
Figure 4.3: Compressive strength development after adjusting for activations energy

### 4.3 Young's modulus

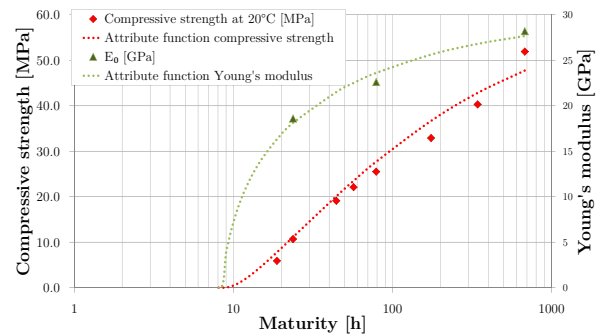
For calculation of Young's modulus, the same values for  $s$  and  $t$ , as were found in last section, were used. The procedure to find parameters  $n_E$  and  $E_0$  to match the characteristic function of Young's modulus is similar to the one used for the compressive strength. The experiments follow SINTEF internal procedures, and the results are found in the test reports [19, 20]. The samples are all concrete cylinders stored at a constant temperature of 20 °C. The points in Figure 4.4 show SINTEF's laboratory results against the attribute function, while Table 4.5 shows the corresponding parameters. Having just a few test data, like in this case, will imply a significant uncertainty in the fitted input data which may influence heavily on the final results.

Table 4.5: Parameters for Young's modulus

NCC 50 % FA		Anlegg 33.3 % FA	
$f_{t28}$	26.99 GPa	$f_{c28}$	27.66 GPa
$t_0$	12.10 h	$t_0$	8.07 h
$s$	0.31	$s$	0.26
$n_E$	0.55	$n_E$	0.29



(a) NCC 50 % FA



(b) Anlegg 33.3 % FA

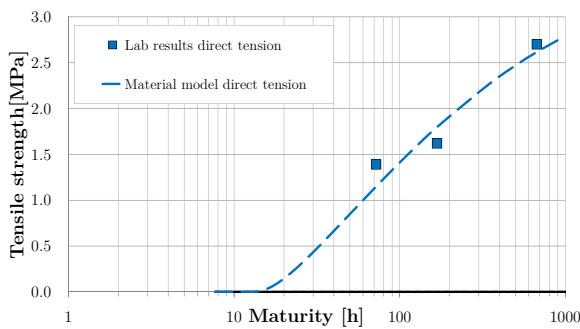
Figure 4.4: Development of Young's modulus and compressive strength with the matching adapted functions.

## 4.4 Tensile strength

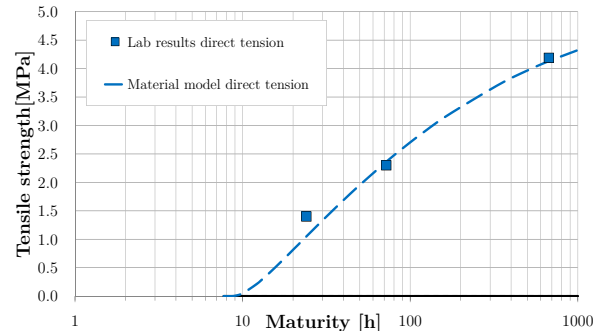
The tensile strength can be measured both by splitting or by direct tension tests. In this study the latter was used. Tensile strength is a very important parameter when it comes to the risk of cracking, since it is directly included in the definition of crack index. Similar to the approach applied to finding Young's modulus, the curve fitting for the tensile strength consist of three samples measured at three different points in time, which is shown in Figure 4.5. As for Young's modulus, the low number of test results, also here, give uncertainties in the estimated tensile strength, which will influence the development function. The parameters in Table 4.6 are, as previously, found by the least squares method, in accordance with Equation 2.12.

Table 4.6: Parameters for tensile strength

NCC 50 % FA		Anlegg 33.3 % FA	
$f_{t28}$	2.62 MPa	$f_{c28}$	4.14 MPa
$t_0$	12.10 h	$t_0$	8.07 h
$s$	0.31	$s$	0.26
$n_t$	1.12	$n_t$	0.95



(a) NCC 50 % FA



(b) Anlegg 33.3 % FA

Figure 4.5: Tensile strength development plotted against maturity

## 4.5 Heat development

The concrete's temperature during the hardening phase is measured by using a so called curing box, or drum. These boxes have a thermometer in the middle connected to a computer that logs temperatures over time. Charts are plotted against the attribute models and found in Appendix B and C. Parameters used in further computations are displayed in Table 4.7.

Table 4.7: Parameters for heat development according to Swedish model

NCC 50 % FA		Anlegg 33.3 % FA	
$W_c$	300 J/kg	$W_c$	331 J/kg
$\lambda_1$	1	$\lambda_1$	1
$t_1$	16.46 h	$t_1$	11.03 h
$\kappa_1$	1.26	$\kappa_1$	1.84

## 4.6 Stiffness development summary

Figure 4.6 gives a chart of the relative development of Young's modulus, tensile strength and compressive strength shown together. It shows that the development of Young's modulus increases much faster from the start compared with the two others parameters. Compared with the results from Kanstad et al. [12], Figure 2.8, the shapes from these two concretes are somewhat different. The tensile strength development is virtually the same as for the compressive strength. The tensile strength will normally have a steeper slope from the start. This may relate to uncertainties associated with measurements of tensile strength.

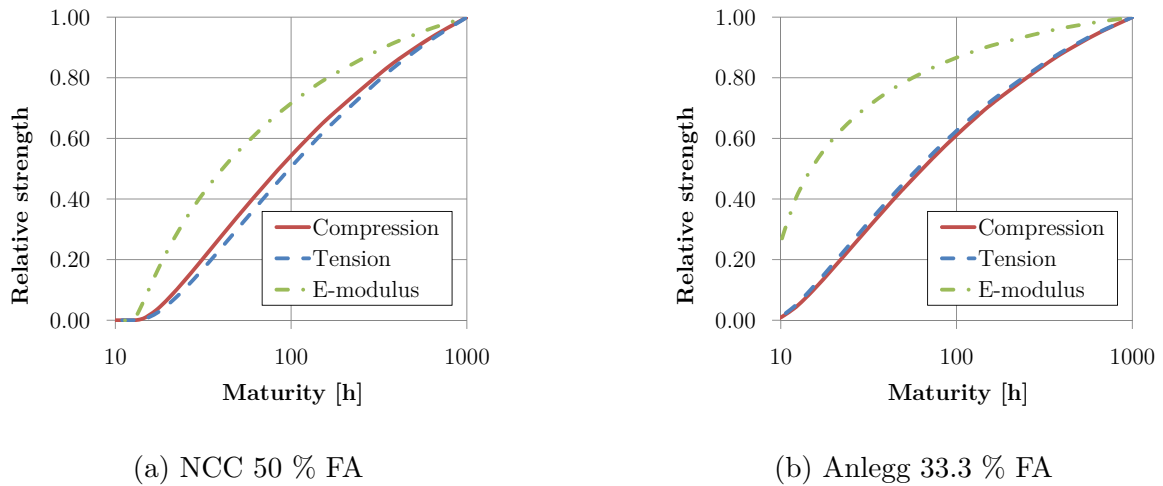


Figure 4.6: Relative development of Young's modulus ( $E$ ), tensile strength ( $f_t$ ) and compressive strength ( $f_c$ ). The properties are all normalized with regard to their 28-day value.

The slow development of tensile strength can have a major impact on one the probability of cracking at a young age. Figure (a) shows the curves closer to each other, compared with (b), which basically is beneficial in order to avoid cracking. Lower Young's modulus will give lower tension at equal strain.

# Chapter 5

## Analysis and Results

### 5.1 Temperature

Figure 5.2 and 5.3 show the results from "CrackTeSt COIN" compared with results Pedersen and Ihme [22] obtained in their master's thesis using the software program "Diana". These are two quite different software, in which "Diana" is a far more general analysis program than what might be said about "CrackTeSt COIN". Apart from the user-friendliness, one can say that the biggest difference between these two computer programs, is that Diana performs analysis in 3D, while "CrackTeSt COIN" sticks to 2D. This will be of great impact on the outcome of the simulations executed when it comes to the stress computation. In this chapter the results will be compared with focus on differences between the two programs when simulations have been done with the same structure and concrete. The concrete used is the "NCC" from the previous chapter.

Figure 5.1 contains graphical representations of the structure in the two programs. They are based on Pedersen and Ihme's thesis and the position of the elements and nodes selected in it. Since "CrackTeSt COIN" is using linear triangular elements, while for Diana quadratic elements was applied, it will be impossible to get results based on exactly equal terms. However, in "CrackTeSt COIN", see Figure 1 (a), the points are selected to represent the elements used in "Diana" and displayed in (b). The choice of elements is made after recommendations by Jonasson [11], one of the software developers, who pointed out using a minimum of 8 elements over the wall thickness.

There are no major differences between the results the two programs present on the basis of the temperature calculations. The one thing to take notice of is the results from "Diana" which tend to react a bit later than the ones from "CrackTeSt COIN". The reason for this deviation is fully understood. It has been made attempts in "CrackTeSt COIN" to adopt the "Diana" results on this matter, but it didn't lead to any enhanced understanding of the difference. After several simulations and evaluations the original results from "CrackTeSt COIN" were concluded

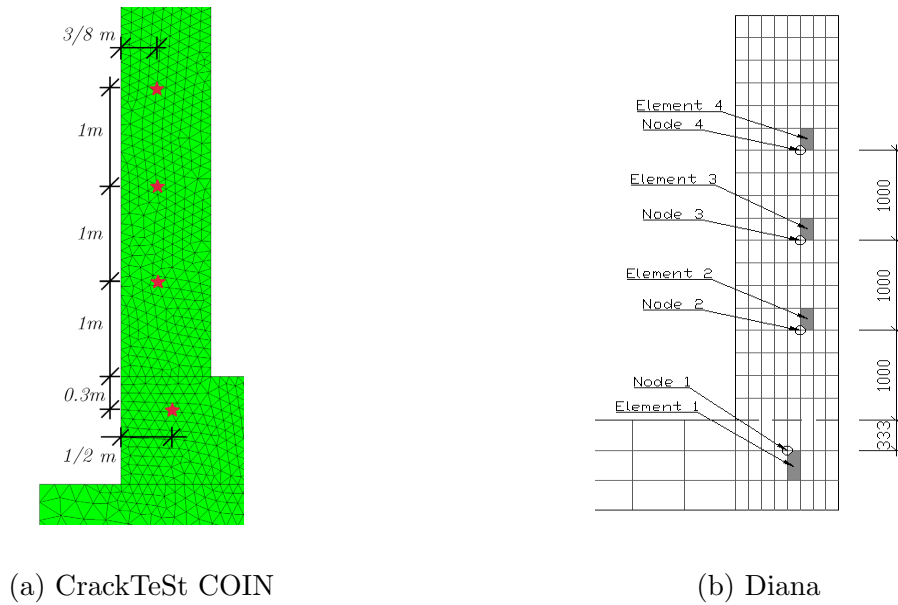


Figure 5.1: Illustration of where the computed results were obtained

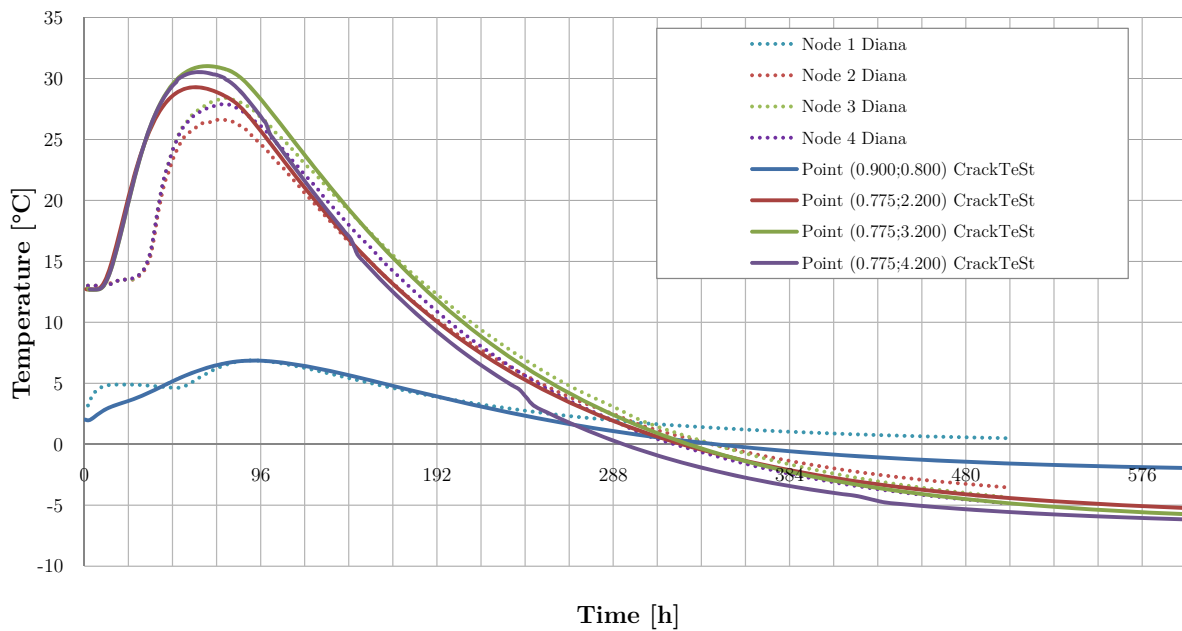


Figure 5.2: Temperature development at an air temperature of  $-7\text{ }^{\circ}\text{C}$ , ground and slab temperature of  $2\text{ }^{\circ}\text{C}$  and a concrete cast temperature of  $13\text{ }^{\circ}\text{C}$

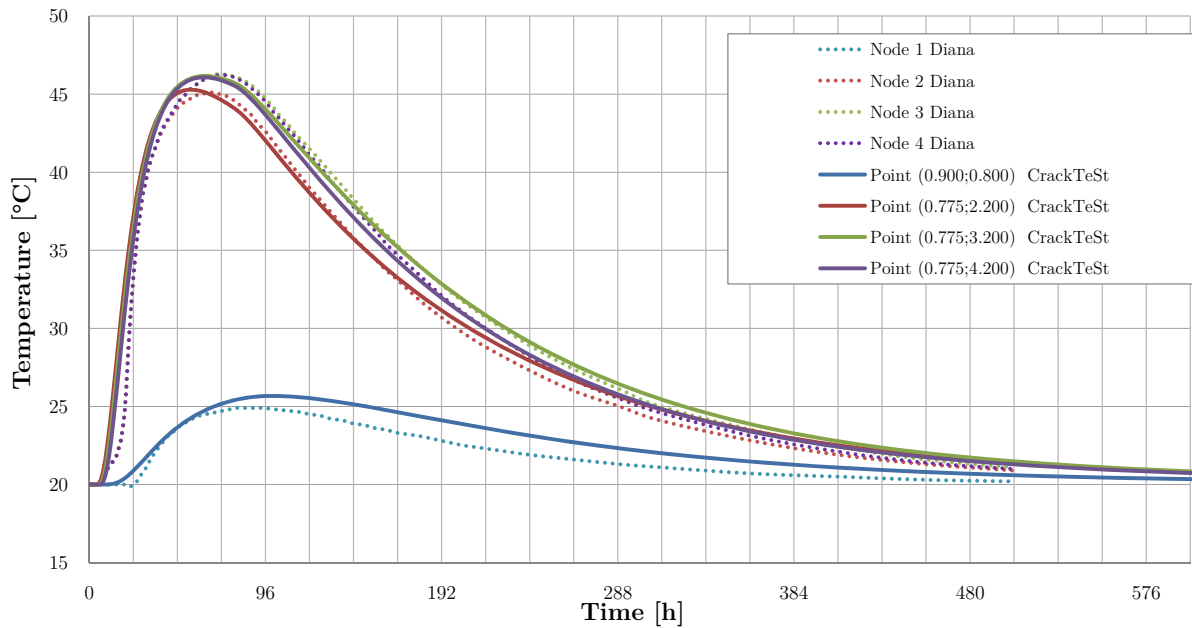


Figure 5.3: Temperature development where all thermal boundary conditions are 20 °C

to be satisfactory. There were also limited knowledge about the model used in "Diana", which gave a bit strange results the first hours in Figure 5.2. It was in cooperation with professor Kanstad discussed how "Diana's" formula for reaction rate in relation to temperature might have influence on the late rise in temperature. The discussion did not, however, reach any specific conclusions, but the late increase probably gave sequential differences which affected the maximum temperature in the same simulation.

Differences in Figure 5.3 are of minor importance and are presumably due to the small differences in the model and input parameters.

## 5.2 Stress

By comparing the stresses, the differences between 2D and 3D models will appear more evident. 2D simulations are plan surface analysis, where the stress varies in the XY-plane according to the boundary conditions. As mentioned in the previous chapter the restraint is full for the rotation around Y-axis, while it is free in terms of rotation around X-axis and translation [17]. In contrast, the "Diana" model is modelled with two symmetry planes represented by restraint in the form of roller support [22]. The model chosen has a restraint of 41 %. Figure 5.4 illustrates a color map displaying the amount of stress through the models, both "CrackTeSt COIN" and "Diana".

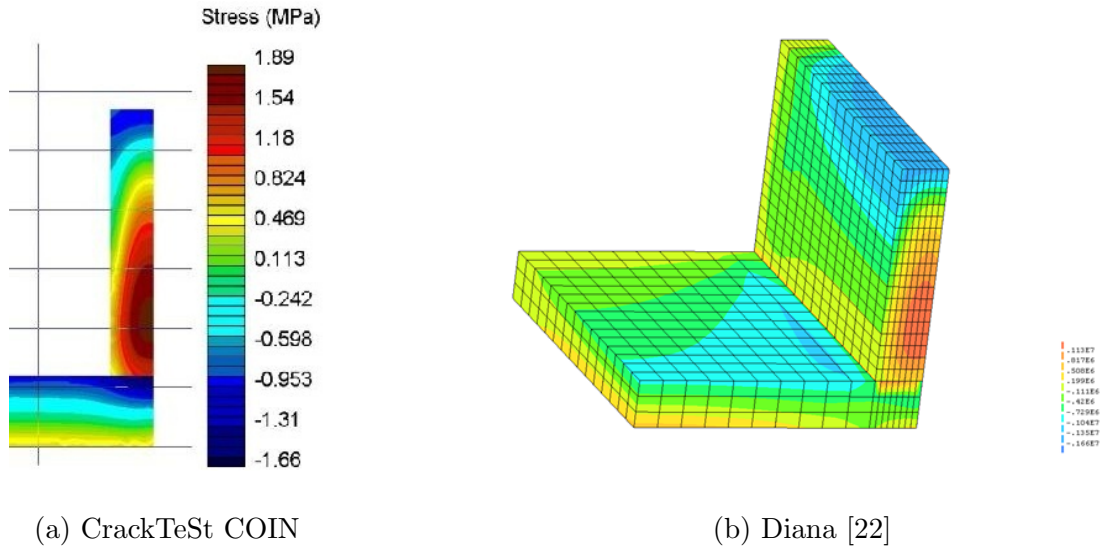


Figure 5.4: Color maps from the two software products at the time, 502 h, with maximum stress

Theory underlining the simplifications made in the two-dimensional analysis, together with the assumption that plane cross-sections remain plane, will make the effect of strain somewhat distorted [23]. The stress will, therefore, be expected to be a bit overestimated, which corresponds well with the results in Figures 5.5 and 5.6. Both figures show basically that the two-dimensional analysis gives either higher or equivalent stresses compared with the results from the three-dimensional. By the way, these findings suit well with the expectations, since in the "Diana" model the volume elements in the exterior wall not are restrained by linear strain over the cross-sectional thickness.

One can also observe the same tendency as for the temperature graphs. The "Diana" function rises a bit slower when it is cold, an effect which is explained in the previous section.

It is worth to notice the big difference on the negative side, compression, of the Y-axis. It is reasonable to assume that this is related to the element sizes and computation differences in the simulations. The major negative deflection in "CrackTeSt COIN" is caused by thermal expansion in a specific point right below the centre of the wall, resulting in compression when the rest of the foundation prevents this. Stress calculations is done in an element, and compared to "Diana" "CrackTeSt COIN" has much smaller elements. The results obtained by "CrackTeSt" are therefore from a more specific area of the structure. The bigger "Diana" elements will obtain the stress results that will be the average of the area size of the element. By creating results showing the average stress over an area equivalent to the size of an "Diana" element in "CrackTeSt COIN", the results showed a curve similar to the curve obtained from "Diana". This showed that the exothermic expansion from the wall creates compression in a small area right beneath the wall.

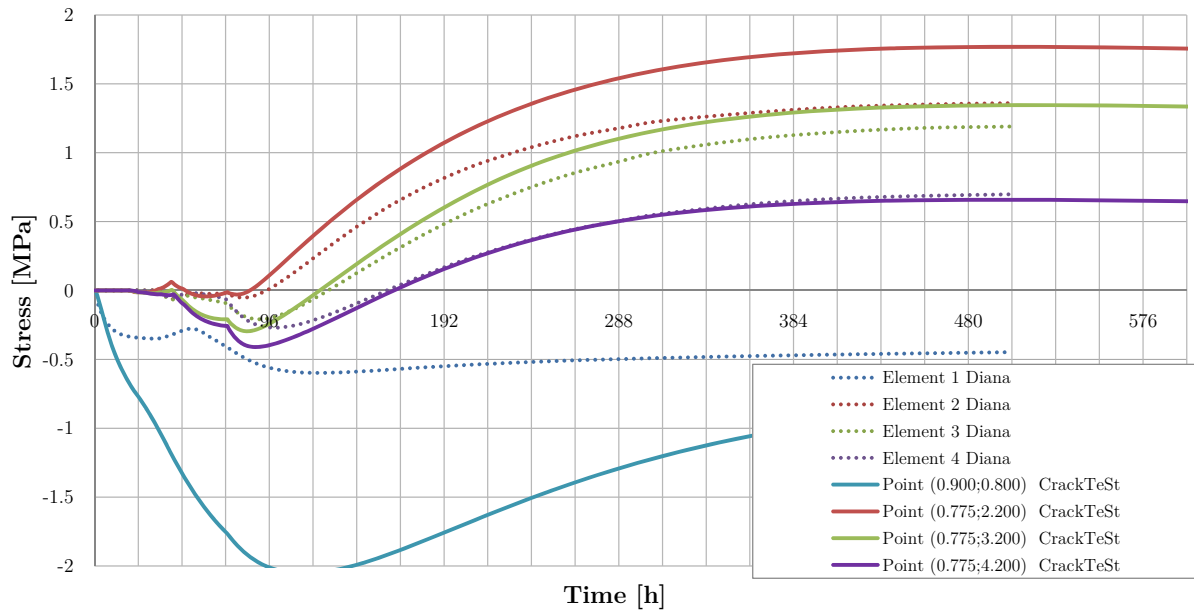


Figure 5.5: Stress development at an air temperature of  $-7\text{ }^{\circ}\text{C}$ , ground and slab temperature of  $2\text{ }^{\circ}\text{C}$  and a concrete cast temperature of  $13\text{ }^{\circ}\text{C}$

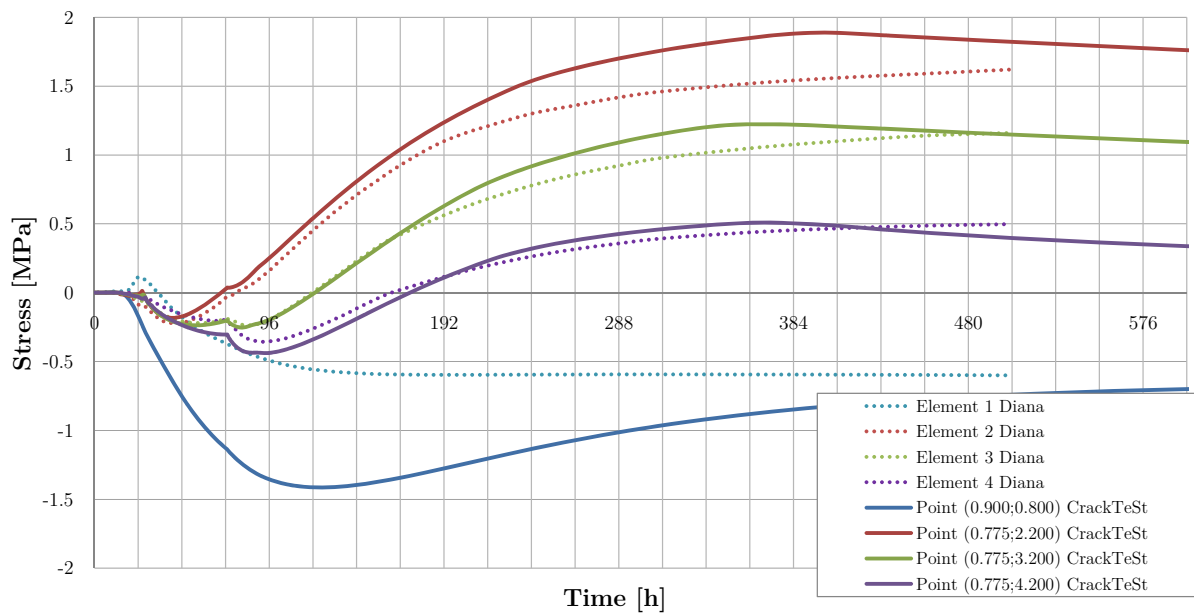


Figure 5.6: Stress development where all thermal boundary conditions are  $20\text{ }^{\circ}\text{C}$

### 5.3 Crack index

Figure 5.7 and 5.8, showing crack indexes do, as expected, not provide results which can not be read from the stress graphs. There should not be any big differences when it comes to computing tensile strength, since the same equation is used. The apparent difference should in this case be due to the simulation of stress development. The trend for the crack index does not seem to differ from the result on stress, and it is reasonable to assume the reasons for the differences are

the same.

By taking a closer look at the results, one notice the differences in crack index results in critically high values for "CrackTeSt COIN". The limit of cracking is set to 0.7, which means "CrackTeSt COIN's" results are too high, even though the concrete under isothermal conditions is over just by a small margin.

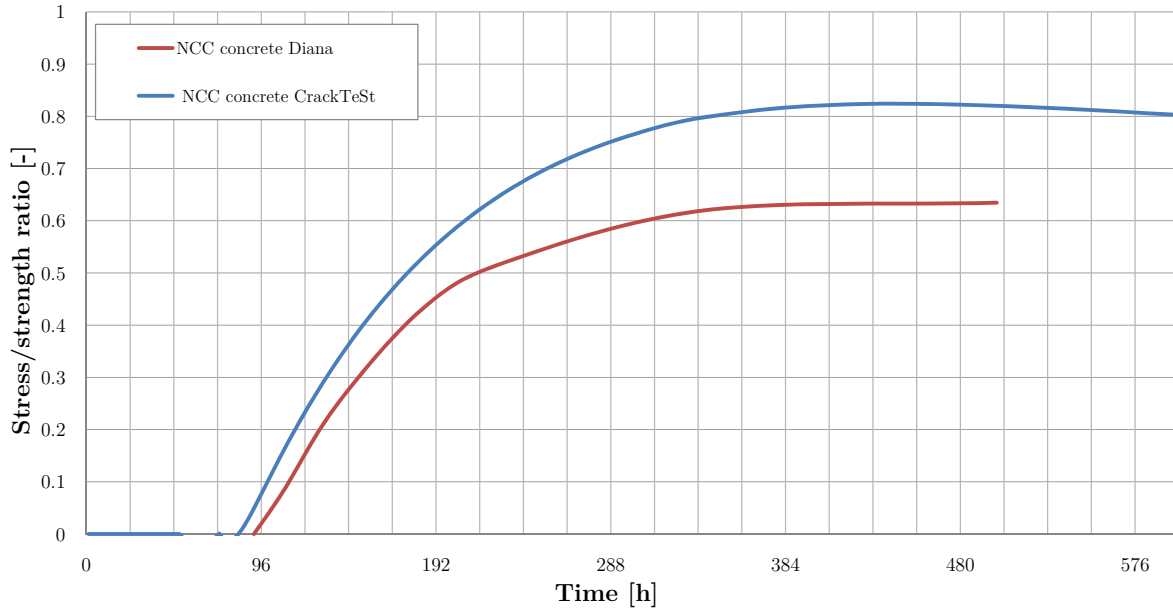


Figure 5.7: Crack index at an air temperature of  $-7\text{ }^{\circ}\text{C}$ , ground and slab temperature of  $2\text{ }^{\circ}\text{C}$  and a concrete cast temperature of  $13\text{ }^{\circ}\text{C}$

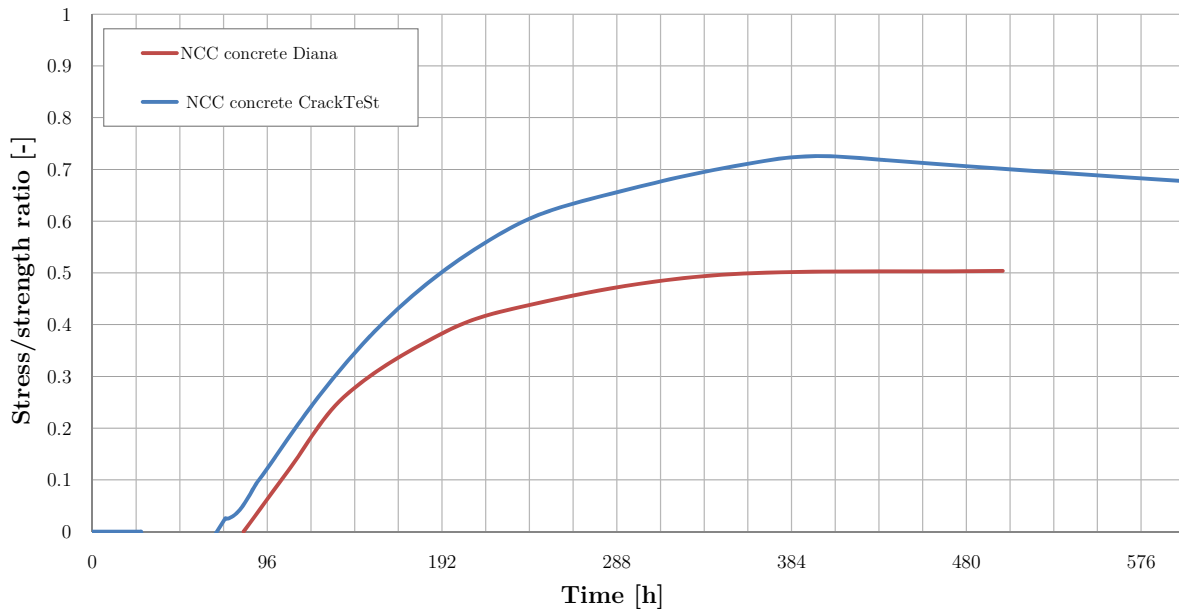


Figure 5.8: Crack index where all thermal boundary conditions are  $20\text{ }^{\circ}\text{C}$

# Chapter 6

## Parameter Study

### 6.1 General

In this part of the thesis the same simulations as in the previous chapter have been done, except three different concretes are compared. The parameters separating the properties of each concrete will be examined more thoroughly regarding how they influence the probability of cracking. The concrete capacity in terms of live and dead load will, however, not be discussed. Although this will probably not be of any problem in the part of the structures computed in this study. The three concretes compared are the two discussed in Chapter 4 in addition to one of the concretes used by Skanska in the Bjørvika submerged tunnel, Appendix D.

Before the simulation results presented, is a chart of measured data isothermal testing of autogenous deformation is displayed Figure 6.1. The figure shows large differences in shrinkage that will have impact on the final results. The deformation findings are inconclusive, and non-existent for the "Bjørvika" concrete after 256 hours and after 521 hours for "Anlegg FA". It is, nevertheless, the data read from Figure 6.1 that are used for simulations in "CrackTeSt COIN".

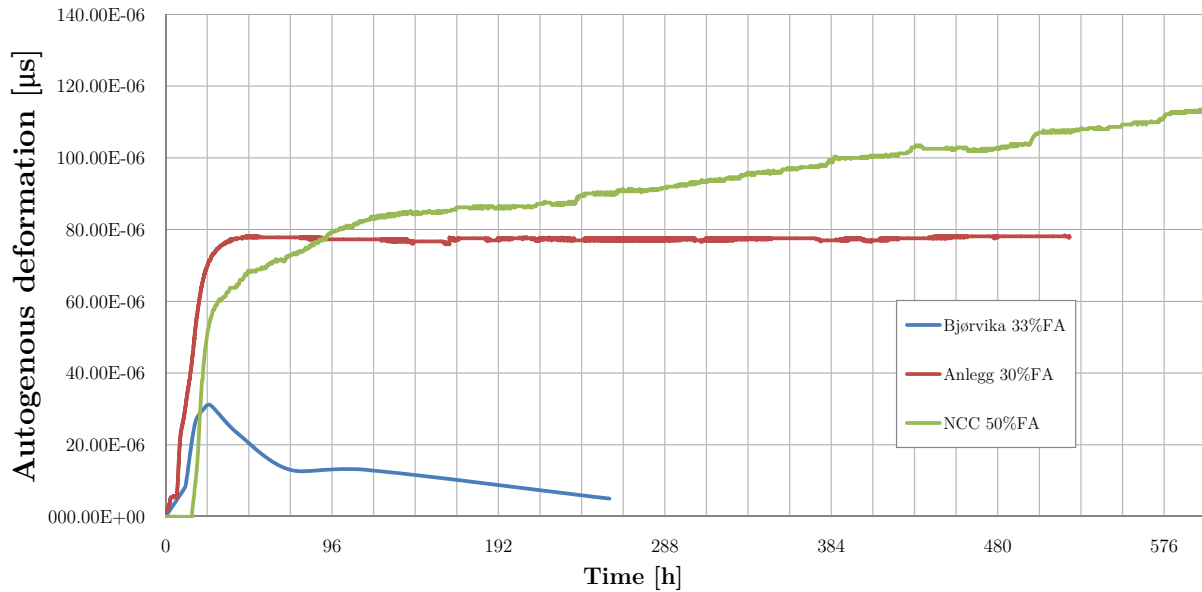


Figure 6.1: Charts from isothermal laboratory tests of autogenous shrinkage

## 6.2 Temperature

Looking at Figure 6.2 and 6.3, one can clearly notice that the NCC concrete differs from the other two in terms of temperature alteration. There is a temperature difference in maximum temperature of approximately  $10\text{ }^{\circ}\text{C}$ , which is considered to be of great significance. Higher temperatures would mean higher temperature gradients that would increase the likelihood of cracks.

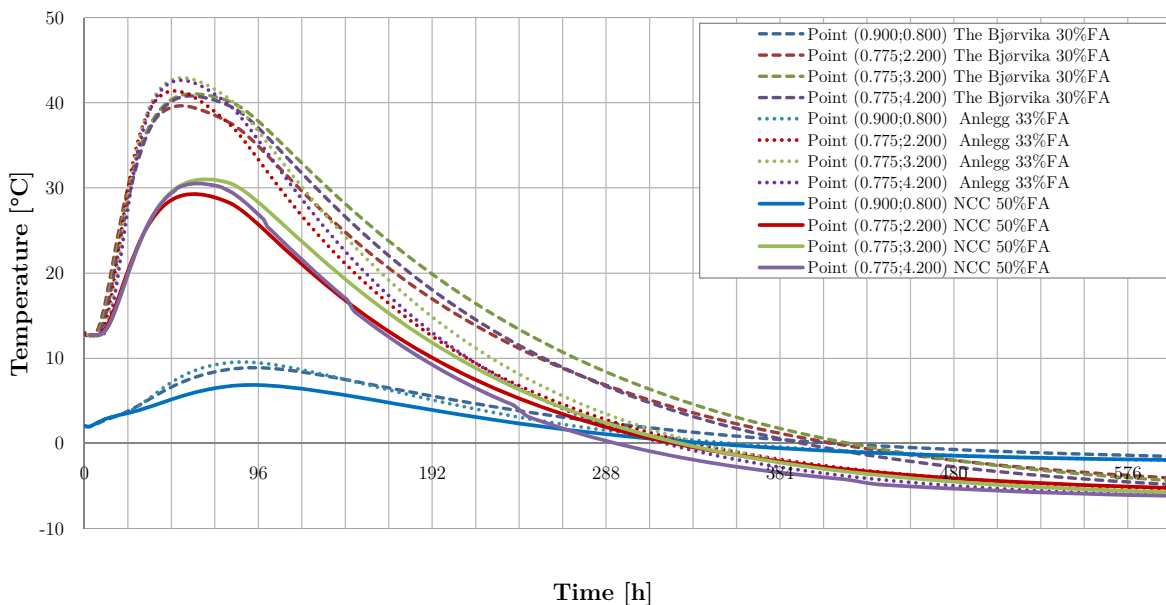


Figure 6.2: Temperature development at an air temperature of  $-7\text{ }^{\circ}\text{C}$ , ground and slab temperature of  $2\text{ }^{\circ}\text{C}$  and a concrete cast temperature of  $13\text{ }^{\circ}\text{C}$

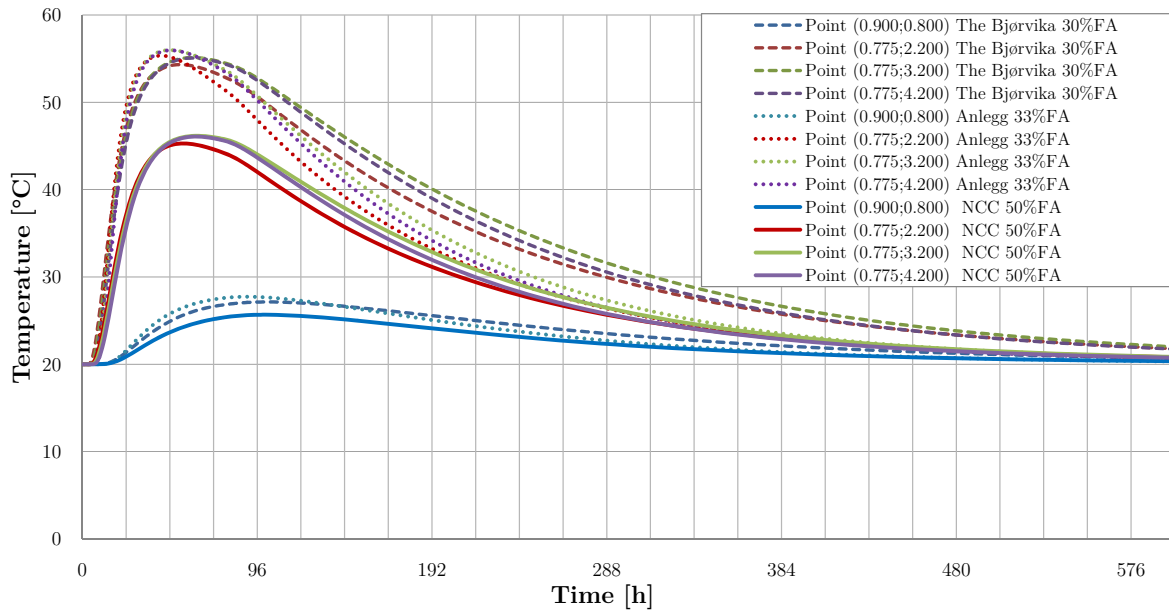


Figure 6.3: Temperature development where all thermal boundary conditions are 20 °C

The difference between the tested concretes is assumed to be due to their content of flying ash, 50 % for the NCC versus 30 % and 33 % for the two others. This is often one of the reasons flying ash is used. It reacts slower, but extends the reaction over a longer period of time. From the input parameters, Appendix B, C and D, one will notice the difference in  $W_\infty$ , from Equation 2.9.  $W_\infty$  is larger for the two concretes with lower content of fly ash. The content of cement and  $W_\infty$ , which are similar for the "NCC" and "Anlegg FA" and a bit higher for the Bjørvika concrete, are multiplied in the heat generation equation in "CrackTeSt COIN". Knowing this, the results are not unexpected.

It is also worth to notice possible differences in the cement, aggregates and other factors that may affect the temperature development of the concrete. Concrete tests are taken at various occasions and the Bjørvika concrete is from a different part of the country as well. Local differences in where cement and aggregates are produced and come from, are known phenomena. The degree of fineness for the cements is for instance not part of the computation, although finer grounded cement will give more heat [9].

## 6.3 Stress

High temperatures are normally correlated with larger development of stress since the reaction rate increases. In this case, see Figure 6.4 and 6.5, it appears not to have any negative effects on the likelihood of cracking. During the first 72 hours as well as all stresses are negative, meaning they are in compression.

The NCC concrete shows the most rapid development under both conditions, although at low temperatures it seems to have lower maximum tension than the other two. In Figure 6.4 "NCC"

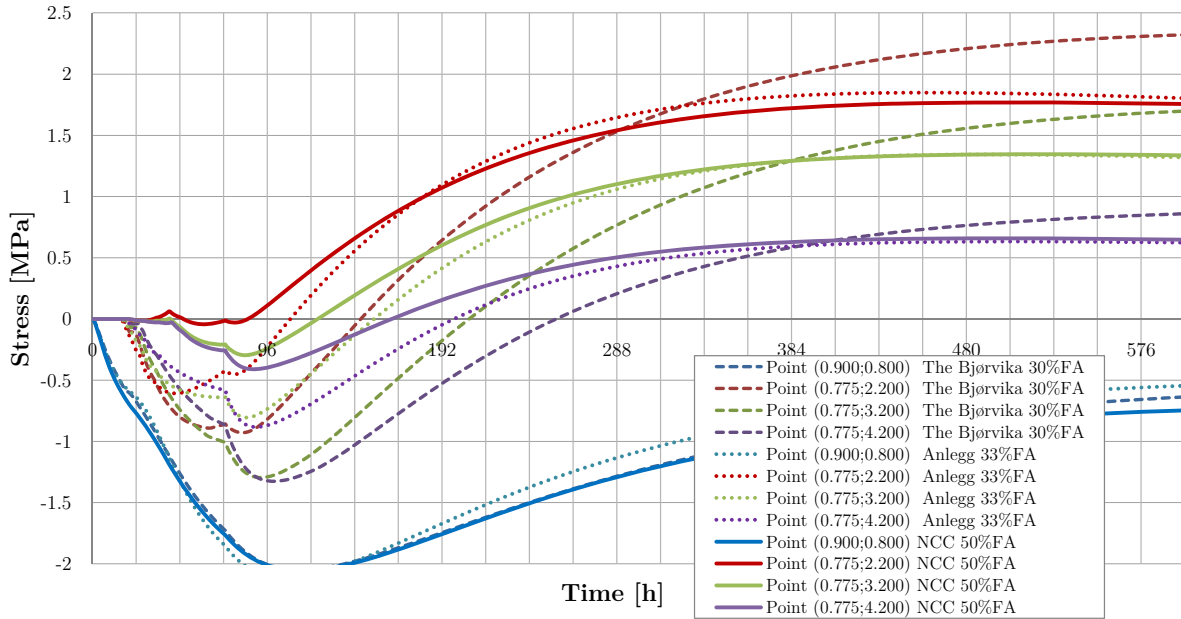


Figure 6.4: Stress development at an air temperature of  $-7\text{ }^{\circ}\text{C}$ , ground and slab temperature of  $2\text{ }^{\circ}\text{C}$  and a concrete cast temperature of  $13\text{ }^{\circ}\text{C}$

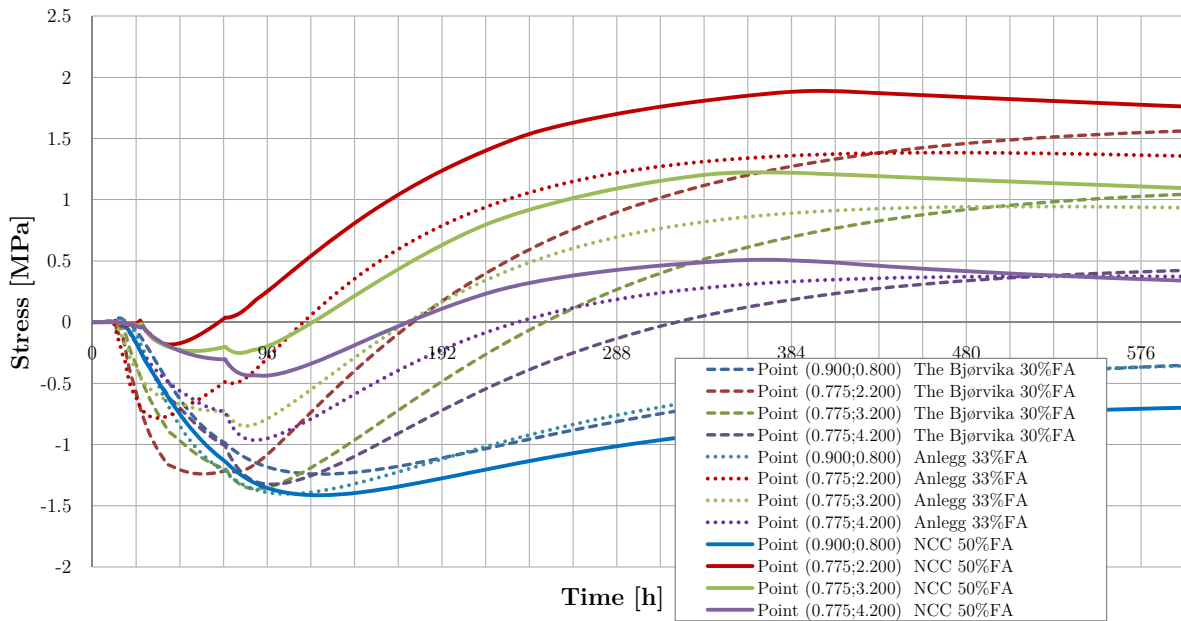


Figure 6.5: Stress development where all thermal boundary conditions are  $20\text{ }^{\circ}\text{C}$

and "Anlegg FA" are virtually following the same pattern after a week, 168 hours. The same conclusion can be made about the simulation under isothermal conditions, only here the "Anlegg FA" concrete tend to stay roughly 0.5 MPa lower than the "NCC" for the point with highest tension.

The Björvika concrete, on the other hand, seems to have a much slower reaction in the beginning and the stress is still continuing to increase when passing 600 hours, 25 days. In the coldest case

the concrete reaches the highest stress of all, at about 2.4 MPa

Stress is seen in context with the development of Young's modulus, which for the "Bjørvika" and "Anlegg FA" concrete rise much faster the first thirty to forty hours. This might help explaining the negative stresses the first few days and why the slower "NCC" concrete has a more rapid stress development.

## 6.4 Crack index

Taking the stress results in to account it is not surprising that the "NCC" concrete has the highest crack index, but how much higher, is difficult to predict. Stress-wise, the concretes were a lot more similar than what can be seen from the crack index chart, by looking at Figure 6.6 and 6.7. The figures show the "NCC" concrete increasing much earlier and reaching a much higher maximum compared to the other two.

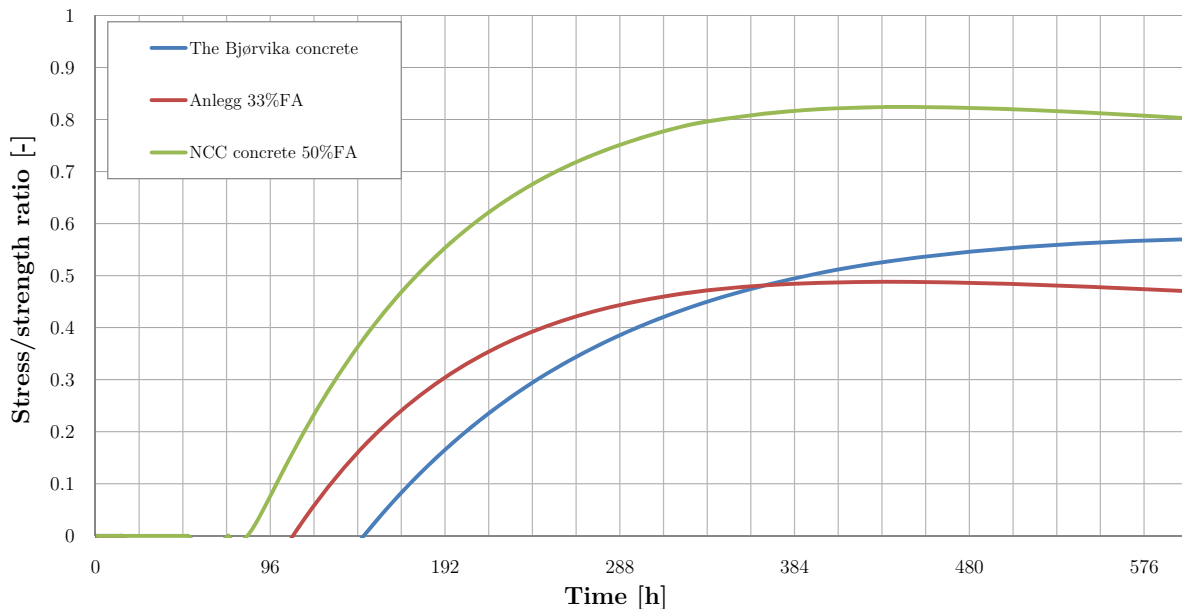


Figure 6.6: Crack index at an air temperature of  $-7\text{ }^{\circ}\text{C}$ , ground and slab temperature of  $2\text{ }^{\circ}\text{C}$  and a concrete cast temperature of  $13\text{ }^{\circ}\text{C}$

The major difference between the three concretes, not shown in the previous section, is the distinction in tensile strength. While "Anlegg FA" and "Bjørvika" concretes have tensile strengths of 4.14 MPa and 4.20 MPa, the "NCC" concrete has a tensile strength of 2.62 MPa. One can safely conclude that the lower tensile strength plays a major role in the "NCC" concrete's high crack index compared to the two others'.

As mentioned in Chapter 5 the crack index is critical high regarding the "NCC" concrete, especially when looking at the simulation done under cold conditions. Considering the other two, both values are well below 0.7 and the likelihood of crack should be minimal.

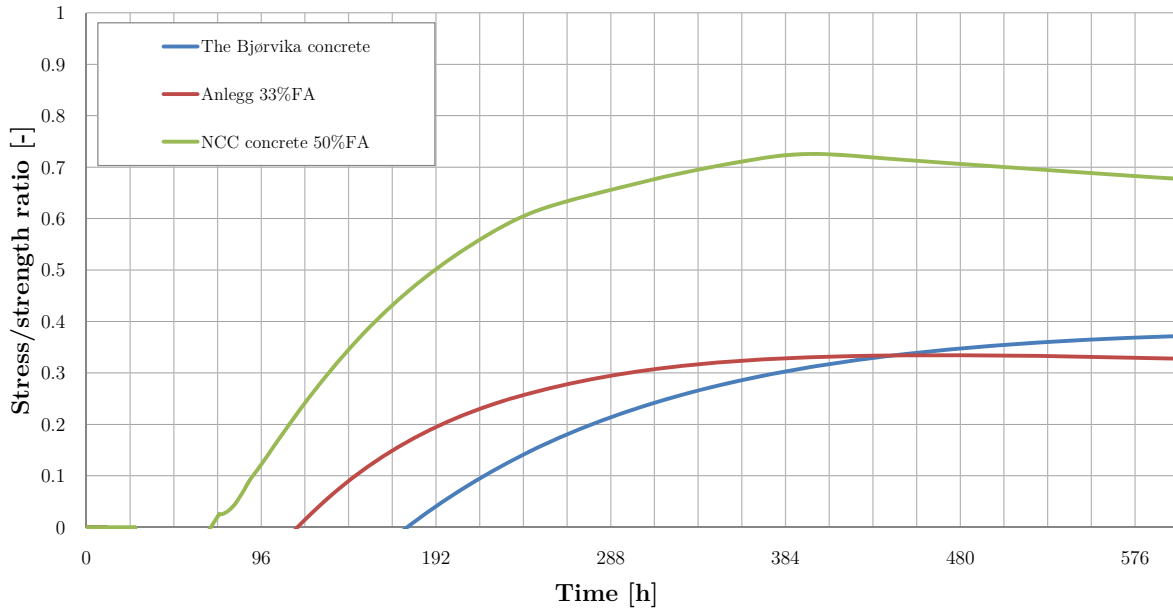


Figure 6.7: Crack index where all thermal boundary conditions are 20 °C

Simulation executed by setting all shrinkage equal to zero indicated that part of the high crack index in the “NCC” concrete is caused by autogenous deformations. While the crack index for the “Bjørvika” and “Anlegg FA” concretes had minimal change when eliminating shrinkage, did the “NCC’s” crack index decrease by almost 22 % under both conditions.

## 6.5 Insulation

The Møllenberg culvert project has been considering to cover the concrete with insulation when the temperature has reached its maximum. To get an indication whether insulation will improve the crack index it has been executed simulations for this alternative as well. Since the insulation is applied after the temperature peak it should not affect the maximum. In Figure 6.8 and 6.9 it is displayed the impact insulation has on the two cases. Both show that the temperatures after reaching their maxima decreases much slower. Slower cooling of the concrete wall should also imply lower temperature gradients compared with the ones without insulation. This may result in lower internal restraint.

When looking at the crack indexes in Figure 6.10 and 6.11 the major difference from the crack indexes in Section 6.4 are when the maxima occur. There are hardly any differences when it comes to the crack index’s maximum value for any of the concretes. It seems like the only effect insulation has on the crack index is a delayed development.

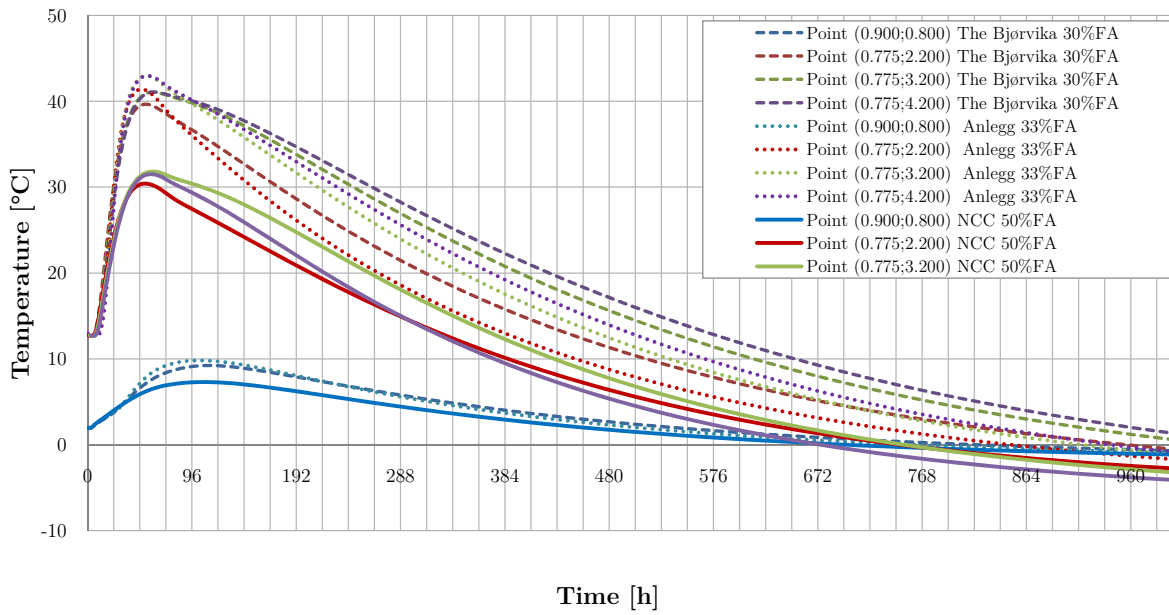


Figure 6.8: Temperature development at an air temperature of  $-7\text{ }^{\circ}\text{C}$ , ground and slab temperature of  $2\text{ }^{\circ}\text{C}$  and a concrete cast temperature of  $13\text{ }^{\circ}\text{C}$

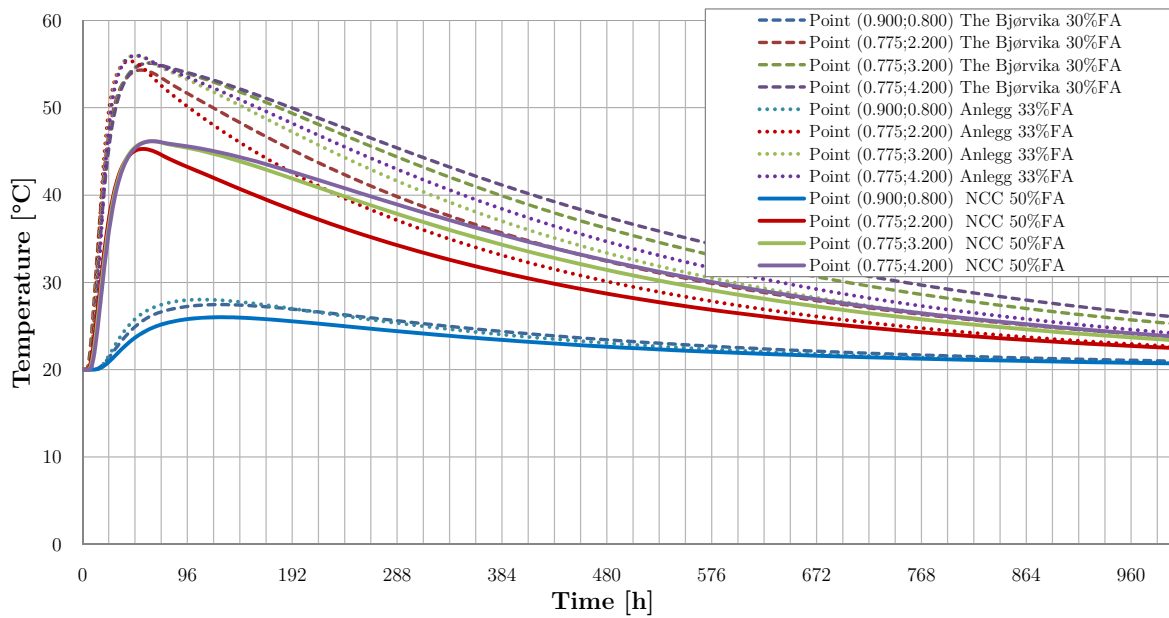


Figure 6.9: Temperature development where all thermal boundary conditions are  $20\text{ }^{\circ}\text{C}$

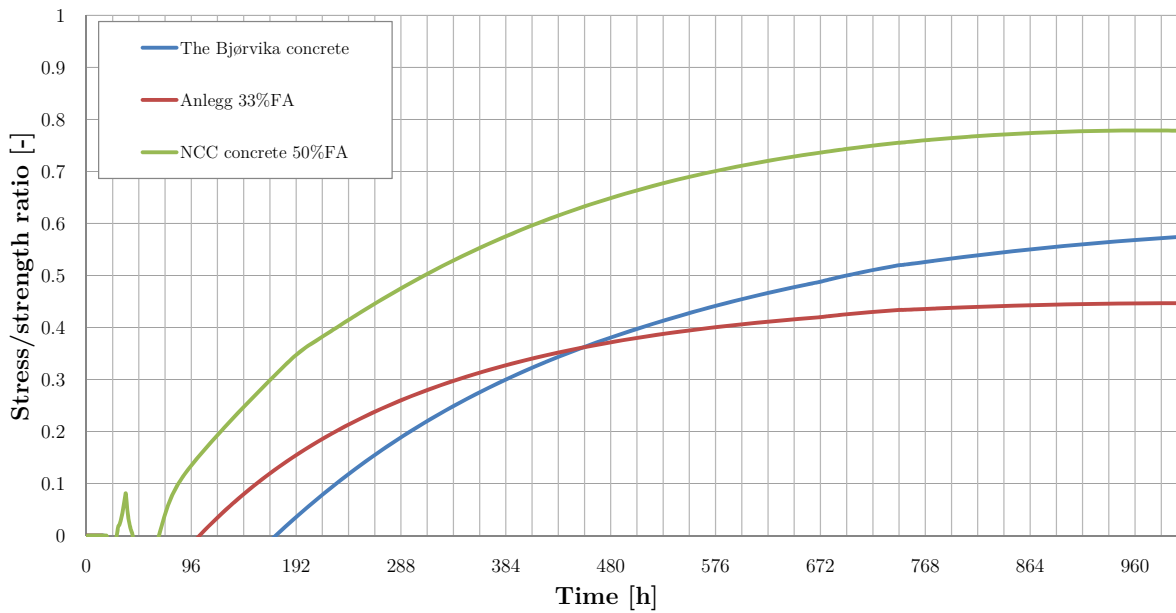


Figure 6.10: Crack index at an air temperature of  $-7\text{ }^{\circ}\text{C}$ , ground and slab temperature of  $2\text{ }^{\circ}\text{C}$  and a concrete cast temperature of  $13\text{ }^{\circ}\text{C}$

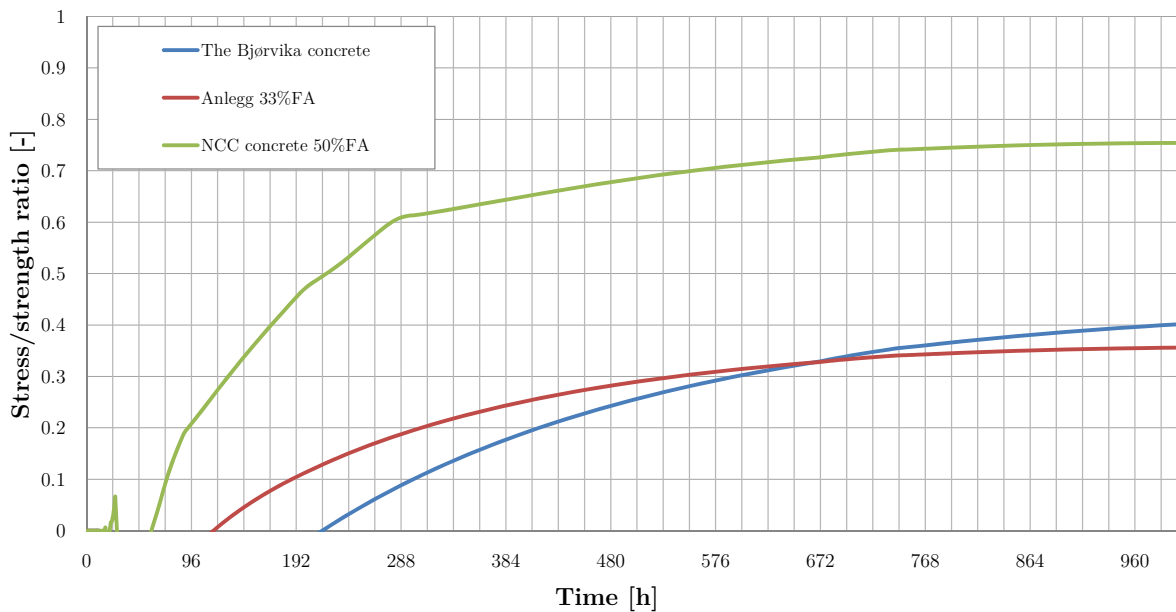


Figure 6.11: Crack index where all thermal boundary conditions are  $20\text{ }^{\circ}\text{C}$

# Chapter 7

## Software Useability

### 7.1 General

Although "CrackTeSt COIN" is still in beta version, the program has been existing under the name of "ConTeSt Pro" for some years already. The program has been customized for Norway by guidelines given by professors at NTNU. It is, adjusted to ensure NTNU's demands and formulas used in Norway. By the way, the software's system requirements are something modern computers do not have any problem to handle.

### 7.2 Graphical user interface

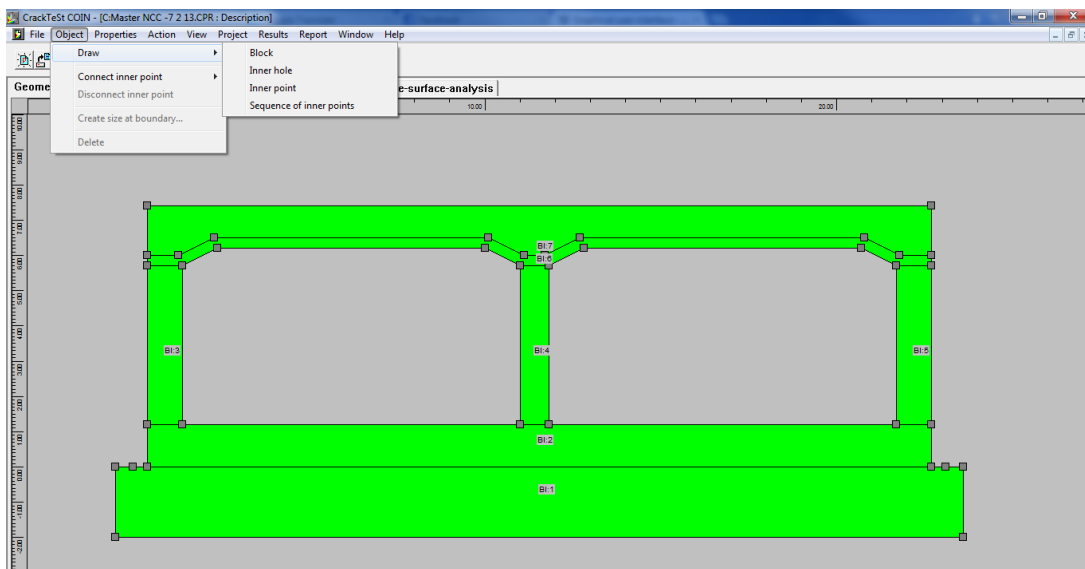


Figure 7.1: Graphical user interface

When you first start using the program, it is a bit unconventional since it differs considerably from the familiar interface used in Windows or Mac. User interface does, therefore, appear

unusual and not very intuitive. Error messages popping up often lack of information and seem incomprehensible. But after some trial and error drawing structures go easy, but there are a few things to remember when using "CrackTeSt COIN".

- First draw the design roughly and then adjust the corner points of the blocks one by one.
- The second thing to remember applies only when using of the stress computation type "Linear line". When using this feature it is important to not have more that one block in x-direction.
- Thirdly one also have to pay attention to which tab is being used. Use of a tab further to the left results in information loss if changes are done and computations must be repeated.

### 7.3 Simulations

Before the simulation can be done, one must give the drawn structure properties. It is possible to choose one of the standard concretes that are included in the software or add variables such as heat and strength development yourself. The same applies when it comes to the formwork and choice of ground (the program requires a ground under the concrete structure [11]). When setting the formwork it is important to notice that a layer of "free surface" needs to be applied when using wind speed higher than zero. Jonasson said that it should have been an error notification when trying to set a wind speed without doing so, this may be added in a later version. Before starting an analysis, "CrackTeSt COIN" also has the option of placing cooling pipes or heating wire, named inner hole and inner point in the program. The simulations in "CrackTeSt COIN" are fast compared with similar computer programs, but by adding these kind of features the simulation time will increase a great deal. Worth noticing is the software's ability to determine filling rate. One can decide when the concrete is poured, and how high steps one want to pour at a time.

Values varying in time are treated in two different ways. Temperature and shrinkage functions are piecemeal linear while the remaining functions are piecewise constant values [17]. Illustrations in Figure show the difference.

As written in Chapter 5 Jonasson did recommend at least 8 elements over the wall thickness to obtain good results. It is possible to increase the number of elements not only in the blocks, but also near the boundaries. However, it is not necessary to modifying properties between adjoining blocks for the program to understand that they are, which must be done for some similar software products.

"CrackTeSt COIN" does its simulations in 2D and when the tunnel is 2.5 km long the section's length is not taken into account in the calculations in this thesis. The program can, although, calculate resilience and joint slip when the length to height ratio of greater than seven. This

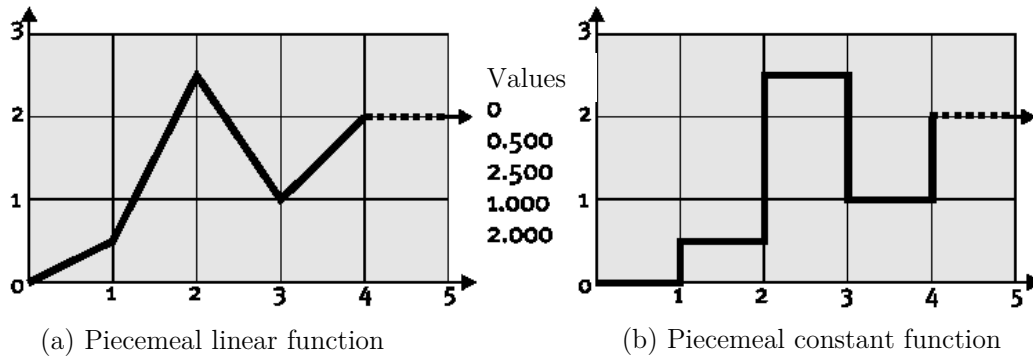


Figure 7.2: Difference between the piecemeal linear and the piecemeal constant functions [17]

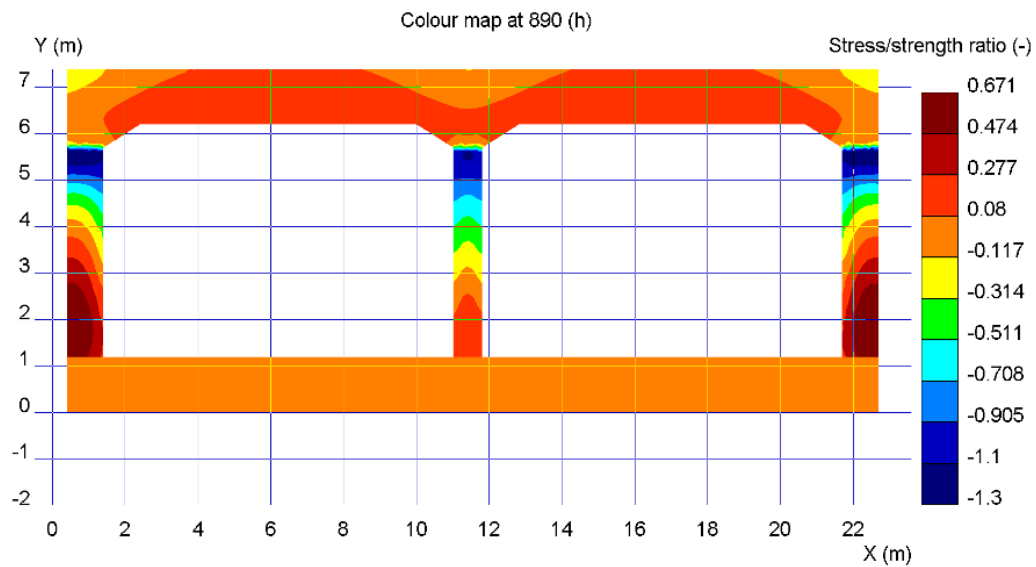


Figure 7.3: Example of color-map results for crack index

is done by a linear function based on the stress results from the cross-section and not from FE analysis.

When it comes to results, there are several opportunities for the user to determine what results to display. One can choose to get result from cross-sections, as in Figure 7.3 or chart from specific points or hole blocks. The possibility of exporting results to image files or to text files are also embedded.

## 7.4 Proposed changes

As emphasized in the last sections, the author's opinion is that the software isn't the most intuitive, even for professionals. This section is intended to propose some changes that would make the software easier to use.

- If this is to become a commercial product, a much larger database should be developed

when it comes to materials. A database of approximately 10 concretes, maybe more, should be sufficient. It would then be quite easy to find a concrete similar to the one used on site.

- An alternative for input of material properties should be direct input of discrete data.
- A possible improvement could be the program obtaining a transition equation by itself. By typing in a  $t_0$  it should be possible for the program to do the rest.
- It would also be nice if it could be a visual function, a graph, to show the heat and strength development after typing in the material parameters.
- The creep computing software RELAX should be integrated in CrackTeSt COIN. This would make it much easier use, in stead of using an additional program that even is DOS command prompt.
- There should be a error message when applying wind speed without adding a layer of "free surface" in addition to the formwork or other outer boundaries.

## Chapter 8

# Conclusion

The Møllenberg culvert is a heavy concrete structure which due to restraint in construction joints, is in great risk of cracking during hardening. To outline the danger of cracking, analysis with use of specially developed FEM software has been performed. Results from the analyses are corresponding well with expectation and theory. It is still believed that the results are somewhat conservative due to the use of 2D computation.

The comparison done between "CrackTeSt COIN" and "4C Temp&Stress" agreed with the anticipation. The major part of the results correspond quite well, while where differences were found they were clearly in affiliation with the creep functions used.

When it comes to the comparison with "Diana", differences between modelling in 2D and 3D appeared clearly. The results also display the impact the finite element size has on the results in numerical simulations.

Fly ash content and temperature have major influence when it comes to crack problems in the hardening phase. It still turns out that it is the tensile strength which has most impact. The statistical significance of the laboratory tests can be questionable, considering the parameter's importance in the equation of crack index. It also appears that the concrete chosen for the Møllenberg culvert may be exposed to cracking, at least if the casting is performed during the summer. Laboratory tests of tensile strength, as well as Young's modulus, at the time the crack index is at its maximum could be a good verification and provide valuable information when establishing the strength development functions.

"CrackTeSt COIN" is basically a well suited program for its purpose when the user has some knowledge of its theoretical basis. It is easy to learn and displays proper and user-friendly results.



## Chapter 9

# Further Work

Suggestions for future research and thesis work are:

- Creating a database of concrete mixtures that can be used in the software like “CrackTeSt COIN”. The laboratory work executed to prepare this database should involve a number of tensile strength tests.
- Doing a comprehensive research on tensile strength development on various concretes. The research should include testing with different amounts of cement, pozzolana and admixtures.
- There should also be done research on how good software programs like “CrackTest COIN” expresses autogenous deformations at various temperatures.
- In addition, could research on how different levels of fly ash affect autogenous deformations be interesting.



# References

- [1] T. E. Page, editor. *VITRUVIUS ON ARCHITECTURE I*. London: William Heinemann LTD, 1929.
- [2] Ø. Bjøntegaard. Teknologirapport nr 2565, Volumendringer og risstendens i betong. Technical report, Statens Vegvesen, Trondheim, 2009.
- [3] Ø. Bjøntegaard. Basis for and practical approaches to stress calculations and crack risk estimation in hardening concrete structures. Technical report, SINTEF, 2011. COIN Project report 31 -2011.
- [4] D. Bosnjak. *Self-Induced Cracking Problems in Hardening Concrete Structures*. PhD thesis, NTNU, Trondheim, 2000. ISBN 82-7984-151-2.
- [5] Statens Vegvesen. vegvesen.no E6 Trondheim-Stjørdal. <http://www.vegvesen.no/Vegprosjekter/e6ost/>. Visited 04.10.2011.
- [6] G. De Schutter and K. Audenaert. *Report 38: Durability of Self-Compacting Concrete - State-of-the-Art Report of RILEM Technical Committee 205-DSC*. 2007. ISBN 978-2-35158-048-6.
- [7] P. Feiesleben Hansen and E.J. Pedersen. Maturity computer for controlled curing and hardening of concrete. Technical report, 1977.
- [8] O. B. Skjølsvik. Beregning og evaluering av rissrisiko pga. fastholdingseffekter i støpeskjøter. Master's thesis, NTNU, Trondheim, 2011.
- [9] S. Jacobsen, E. J. Sellevold, M. Maage, S. Smeplass, K. O. Kjellsen, J. Lindgård, R. Myrdal, and Ø. Bjøntegaard. *Concrete Technology 1*. NTNU, Trondheim, 2010. ISBN: 82-7482-098-3.
- [10] S. Smeplass. *Calor, program documentation*. Sintef FCB-raport, 1988. ISBN 82-595.5096-2.
- [11] Lecture with J.E. Jonasson 12. -13. September 2011.
- [12] T. Kanstad, T. A. Hammer, Ø. Bjøntegaard, and E. J. Sellevold. Mechanical properties of young concrete: part II: Determination of model parameters and test program proposals. *Materials and Structures*, 36(4):226–230, 2003.

- 
- [13] J. E. Jonasson, M. Emborg, L. Elfgren, and K. Wallin. How to build crack-free durable concrete structures-concrete hardening technology including modelling of shrinkage, creep and temperature of young concrete and its influence on durability and lifetime. *ISLECI 2009: The 4th International Symposium on Lifetime Engineering of Civil Infrastructure*, 2009.
- [14] O. B. Skjølvik. Rapport for sammenligning CrackTeSt COIN og 4C Temp&Stress - Betesting av CrackTeSt COIN. Technical report, Skanska Norge AS, August 2011.
- [15]
- [16] W. N. Findley, J. S. Lai, and K. Onaran. *Creep and relaxation of nonlinear viscoelastic materials: with an introduction to linear viscolasticity*, volume 18. North-Holland Publishing Company, Amsterdam, 1976.
- [17] *ConTeSt Pro - User's Manual*. JEJMS Concrete AB, 2008.
- [18] J.E. Jonasson and G. Westman. Conversion of creep data to relaxation data by the program RELAX. Technical report, Luleå University of Technology, 2001. ISBN 91-89580-45-1.
- [19] Prøvingrapport, TUNNEL MØLLENBERG - Ung Betong LVB 100% FA, Project no: 3D0593.42, Report no: 33409/A. Technical report, SINTEF Byggforsk, 2011.
- [20] Prøvingrapport, TUNNEL MØLLENBERG, Project no: 3D0593.31, Report no: 33380. Technical report, SINTEF Byggforsk, 2011.
- [21] Ø. Bjøntegaard. NOR-CRACK Report 3.2. Technical report, SINTEF, 2005.
- [22] T. E. Pedersen and T. H. Ihme. Betongkonstruksjoner i herdefasen analysert med elementmetoden: Bestemmelse av risiko for riss i Møllenberg Løsmassetunnel. Master's thesis, NTNU, Trondheim, 2011.
- [23] S. F. Gjessing. Bergning og evaluering av rissrisiko på grunn av fastholdingseffekter i støpeskjøter. Master's thesis, NTNU, Trondheim, 2008.
- [24] D. Atrushi, Ø. Bjøntegaard, T. Kanstad, and E. J. Sellevold. Creep deformations in hardening concrete: Test method investigations and the effect of temperature. *IPACS Document, Subtask, 3*, 2001.
- [25] G. Ji. *Cracking Risk of Concrete Structures in the Hardening Phase*. PhD thesis, NTNU, 2008.
- [26] Standard Norge. NS-EN 1992-1-1:2004+NA:2008 Eurocode 2: Design of concrete structures - Part 1-1: General rules and rules for buildings. European committee for standardization, 2008.

## Appendix A

# Material Parameters from Oliver

See next page

Parameters from retest of Oliver Berget Skjølvsvik's report in CrackTest COIN

Young concrete -heat properties					
		Ny Anlegg	Anlegg FA20	Anlegg FA40	
Temp	(°C)	Constant	20	Constant	20
Density	(kg/m <sup>3</sup> )		2 400	2 335	2 400
Heat capacity	(J/kg K)		1 030	1 000	1 000
Heat conductivity	(W/m K)	0 (h)	2.0	0 (h)	2.0
Qinfinite	(J/kg)		364 600	350 000	350 907
C	(kg/m <sup>3</sup> )		384.3	399.9	348.0
t1	(h)		10	11	10
Kappa	(-)		2.17	1.53	2.29
te0	(h)		0	0	0
BetaD	(-)		1	1	1
Aset	(J/mol)		24 942	32 000	26 000
Bset	(J/mol K)		2 494	500	50
A	(J/mol)		24 942	32 000	36 000
B	(J/mol K)		2 494	500	50
Fcc288	(MPa)		81.0	50.7	50.7
s	(-)		0	0	0
TimeInitial	(h)		8	8	8
TimeFinal	(h)		11	11	11
nSet	(-)		1	2	2.0
FccSet	(MPa)		1.E-300	1.00E-300	1.00E-300
ncc28d	(-)		0.5	0.53	0.5

Non-hydrating material -heat properties					
		Ny Anlegg	Anlegg FA20	Anlegg FA40	
Temp	(°C)	Constant	10	Constant	10
Density	(kg/m <sup>3</sup> )		2 400	2 335	2 400
Heat capacity	(J/kg K)		1 030	1 000	1 000
Heat conductivity	(W/m K)		2.0	2.0	2.0

Young concrete- mechanical properties					
		Ny Anlegg	Anlegg FA20	Anlegg FA40	
E-modulus	(GPa)		34.3	29.3	29.3
RelTime1	(d)		0.005	0.005	0.005
TimeZero	(d)		0.458333	0.458333	0.5
Number of ages			20	20	20
Number of rel.units			8	8	8
Fcc28	(MPa)		81	50.7	50.7
Fct28	(MPa)		4.44	3.1	4.2
nct	(-)		0.658	0.708	0.7
AlphaTemp	(1/K)		9.2E-06	7.30E-06	7.20E-06

Non-hydrating material- machanical properties				
		Ny Anlegg	Anlegg FA20	Anlegg FA40
AlphaTemp	(1/K)	7.3E-06	7.30E-06	7.20E-06
E-modulus	(GPa)	29.3	29.3	39.84
Fcc	(MPa)	81	50.7	50
Fct	(MPa)	4.44	3.13	3

Outer boundary type			
Forskaling			
Temp	(°C)	5	
Wind	(m/s)	1	
External power	(W/m2)	0	
Description of Insulation	(h)	(W/K m2)	
	0	6.36364	0.022(m)Wood/Plywood
	24	1000	Free surface
	1000	1000	Free surface
HTC	0	3.81891	
	24	9.45966	
	1000	9.45966	

Filling time		
(h)	(m)	
	0	0
	1	4
	2	7

Outer boundary type			
Fri flate			
Temp	(°C)	5	
Wind	(m/s)	1	
External power	(W/m2)	0	
Description of Insulation	(h)	(W/K m2)	
	0	6.36364	Free surface
	1000	1000	Free surface
HTC	0	9.45966	
	1000	9.45966	

Outer boundary type		
Grunn		
Temp	(°C)	5
Wind	(m/s)	1
External power	(W/m2)	0
Description of Insulation	(h)	(W/K m2)
	0	900
HTC	0	900



## Appendix B

# Material Parameters for NCC 50% FA per binder

See SINTEF Test Report, project no: 3D0593.42, Report no: 33409/A

See next pages

**Adiabatic temperature and isothermic heat**

(v 2.7 ss 2004-01-07)

**SKANSKA**

**Concrete parameters**

Temp. trans. coeff.	0.0040
Density	2375
Heat capacity (fresh)	1.03
Heat capacity (hardened)	1.03
Cement content	332
Set time	12.1
A - set time	40742
B - set time	273
A - hydration	40742
B - hydration	273
Adia. start temperature	19.5

**Temp. trans. coeff.**

dQ/dm	0.07
m>	250
m<	300

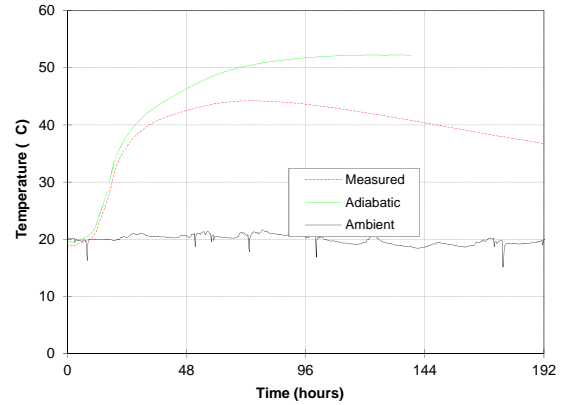
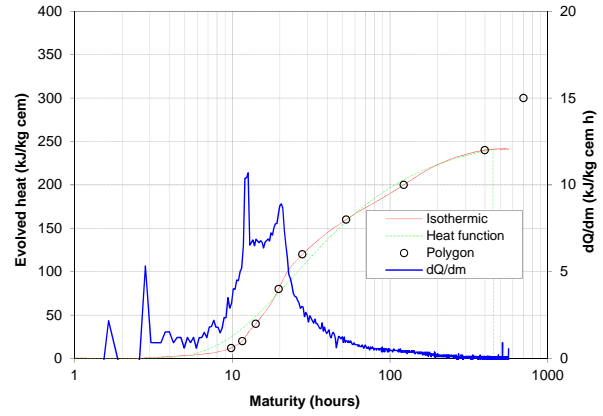
**Heat function**

M-limit	450
Q <sub>∞</sub>	257
τ	24.38
α	0.93
R <sup>2</sup>	0.9733
ΣΔ <sub>Q</sub>	12997

**Heat polygon**

Reference heat [kJ/kg cem]	Corresp. maturity [h]
0	-0.3
12	9.8
20	11.6
40	14.1
80	19.7
120	27.8
160	52.7
200	122.1
240	398.5
300	701.8

Adapt the temperature transmission coefficient: <Ctrl> t  
Adapt the heat function: <Ctrl> h



**Project**

Name	Løsmassetunnel 100% FA
Test id	SINTEF rapportnr: 33380
Perf. by	Christian K Sandvik
Date	28.11.2011

Time [h]	Concrete temperature [C]	Ambient temperature [C]	Maturity [h]	Acc. heat pr. cem. [kJ/kg cem]	Adiabatic time [h]	Adiabatic temperature [C]
0.0	18.8	20.1	0	0.0	0.0	19.5
0.3	18.9	20.1	0.2	0.6	0.2	19.6
0.5	19.0	20.2	0.5	0.9	0.5	19.6
0.8	19.0	20.2	0.7	0.9	0.7	19.6
1.0	18.9	20.1	0.9	0.6	1.0	19.6
1.3	18.9	20.1	1.2	0.5	1.2	19.6
1.5	18.8	20.1	1.4	-0.2	1.4	19.5
1.8	18.9	20.1	1.6	0.3	1.7	19.5
2.0	18.9	20.2	1.9	0.3	1.9	19.5
2.3	18.8	20.2	2.1	-0.2	2.2	19.5
2.5	18.8	20.2	2.3	-0.3	2.4	19.5
2.8	18.8	20.2	2.6	-0.3	2.6	19.5
3.0	19.0	19.5	2.8	0.9	2.9	19.6
3.3	19.0	19.9	3.0	1.1	3.1	19.7
3.5	19.0	20.0	3.3	1.4	3.4	19.7
3.8	19.1	19.9	3.5	1.6	3.6	19.7
4.0	19.1	19.9	3.8	1.9	3.8	19.8
4.3	19.2	19.7	4.0	2.3	4.1	19.8
4.5	19.2	19.8	4.2	2.5	4.3	19.8
4.8	19.2	19.8	4.5	2.8	4.6	19.9
5.0	19.3	19.8	4.7	3.1	4.8	19.9

## Konvertering av egenskapsfunksjoner

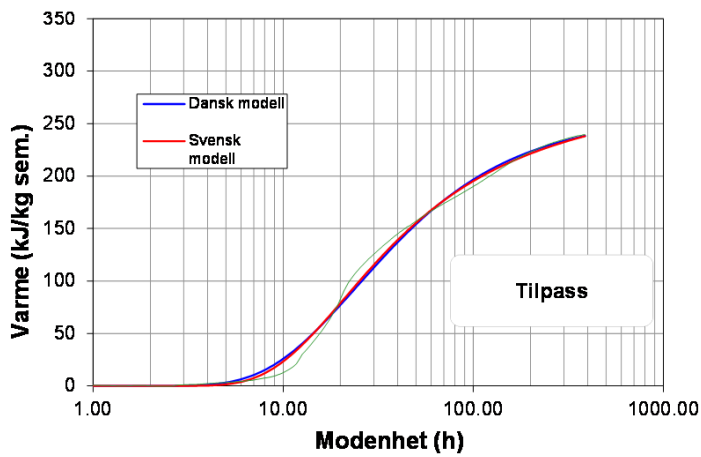
Dansk modell	
$Q_\infty$	257
$\tau$	24.38
$\alpha$	0.93

$$Q = Q_\infty \cdot e^{\left(-\frac{\tau}{M}\right)^\alpha}$$

Svensk modell	
$W_c$	300
$\lambda_1$	1.000
$t_1$	16.46
$\kappa_1$	1.26

$$Q = W_c \cdot e^{\left(-\lambda_1 \cdot \ln\left(1 + \frac{t_e}{t_1}\right)\right)^{-\kappa_1}}$$

Kv.sumsav.	7351
------------	------



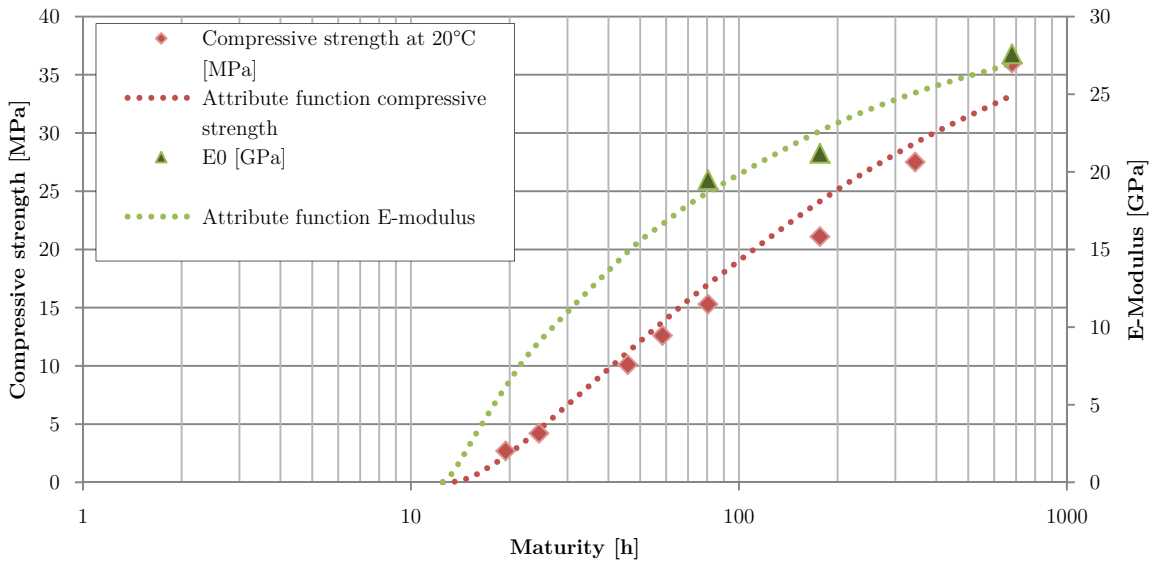
$$f_c(t_e) = f_{c28} \cdot \exp \left[ s \left( 1 - \sqrt{\frac{28}{\frac{t_e}{24} - \frac{t_0}{24}}} \right) \right] \quad (2.11)$$

$$E_c(t_e) = E_{c28} \cdot \left\{ \exp \left[ s \left( 1 - \sqrt{\frac{28}{\frac{t_e}{24} - \frac{t_0}{24}}} \right) \right] \right\}^{nE} \quad (2.13)$$

Maturity [h]	Compressive strength at 20°C [MPa]	Attribute function compressive strength	E0 [GPa]	Attribute function E-modulus	Least square error
-	-	-	-	-	-
15.50	-	0.55	-	2.84	-
15.80	-	0.66	-	3.14	-
19.44	2.70	2.24	-	6.15	-
24.57	4.20	4.52	-	9.04	-
45.81	10.10	11.18	-	14.84	-
58.50	12.60	13.76	-	16.63	-
80.50	15.30	17.00	19.50	18.67	0.68
176.50	21.10	24.12	21.20	22.63	2.03
344.50	27.50	29.14	-	25.09	-
680.50	36.00	33.25	27.60	26.98	0.39
					3.11

fc28	33.27
s	0.31
t0	12.10

Ec28	26.99
s	0.31
t0	12.10
nE	0.55

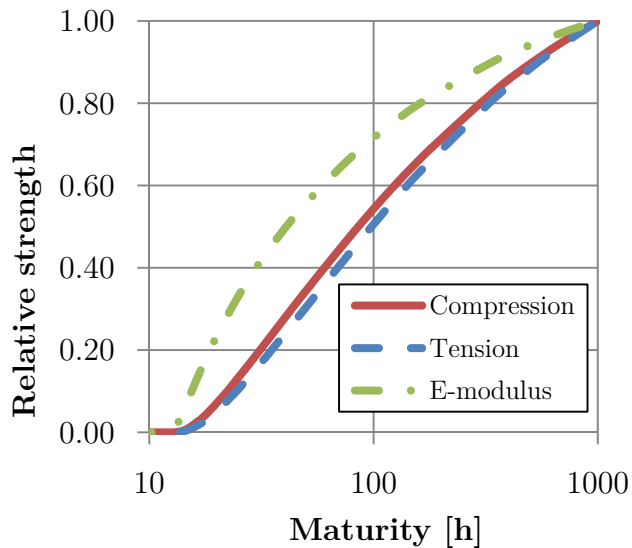
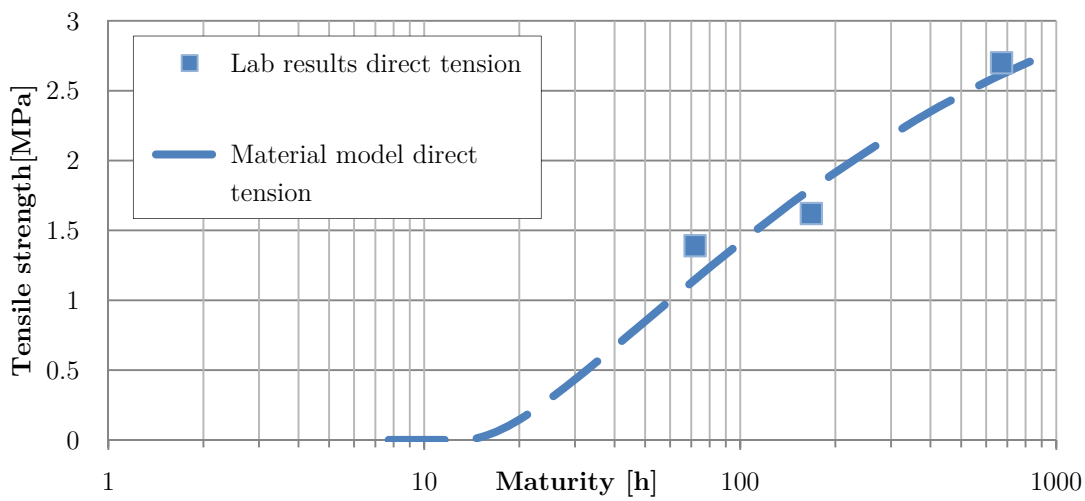


Tensile strength

$$f_t(t_e) = f_{t28} \cdot \left\{ \exp \left[ s \left( 1 - \sqrt{\frac{28}{\frac{t_e}{24} - \frac{t_0}{24}}} \right) \right] \right\}^{n_t} \quad (2.12)$$

Age	Maturity [h]	Lab results direct tension	Material model direct tension	Least square error
18	22	0	0.2073779	0
24	29	0	0.4176091	0
48	57	0	0.9503006	0
72	81	1.39	1.239564	0.022631
168	177	1.62	1.8328294	0.045296
336	345	0	2.2631054	0
672	681	2.7	2.6223586	0.006028
				0.073955

ft28	2.62
s	0.31
t0	12.10
nt	1.12



RELAX

creepinp.ire:

NCC

7 3 9 3

0.001 0.1

FileNameCreep.txt

Filenamecreep.txt:

7

26.99 28 0.31 0.55

1.47 0.24 0.24 0.0

0.504 1.9 18

NCC.rel:

10	8	0.00500	0.50400						
	0.503	0.604	1.301	2.804	6.040	13.013	28.035	60.400	
130.128	280.352								
	0.01	0.01	0.01	0.01	0.01	0.01	0.01	0.01	0.01
0.4011	-0.1700	2.1337	-0.0006	-0.3769	-0.2330	-0.5203	0.2849		
1.5255	1.2723	2.6669	0.6924	1.1562	1.2518	2.2508	-1.2470		
1.9951	2.0235	3.1580	1.3682	2.1955	2.3063	4.1844	-2.3298		
2.1509	2.4037	3.4642	2.1939	3.0233	3.1827	5.7528	-3.2852		
2.1207	2.5600	3.5142	3.2168	3.7732	3.9594	7.1133	-4.3019		
1.9926	2.5345	3.4815	3.8042	4.0713	4.1714	7.4371	-3.1735		
1.7195	2.2594	3.2196	3.7372	4.0109	3.9272	6.9271	-1.0666		
1.4750	1.9926	2.9337	3.5987	3.9900	3.7487	6.4556	0.8955		
1.2592	1.7401	2.6405	3.3931	3.9610	3.6482	6.0269	2.7233		

Shrinkage:

Maturity [h]	Autogenous shrinkage [ $10^{-6}$ ]:
0	0
12	0
15	-0.000003
17	-0.000018
22	-0.000025
26	-0.000030
72	-0.000046
116	-0.000078
256	-0.000104
800	-0.000140



## Appendix C

# Material Parameters for Anlegg 33.3% FA per binder

See SINTEF Test Report, project no: 3D0593.31, Report no: 33380

See next page

**Adiabatic temperature and isothermic heat**

(v 2.7 ss 2004-01-07)

**SKANSKA**

**Concrete parameters**

Temp. trans. coeff.	0.0042
Density	2340
Heat capacity (fresh)	1.03
Heat capacity (hardened)	1.03
Cement content	334
Set time	8.07
A - set time	33792
B - set time	386
A - hydration	33792
B - hydration	386
Adia. start temperature	20

**Temp. trans. coeff.**

dQ/dm	0.1
m>	150
m<	200

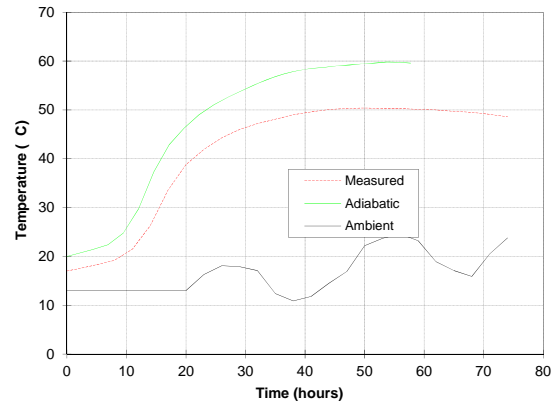
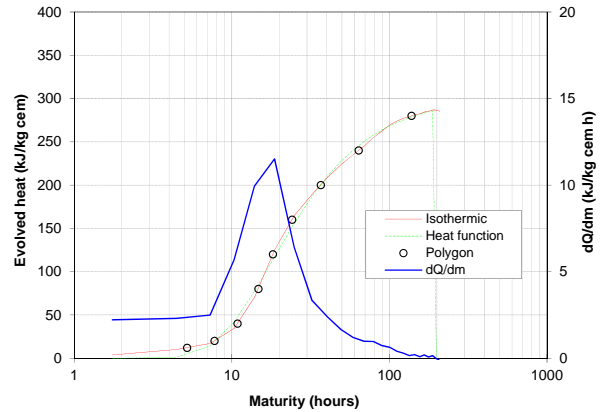
**Heat function**

M-limit	190
Q <sub>e</sub>	301
τ	17.82
α	1.25
R <sup>2</sup>	0.9887
ΣΔ <sub>Q</sub>	454

**Heat polygon**

Reference heat [kJ/kg cem]	Corresp. maturity [h]
0	0.0
12	5.2
20	7.8
40	10.9
80	14.8
120	18.2
160	24.1
200	36.7
240	63.9
280	138.3

Adapt the temperature transmission coefficient: <Ctrl> t  
Adapt the heat function: <Ctrl> h



**Project**

Name	Løsmassetunnel 50% FA
Test id	SINTEF rapportnr: 33380
Perf. by	Christian K Sandvik
Date	28.11.2011

Time [h]	Concrete temperature [C]	Ambient temperature [C]	Maturity [h]	Acc. heat pr. cem [kJ/kg cem]	Adiabatic time [h]	Adiabatic temperature [C]
0.0	17.0	13.0	0	0.0	0.0	20.0
2.0	17.5	13.0	1.7	3.9	1.7	20.5
5.0	18.3	13.0	4.5	10.1	4.3	21.4
8.0	19.2	13.0	7.3	17.2	6.9	22.4
11.0	21.5	13.0	10.3	34.5	9.5	24.8
14.0	26.3	13.0	13.9	70.3	12.0	29.8
17.0	33.6	13.0	18.7	124.8	14.6	37.3
20.0	38.8	13.0	24.9	164.7	17.2	42.8
23.0	41.9	16.3	32.3	189.3	19.7	46.3
26.0	44.3	18.1	40.5	209.0	22.2	49.0
29.0	46.0	17.9	49.5	233.8	24.7	51.1
32.0	47.2	17.1	59.0	235.2	27.1	52.6
35.0	48.1	12.4	68.9	245.0	29.5	54.0
38.0	49.0	10.9	79.2	254.9	31.9	55.4
41.0	49.6	11.8	89.8	262.7	34.2	56.4
44.0	50.1	14.5	100.6	269.5	36.5	57.4
47.0	50.3	16.9	111.6	274.0	38.8	58.0
50.0	50.4	22.2	122.6	277.3	41.0	58.5
53.0	50.3	23.7	133.7	279.0	43.2	58.7
56.0	50.3	24.6	144.7	281.3	45.3	59.0
59.0	50.1	23.2	155.6	282.4	47.5	59.2
62.0	50.0	18.9	166.5	284.5	49.6	59.5
65.0	49.7	17.1	177.3	285.3	51.7	59.6
68.0	49.5	15.9	188.1	286.9	53.7	59.8
71.0	49.1	20.5	198.6	286.6	55.7	59.8
74.0	48.6	23.8	209.1	285.3	57.7	59.6

## Konvertering av egenskapsfunksjoner

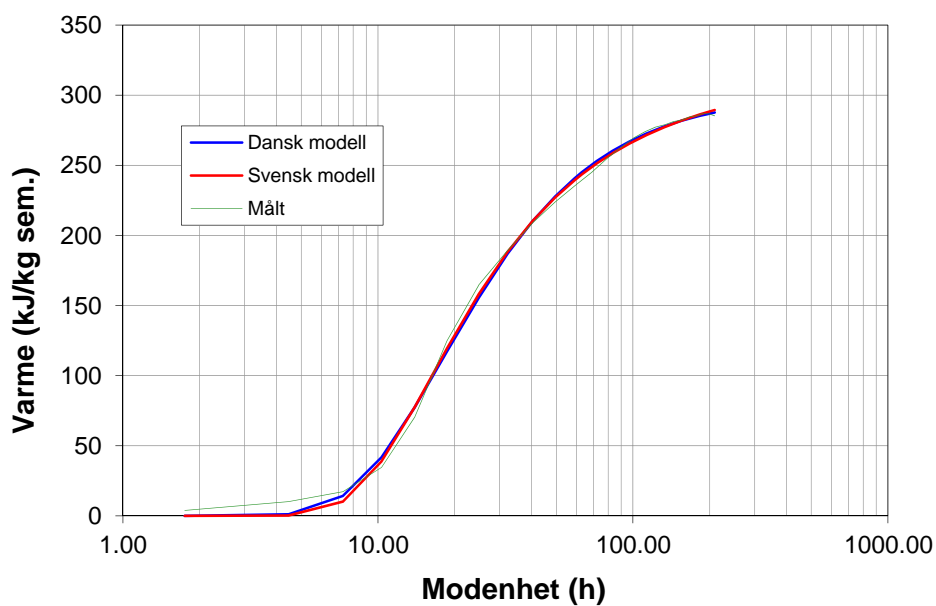
Dansk modell	
$Q_\infty$	301
$\tau$	17.82
$\alpha$	1.25

$$Q = Q_\infty \cdot e^{\left(-\frac{\tau}{M}\right)^\alpha}$$

Svensk modell	
$W_c$	331
$\lambda_1$	1.000
$t_1$	11.03
$\kappa_1$	1.84

$$Q = W_c \cdot e^{\left(-\lambda_1 \cdot \ln\left(1 + \frac{t_e}{t_1}\right)\right)^{-\kappa_1}}$$

Kv.sumsav.	400
------------	-----



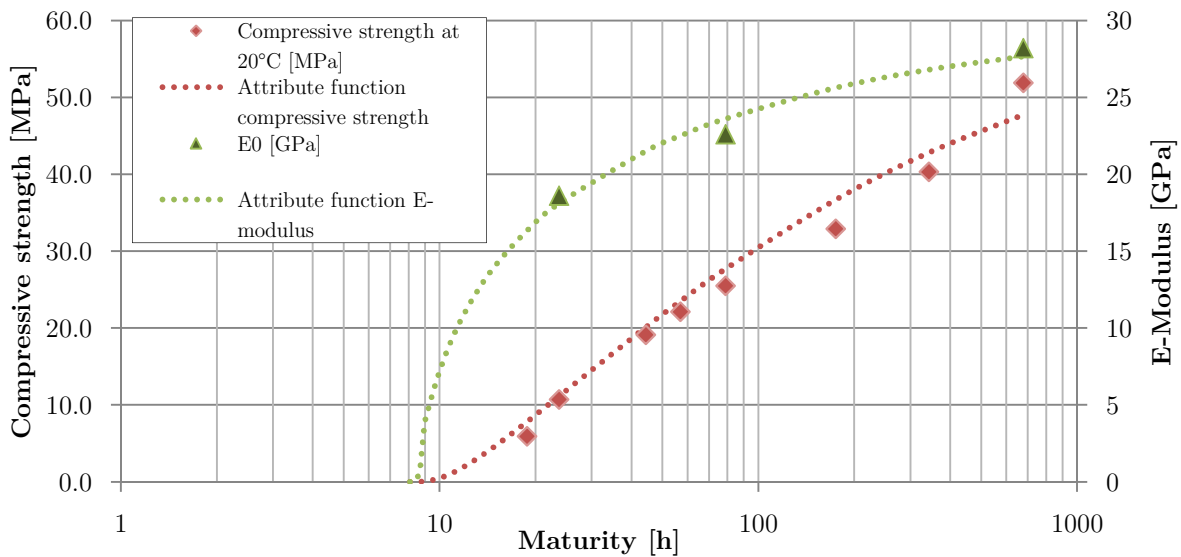
$$f_c(t_e) = f_{c28} \cdot \exp \left[ s \left( 1 - \sqrt{\frac{28}{\frac{t_e}{24} - \frac{t_0}{24}}} \right) \right] \quad (2.11)$$

$$E_c(t_e) = E_{c28} \cdot \left\{ \exp \left[ s \left( 1 - \sqrt{\frac{28}{\frac{t_e}{24} - \frac{t_0}{24}}} \right) \right] \right\}^{n_E} \quad (2.13)$$

Maturity [h]	Compressive strength at 20°C [MPa]	Attribute function compressive strength	E0 [GPa]	Attribute function E-modulus	Least square error
8.07	-	0.00	-	0.00	-
11.67	-	1.73	-	10.53	-
13.00	-	2.91	-	12.25	-
18.79	5.90	7.79	-	16.32	-
23.71	10.70	11.14	18.60	18.11	0.24
44.36	19.10	20.09	-	21.50	-
56.93	22.10	23.48	-	22.50	-
78.93	25.50	27.69	22.60	23.61	1.01
174.93	32.90	36.68	-	25.62	-
342.93	40.30	42.81	-	26.80	-
678.93	51.90	47.74	28.20	27.66	0.29
					1.54

fc28	47.75
s	0.26
t0	8.07

Ec28	27.66
s	0.26
t0	8.07
nE	0.29

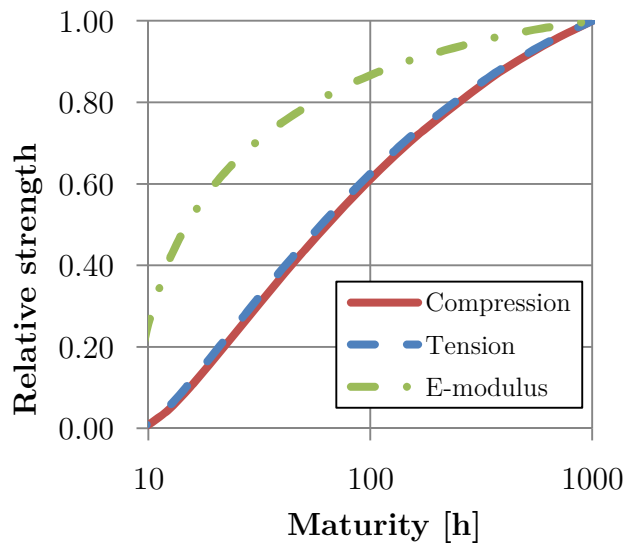
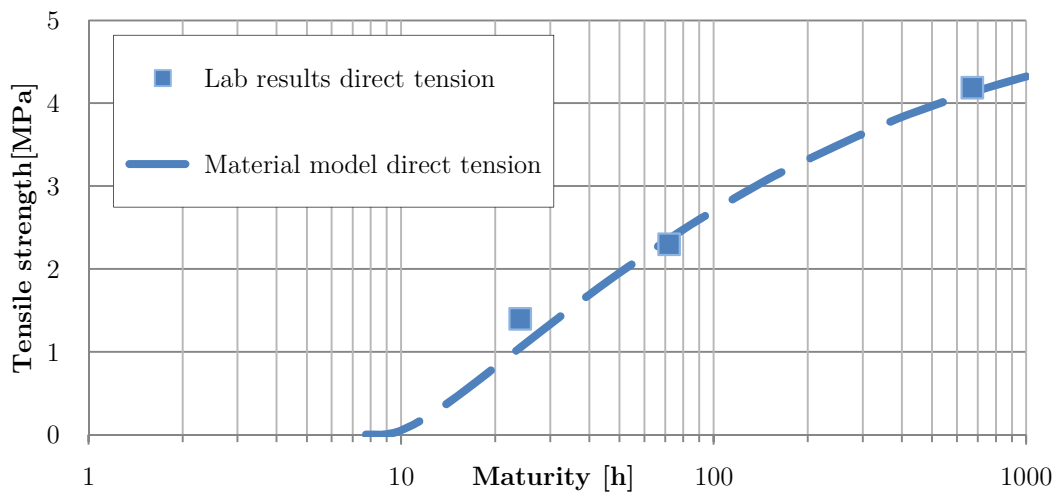


Tensile strength

$$f_t(t_e) = f_{t28} \cdot \left\{ \exp \left[ s \left( 1 - \sqrt{\frac{28}{\frac{t}{24} - \frac{t_0}{24}}} \right) \right] \right\}^{n_t} \quad (2.12)$$

Age	Maturity [h]	Lab results direct tension	Material model direct tension	Least square error
18	21	0	0.8941577	0
24	28	1.4	1.2629869	0.018773
48	55	0	2.061979	0
72	79	2.3	2.4606391	0.025805
168	175	0	3.2170051	0
336	343	0	3.7281605	0
672	679	4.19	4.1362723	0.002887
				0.047464

ft28	4.137153612
s	0.262035217
t0	8.072665435
nt	0.953483691



RELAX

creepinp.ire:

Anlegg FA  
 7 3 9 3  
 0.001 0.1  
 FileNameCreep.txt

Filenamecreep.txt:

7  
 27.66 28 0.26 0.29  
 1.23 0.28 0.3 0.0  
 0.336 1.9 18

Anlegg FA.rel:

10	8	0.00500	0.33600						
	0.335	0.436	0.939	2.024	4.360	9.393	20.237	43.600	
93.933	202.373								
	0.01	0.01	0.01	0.01	0.01	0.01	0.01	0.01	0.01
1.3215	0.8249	4.8221	0.1278	0.0207	0.2001	0.2749	-0.2240		
2.1648	2.3093	4.7954	1.2878	2.1046	2.3102	4.3436	-3.4591		
2.2010	2.7389	4.8695	2.0821	3.2138	3.4773	6.5604	-5.2395		
2.0351	2.7729	4.7792	2.9361	4.0510	4.4039	8.2748	-6.6768		
1.7939	2.6275	4.4554	3.9124	4.8039	5.2229	9.7516	-8.0857		
1.5279	2.4144	3.9263	4.8642	5.5654	5.9044	10.9603	-9.2932		
1.2762	2.0683	3.5227	4.6922	5.3792	5.4635	10.0411	-5.9534		
1.0462	1.7352	3.0550	4.3848	5.2666	5.1240	9.2127	-3.1150		
0.8553	1.4434	2.6164	3.9842	5.1465	4.9063	8.4717	-0.5346		

Shrinkage:

Maturity [h]	Autogenous shrinkage [ $10^{-6}$ ]:
0	0
8	0
12	-0.000032
17	-0.000052
24	-0.000069
42	-0.000077
800	-0.000077



## Appendix D

# Material Parameters for Anlegg 30% FA per binder from the Bjørvika tunnel

See next pages

## **Lavvarmebetong: Input for spenningsberegninger**

### **Innhold**

1	RESEPT .....	2
2	MATEMATISKE MODELLER .....	2
3	DIVERSE INPUTPARAMETRE .....	2
4	VARMEUTVIKLING .....	3
5	AUTOGEN DEFORMASJON .....	3
6	TRYKKFASTHET .....	4
7	E-MODUL .....	5
8	STREKKFASTHET .....	6

Vedlegg 1 Tabellerte inngangsdata

## 1 Resept

Materialer	Resept kg/m <sup>3</sup>
Anleggsement FA	388.9
Elkem Microsilica	11.0
Fritt vann	162.3
Absorbert vann	9.7
Årdal 0 - 8 mm	968.4
Eklogitt 5.6 - 16mm	296.2
Eklogitt 16 - 22mm	593.5
Luft	5%
Sika Viscocrete HT-250	3.5
Sika AER (1:9)	1.5

## 2 Matematiske modeller

To modeller er tilpasset forsøksdataene, disse er CEB-FIP Modell Code 1990 (MC) likningen og Friesleben-Hansen (FH) likningen:

MC-likningen: 
$$X(t_e) = X_{28} \cdot \left\{ \exp \left[ s \cdot \left( 1 - \sqrt{\frac{28}{t_e - t_0}} \right) \right] \right\}^n$$

hvor  $X(t_e)$  er egenskapen ved tiden (modenheten)  $t_e$ ,  $X_{28}$  er egenskapen etter 28 døgn,  $s$  og  $n$  er modellparametere og  $t_0$  er tiden hvor spenninger begynner å bygges opp (avbinding).

FH-likningen: 
$$X(t_e) = X_{\infty} \cdot \exp \left[ - \left( \frac{\tau}{t_e} \right)^{\alpha} \right]$$

hvor  $X_{\infty}$  er egenskapen etter lang tid,  $\tau$  og  $\alpha$  er modellparametere.

## 3 Diverse inputparametere

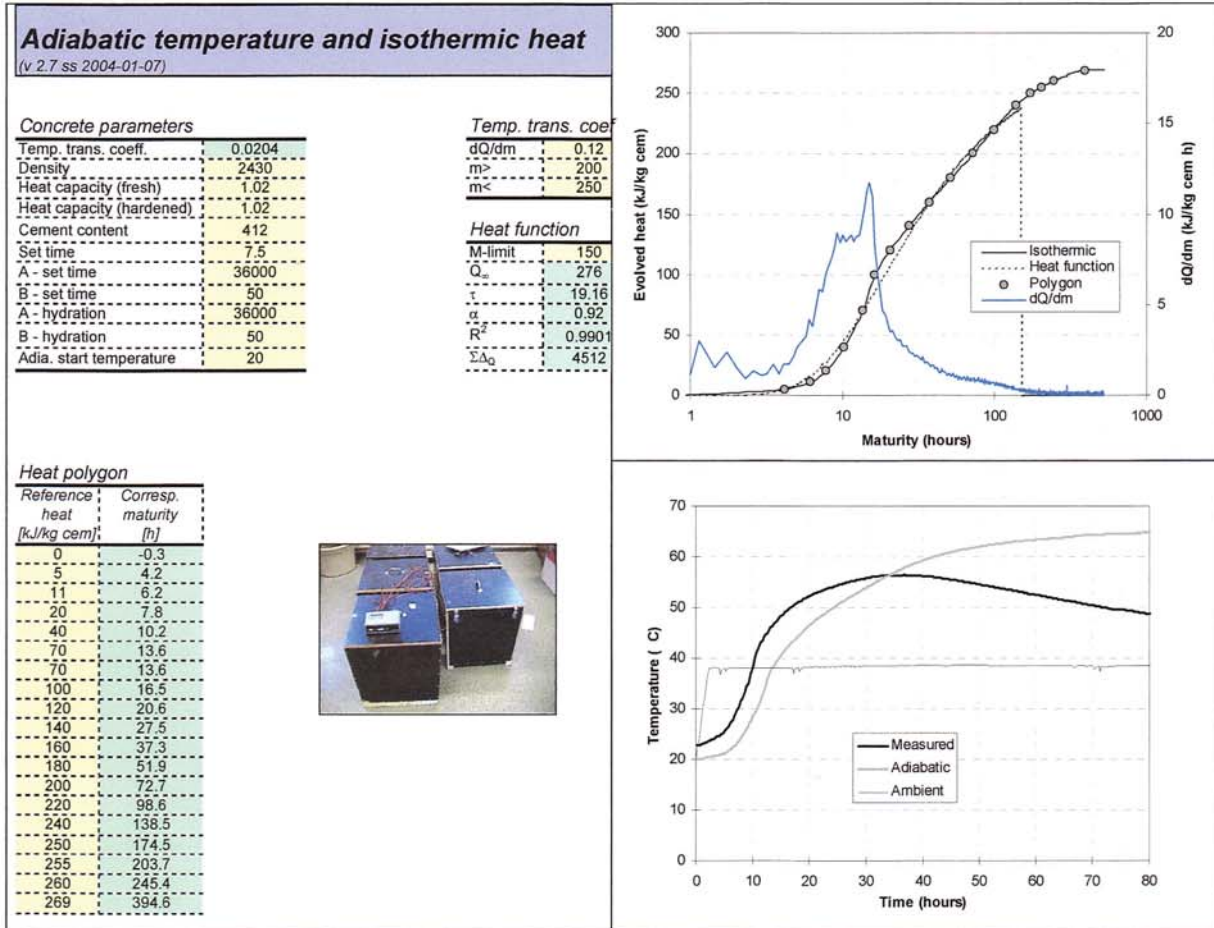
$t_0 = 11$  modenhets timer

Aktiveringsenergi: Parameter A = 36000 kJ/mol, parameter B = 50 kJ/(mol x °C)

Varmeutvikling og termisk dilatasjon: Densitet = 2430 kg/m<sup>3</sup>, varmekapasitet = 1.02 kJ/(kg x °C),  
Termisk utvidelseskoeffisient ( $\alpha_T$ ) =  $7.3 \times 10^{-6}/^{\circ}\text{C}$

Kryp: Default kryptformulering i 4C-Temp&Stress

### 4 Varmeutvikling



### 5 Autogen deformasjon

Modenhets [timer]	Autogent svinn [10 <sup>-6</sup> ]
11	0
12	-8
17	-10
22	-26
26	-30
42	-31
72	-23
116	-13
256	-5

NB: Negative strain is shrinkage

## 6 Trykkfasthet

### TRYKKFASTHET

Tillegg  
 Frieleber-Hansen (FH) modell (C1st f)  
 Modelcode 1990 (MC90) modell (C1st m)

$Q_0 =$	59.8
$\tau =$	46.13
$\alpha =$	0.70

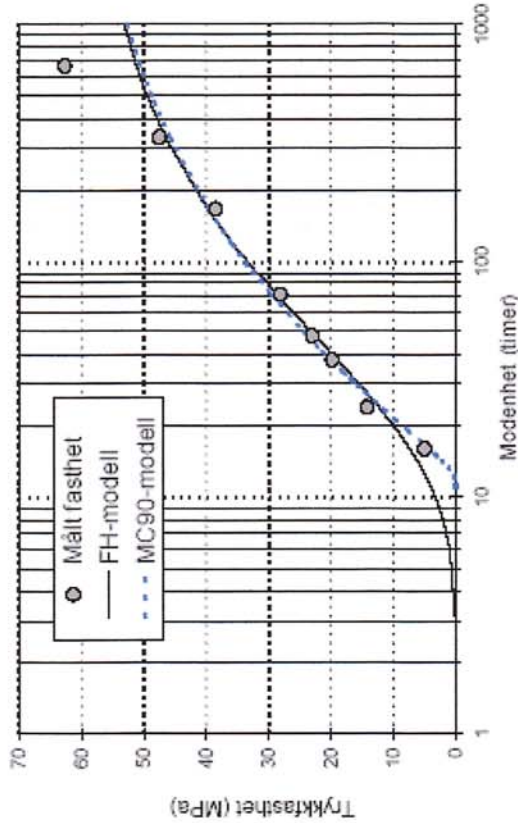
$f_{cs} =$	50.7
$s =$	0.23
$t_0 =$	11.0

Modenhets- (timer)	Fasthet (MPa)		Kv avvik		Fasthet		Kv avvik	
	FH-Modell	MC90-Modell	FH-Modell	MC90-Modell	MC90-Modell	MC90-Modell	MC90-Modell	MC90-Modell
16	5.0	7.4	5.7	4.3	0.4			
24	14.2	12.4	3.4	12.0	4.6			
36	19.8	19.0	0.6	20.1	0.1			
46	23.0	22.6	0.1	23.8	0.6			
72	28.1	28.7	0.4	29.6	2.2			
168	36.5	39.9	1.8	39.5	1.1			
336	47.5	46.6	0.9	45.8	3.0			
<b>672</b>								
Sum kv avvik:								
			12.9		12.0			

NBH	Barnesens testser, flere punkter	
	Fasthet	Fasthet
1	0.0	0.0
3	0.1	0.2
6	0.9	0.9
8	2.0	2.0
9	2.6	3.2
10	3.3	5.5
11	4.0	7.6
12	4.6	9.5
13	5.3	11.3
14	6.0	12.8
18	8.7	14.2
24	12.4	15.5
30	15.5	16.6
36	18.2	19.6
48	22.6	22.1
60	26.0	24.1
72	28.7	29.8
96	32.8	33.4
120	35.8	36.0
168	30.9	39.5
336	46.6	45.8
500	49.5	48.7
672	51.3	50.6
1000	53.2	52.8

NBH  
 Reddetall (28 d)  
 er utføst dvs. modellene  
 undersøkt for styrken  
 etter 336 t (2 uker).



### 7 E-modul

#### E-modul

**Tilpass**

Frieston-Hansen (FH) modell (C21 f)  
 Modcode 1990 (MC90) modell (C21 m)

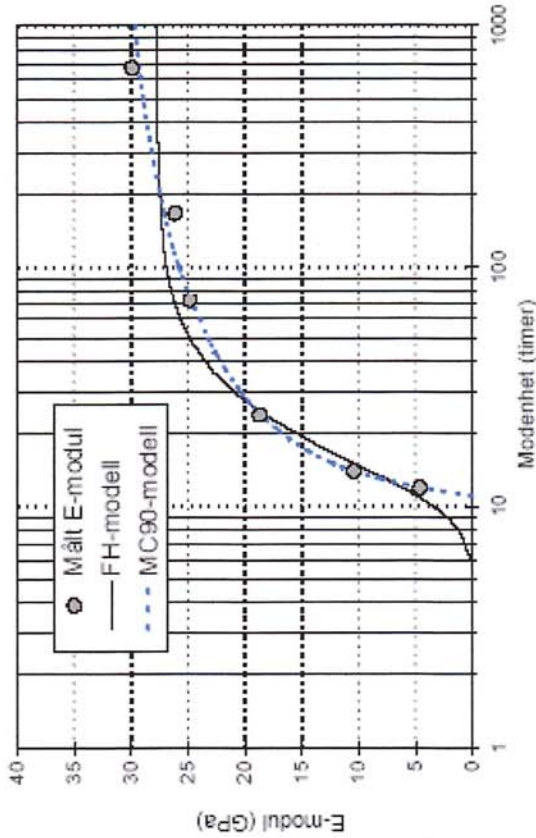
$\eta_E =$	0.3
$E_{0.28} =$	29.3
$S =$	0.23
$f_0 =$	11.0

$E_a =$	27.7
$\nu =$	14.92
$\alpha =$	1.84

Modenhets (timer)	E-modul (MPa)		Kv avvik		E-modul		Kv avvik		
	FH-Modell	MC90-Modell	FH-Modell	MC90-Modell	FH-Modell	MC90-Modell	FH-Modell	MC90-Modell	
24	15.7	15.3	0.2	0.0	18.5	18.5	0.0	0.0	
72	24.8	26.2	2.0	0.0	24.7	24.7	0.0	0.0	
168	26.1	27.4	1.6	0.9	27.0	27.0	0.9	0.9	
672	29.9	27.7	4.9	0.4	29.2	29.2	0.4	0.4	
12	4.6	6.2	2.6						
14	10.4	9.0	2.0						
Sum kv avvik=		13.4				1.4			

NB!!  
 Røde tall er tatt fra  
 MC90-modellen for å  
 tvinge FH-modellen  
 ned for elubinding

Timer	Beregnete verdier, fers.punkter	
	E-modul	E-modul
1	0.0	0.0
3	0.0	4.6
6	0.1	8.1
8	1.2	10.4
9	2.2	12.1
10	3.4	14.4
11	4.6	16.0
12	6.2	17.2
13	7.6	18.1
14	9.0	18.9
18	13.6	19.5
24	18.3	20.1
30	21.0	20.5
36	22.7	21.6
48	24.7	22.5
60	25.6	23.1
72	26.2	24.7
96	26.8	25.6
120	27.1	26.3
168	27.4	27.0
336	27.6	28.3
500	27.7	28.9
672	27.7	29.2
1000	27.7	29.6



### 8 Strekkfasthet

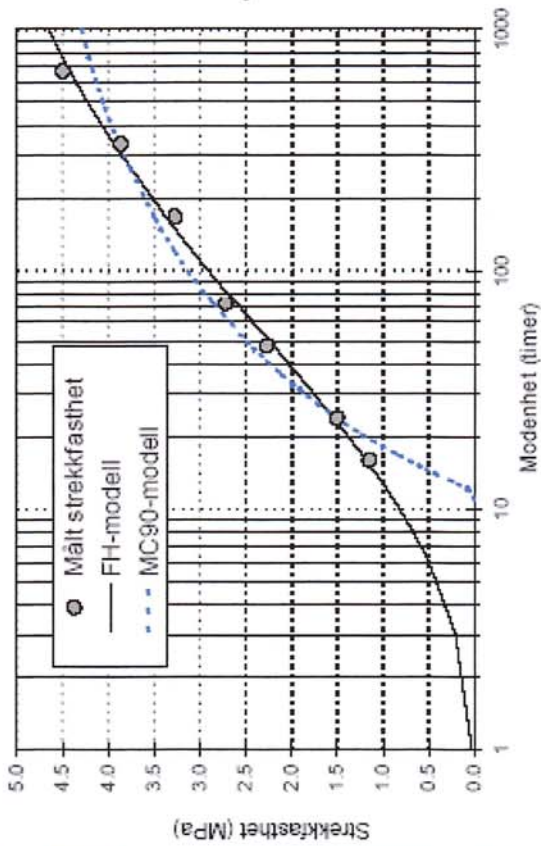
**STREKKFASTHET**

**Tillegg**

Friskiben-Hansen (FH) modell (Ctil f)  
 Modellsids 1990 (MC90) modell (Ctil m)

$n_1 =$	0.7
$f_{28} =$	4.2
$s =$	0.23
$f_{\phi} =$	11.0

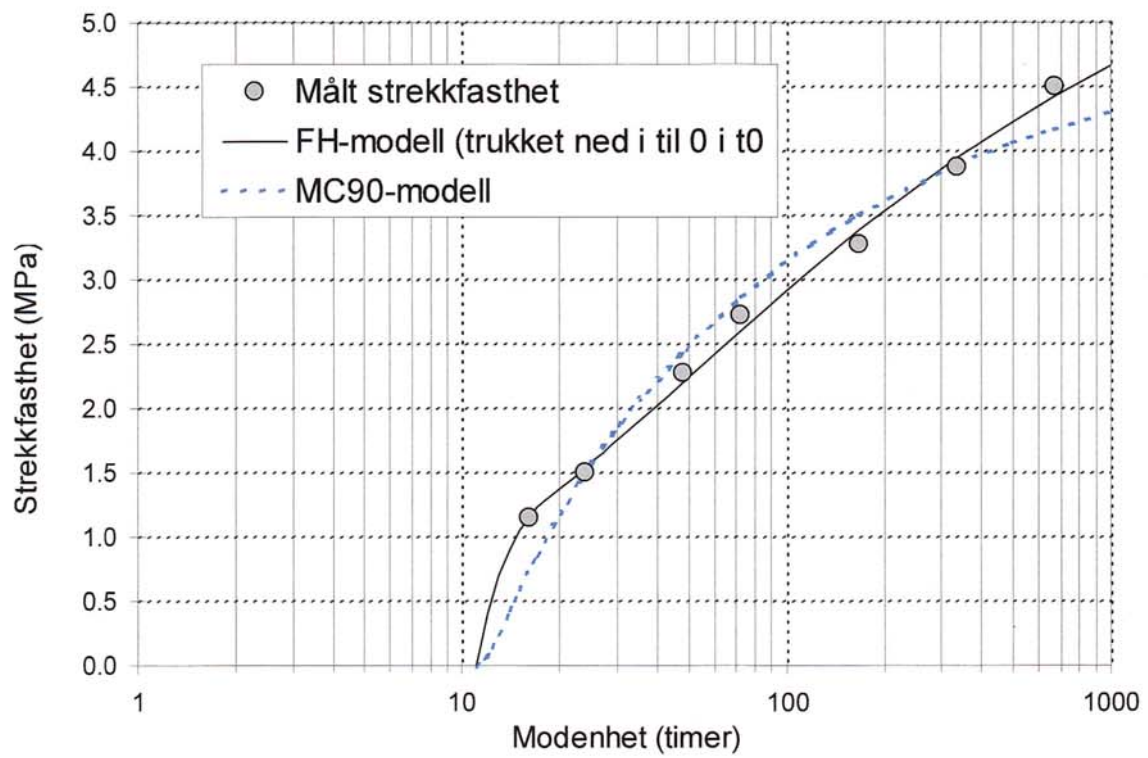
$f_{90} =$	6.1
$\tau =$	50.56
$\alpha =$	0.43



Modenhhet (timer)	Strekkf. (MPa)		Kv. avvik		Kv. avvik	
	FH-Modell	MC90-Modell	FH-Modell	MC90-Modell	MC90-Modell	MC90-Modell
16	1.15	1.2	0.0	0.7	0.2	0.2
24	1.50	1.5	0.0	1.5	0.0	0.0
48	2.27	2.2	0.0	2.4	0.0	0.0
72	2.72	2.6	0.0	2.9	0.0	0.0
168	3.27	3.4	0.0	3.5	0.1	0.0
336	3.87	3.9	0.0	3.9	0.0	0.0
672	4.50	4.4	0.0	4.2	0.1	0.1
Sum kv avvik=			0.0			0.4

Beregnete verdier, flere punkter		
Timer	Strekkf.	Strekkf.
1	0.0	0.0
11	0.2	0.1
3	0.5	0.2
6	0.7	0.4
9	0.7	0.6
10	0.8	0.0
11	0.9	1.1
12	1.0	1.3
13	1.0	1.4
14	1.1	1.0
18	1.3	1.7
24	1.5	1.8
30	1.8	1.9
36	1.9	2.1
48	2.2	2.3
60	2.4	2.5
72	2.6	2.9
96	2.9	3.1
120	3.1	3.3
168	3.4	3.5
336	3.9	3.9
500	4.2	4.1
672	4.4	4.2
1000	4.7	4.3



## Vedlegg 1 Tabellerte inngangsdata

Varme:

Modenhets [timer]	Varme [kJ/kg]
0	0
4.2	5
6.2	11
7.8	20
10.2	40
13.6	70
13.6	70
16.5	100
20.6	120
27.5	140
37.3	160
51.9	180
72.7	200
98.6	220
138.5	240
174.5	250
203.7	255
245.4	260
394.6	269

Autogent svinn (negativ tøyning er svinn):

Modenhets [timer]	Autogent svinn [10 <sup>6</sup> ]
11	0
12	-8
17	-10
22	-26
26	-30
42	-31
72	-23
116	-13
256	-5

Mekaniske egenskaper:

Trykkfasthet:		E-modul:		Strekkfasthet:	
Modenhets	Fasthet	Modenhets	E-modul	Modenhets	Strekkf.
11	0.0	11	0.0	11	0
12	0.2	12	4.6	12	0.4
13	0.9	13	8.1	13	0.7
14	2.0	14	10.4	14	0.9
15	3.2	15	12.1	15	1.1
17	5.5	17	14.4	17	1.2
19	7.6	19	16.0	19	1.3
21	9.5	21	17.2	21	1.4
23	11.3	23	18.1	23	1.5
25	12.8	25	18.9	25	1.6
27	14.2	27	19.5	27	1.7
29	15.5	29	20.1	29	1.7
31	16.6	31	20.5	31	1.8
37	19.6	37	21.6	37	2.0
43	22.1	43	22.5	43	2.1
49	24.1	49	23.1	49	2.2
73	29.8	73	24.7	73	2.6
97	33.4	97	25.6	97	2.9
121	36.0	121	26.3	121	3.1
168	39.5	168	27.0	168	3.4
336	45.8	336	28.3	336	3.9
500	48.7	500	28.9	500	4.2
672	50.6	672	29.2	672	4.4
1000	52.8	1000	29.6	1000	4.7

Trykkfastheten og E-modulen er uttrykt ved MC-likningen, mens strekkfastheten ved FH-likningen, men trukket ned til 0 i  $t_0$  som vist i figuren i Kapittel 8.

## Konvertering av egenskapsfunksjoner

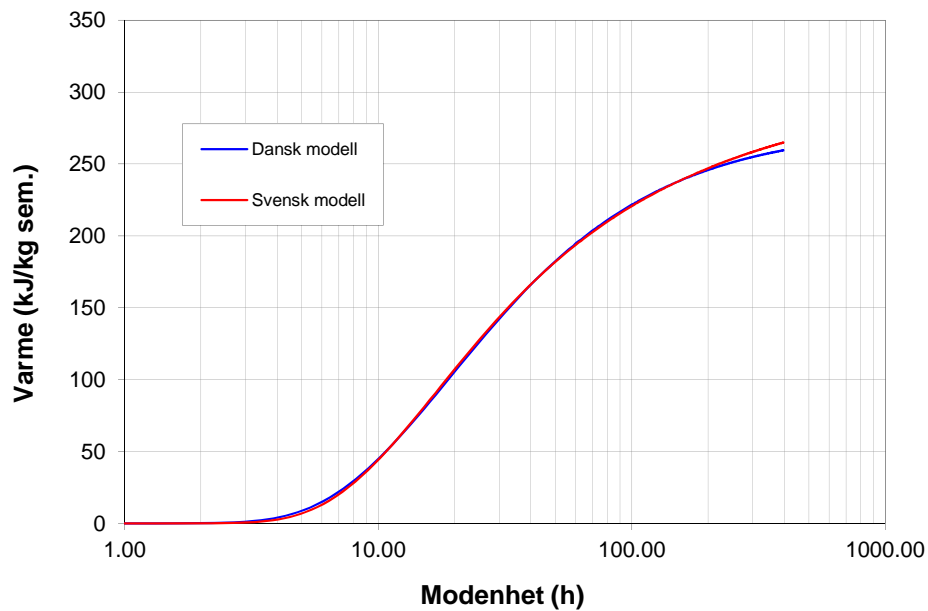
Dansk modell	
$Q_\infty$	276
$\tau$	19.16
$\alpha$	0.92

$$Q = Q_\infty \cdot e^{\left(-\frac{\tau}{M}\right)^\alpha}$$

Svensk modell	
$W_c$	341
$\lambda_1$	1.000
$t_1$	14.22
$\kappa_1$	1.13

$$Q = W_c \cdot e^{\left(-\lambda_1 \cdot \ln\left(1 + \frac{t_e}{t_1}\right)\right)^{-\kappa_1}}$$

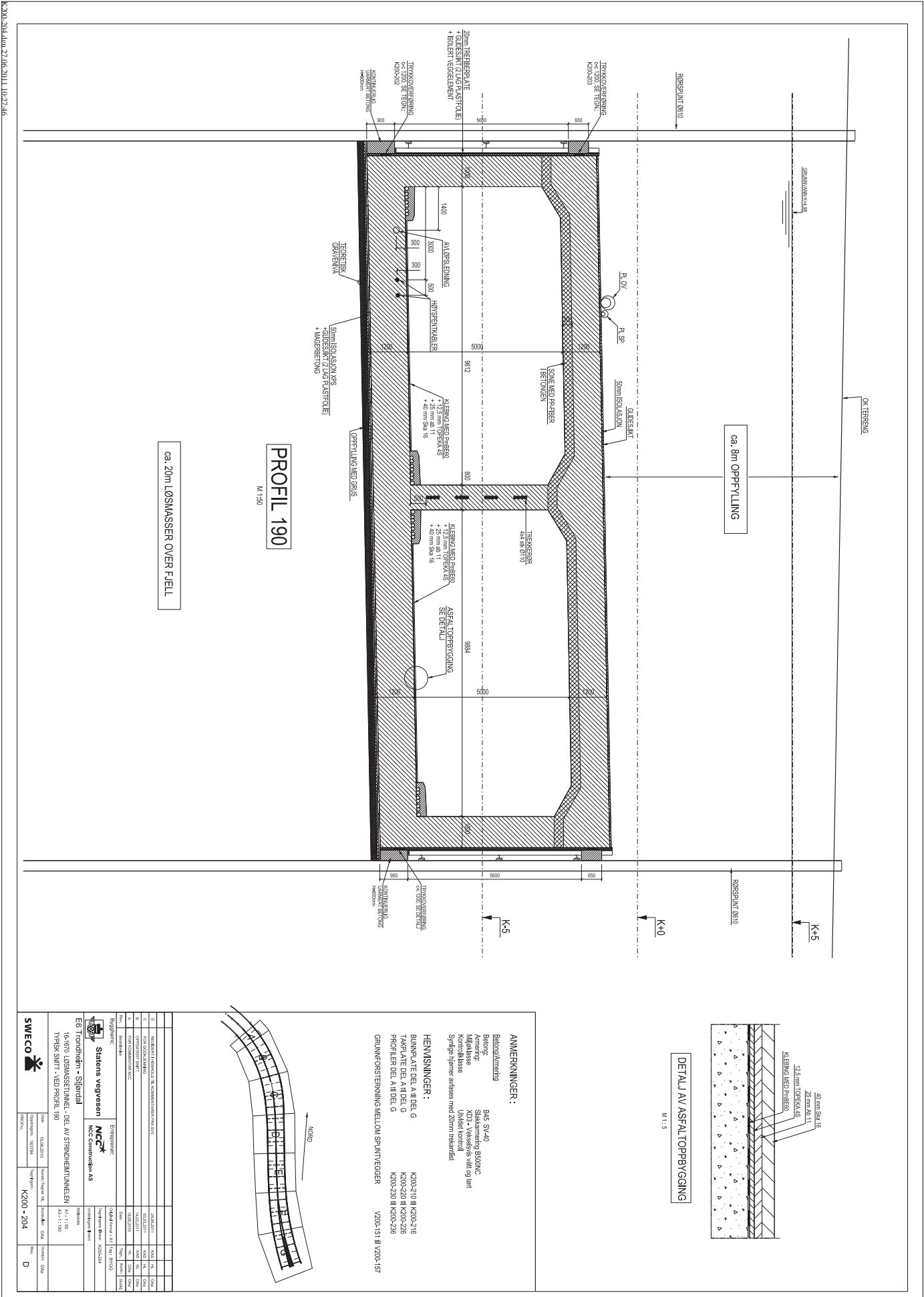
Kv.sumsav.	169
------------	-----



## Appendix E

# Geometry of the Møllenberg tunnel

See next page



K200-204.dwg 27.06.2011 10:27:46

